EVALUATING TISSUE CULTURE PLATFORMS FOR USE IN DRUG DEVELOPMENT: A MULTI-METHOD VALIDATIONAL APPROACH

By

CARRIE LYNN GERMAN

Bachelor of Science in Secondary Education

Oklahoma State University

Stillwater, Oklahoma

2006

Master of Science in Chemical Engineering

Oklahoma State University

Stillwater, Oklahoma

2014

Submitted to the Faculty of the

Graduate College of the

Oklahoma State University

in partial fulfillment of

the requirements for

the Degree of

DOCTOR OF PHILOSOPHY

December, 2017

EVALUATING TISSUE CULTURE PLATFORMS FOR USE IN DRUG DEVELOPMENT: A MULTI-METHOD VALIDATIONAL APPROACH

Dissertation Approved:

Dr. Sundar Madihally

Dissertation Adviser

Dr. Ashlee Ford Versypt

Dr. AJ Johannes

Dr. Carey Pope

Name: Carrie Lynn German

Date of Degree: DECEMBER, 2017

Title of Study: EVALUATING TISSUE CULTURE PLATFORMS FOR USE IN DRUG DEVELOPMENT: A MULTI-METHOD VALIDATIONAL APPROACH

Major Field: Chemical Engineering

Abstract: There has been significant interest in the development of synthetic tissue constructs for drug screening. Multiple approaches to developing tissue cultures that mimic *in vivo* conditions have been investigated, including three dimensional (3D) culturing and co-culturing. Little work has been done to develop *in silico* tools that provide drug pharmacokinetic (PK) profiles that can tie *in vitro* results to clinical data. In this regard, the possibility of integrating data and models into a 3D computational simulation using acetaminophen (APAP) as a case study was explored. Of particular concern with synthetic tissue constructs is maintenance of cellular functions. Thus, the effect of culturing 2 different hepatic cell lines (HepG2 and HepaRG) in 2D and 3D, using monoculture and co-culturing techniques, on enzyme activity, protein and urea section were investigated. A computational fluid dynamics software (Comsol) was used to create a 3D geometry based on 24-well and 96-well plate configurations. The effects of i) considering a total contribution to metabolism versus individualized contribution for CYP and UGT isoforms, ii) evaluating individualized metabolism based on isoform contributions and abundance, iiI) dosage and cell number, and iv) tissue culture size on APAP metabolism for 24 h were evaluated *in silico*. Obtained metabolic profiles were compared with the clinical data. APAP-GSH formation was over-predicted when rates of individual CYP isoform kinetics were simulated. When relative contributions of activity of each isoform was incorporated, metabolic distribution agreed with clinical data. Increased APAP content decreased APAP-Sulfation yield. Increased cell number increased APAP conversion and all metabolite yields. Simulation results validated by clinical data were compared with the various culturing systems. Results demonstrated that co-culturing had the greatest effect on PK results, as well as enzyme activity and protein and urea synthesis.

TABLE OF CONTENTS

LIST OF TABLES

Table Page

LIST OF FIGURES

Figure Page

Chapter II

Chapter III

Chapter IV

Chapter V

CHAPTER I

INTRODUCTION

Most big pharmaceutical companies work on developing multiple drugs at once and spend billions of dollars per successfully developed new medication due to an alarming nearly 95% drug failure rate in human trials [1]. Moreover, drugs that receive FDA approval to go to market only to be recalled due to safety inadequacies are even more costly. The extremely high initial cost of new drugs is a result of the need to recuperate development costs of these failed drugs. The need for less expensive and more efficient methods of screening drug effectiveness and safety prior to investigation in humans and the heavy monetary investments human trials require are vital to increasing safety and decreasing the cost of medications for both producers and consumers.

Drug failure in human trials can be traced back to the use of poorly predictive preclinical models, indicating serious limitations in preclinical testing as well as large gaps in knowledge of drug-specific metabolism [2]. Animal models are the current standard for evaluating preclinical drug safety and efficacy. Unfortunately, animal models, while good for predicting efficacy, are poor

models for predicting human toxicity. As a result, there is a sway toward the incorporation of tissue culture and computational models for evaluating preclinical toxicity, particularly those pertaining to liver metabolism. Improving preclinical models for evaluating human toxicity at the preclinical level holds the greatest potential for increasing the overall efficiency of the drug development process.

A wide variety of tissue culture techniques and environmental setups have been investigated in an attempt to create predictive hepatic models. Some of these techniques include monocultures or cocultures, 2D or 3D environments, and whole liver cells or liver microsomes. Additionally, liver tissue cocultures can involve the growth of hepatocytes with endothelial, kupffer, or stellate cells, and numerous methods for creating 3D environments have been investigated. Different labs have different setups for evaluating the same metabolic function and yet obtain different results. Also, drug screening requires high-throughput analysis, thus rendering environments the size of the whole human liver incompatible. Thus, a method that both scales between local tissue metabolic response and whole-body response and that validates experimental results using *in vivo* data is necessary. Computational modeling is useful in addressing these requirements.

Due to the challenges of mathematically modeling the complexities of the human body, *in silico* research in drug development did not gain a significant increase in application until the late 1990's [3, 4]. The U.S. FDA's Office of Clinical Pharmacology (OCP) has used modeling and simulation strategies to address a variety of drug development issues over the past decade. The FDA has made appeals for innovation in modeling areas (computational and experimental) and collaboration between FDA, industry, and academic scientists [5]. Improvement in drug development efficiency requires the employment of a combination of experimental and computational models from full body down to the cellular level to tell the interactive story between the body and a specific drug [5],[6].

This project was split into three aims and employed a "learn and confirm" or synergistic approach to the creation of an *in vitro*/*in silico* drug development platform for which metabolic and hepatic function data could be validated by comparison against clinical data.

1.1 Aim 1: Develop a computational model to connect liver tissue culture metabolic data with clinical and experimental data for validation purposes.

The purpose of Aim 1 was to develop a computational model incorporating Fick's aw of diffusion, mass balance, and Michaelis-Menten reaction kinetics for a constant volume, static bioreactor capable of producing transient metabolic profiles for a drug. APAP was selected for investigation due to the large amount of metabolic data available in literature. The first goal was to obtain metabolic profiles from simulation that matched clinical data, using a physiologically relevant hepatocyte density. Numerous kinetic constants for the same pathway (bioactivation, sulfation, or glucuronidation) or specific enzyme were evaluated along with multiple approaches to representing reaction rates (i.e. on a specific enzyme or grouped sum basis). Results demonstrated that consideration of the bioactivation reaction rate on individual enzyme basis weighted by each enzyme's contribution to metabolism yielded results that most closely matched clinical data. After validation of the kinetic constants and reaction rate equations, the computational model was used to scale down cell densities to those more appropriate for high-throughput applications. The effects of cell density, initial dose, and bioreactor size on metabolic distribution were evaluated. The computational model helped by evaluating multiple metabolic profiles simultaneously and validating reaction rate constants with clinical data. Results demonstrated that both dose and cell density changes affect metabolic profiles; however, metabolism did not appear to be sensitive to well size, allowing for up or down scaling.

1.2 Aim 2: Create a tissue culture environment mimicking simulated geometry to investigate differences in hepatocyte behavior using an immortalized cell line (HepG2) and varying culture techniques (monoculture versus coculture with endothelial cells and 2D versus 3D).

HepG2 cells, a hepatocarcinoma cell line are commonly used to evaluate liver functions. As evidence, they are being used in the government collaborative project, Tox21. The highly proliferative state of these cells make them desirable and easy to maintain. However, there is concern as to their predictive capabilities and ability to maintain function due to their classification as a cancerous cell line. This aim examined HepG2 abilities to i) maintain liver specific functions (protein synthesis) over an eight-day culture period and ii) mimic clinical metabolic metabolism of APAP. Multiple cell culture techniques were used to determine which setup more closely matched the transient metabolic profiles obtained from the simulation mimicking experimental setup. Monoculture experiments in 2D were performed to provide a base case. Coculture experiments and 3D experiments were performed to determine whether these conditions would promote cell-cell communication similar to *in vivo* conditions, yielding metabolic and functionality results similar to clinical data. Coculture experiments were performed with Liver Sinusoidal Endothelial Cells (LSEC) and Human Umbilical Vein Endothelial Cells (HUVEC) to determine whether the endothelial cell source affected results. Reorganization of cells in culture was observed in 2D. In 3D, multiple methods were used to validate that cells were distributed in all dimensions. Assessment of hepatocyte viability was comparable across all experimental setups and cultures, and HUVEC demonstrated higher viability than LSEC in both 2D and 3D cultures. Protein secretion was comparable for 2D and 3D within respective cultures until Day 9 (post dosing). 3D coculture with HUVEC yielded an APAP consumption profile that more closely matched simulation and thus clinical data. The trend for APAP-sulfate production was observed in simulation and experimental metabolic profiles. APAP-glucuronide production in experimentation did not match well with simulation, indicating that the

glucuronidation pathway in HepG2 cells is less active than primary hepatocytes *in vivo*. Enzymatic activity for CYP3A4 was higher in coculture with HUVEC for 2D and 3D cultures. HepG2 tissue culture models demonstrated sensitivity to the endothelial cell line used.

1.3 Aim 3: Create a tissue culture environment mimicking simulated geometry to investigate differences in hepatocyte behavior using a terminally differentiated cell line (HepaRG) and varying culture techniques (monoculture versus coculture with endothelial cells and 2D versus 3D).

HepaRG is a terminally differentiated hepatocarcinoma cell line with reportedly higher enzymatic activity and the ability to maintain cell functions for longer periods of time, relative to HepG2. A major difference between HepG2 and HepaRG is that HepaRG line does not proliferate. The same analyses were performed in Aim 2 and 3 for comparison purposes. Reorganization of hepatocytes and endothelial cells, both LSEC and HUVEC, was again observed in all 2D cultures. Endothelial cells were observed to attach in and around established HepaRG colonies, suggesting cell-cell communication. Morphological changes were observed in HepaRG cells between Day 1 to Day 3, in agreement with previously reported occurrences of the formation of bile canaliculi. For both monoculture and cocultures, cells were confirmed to be distributed in 3D. Hepatocyte viability was comparable with initial seeding for 3D monoculture and 2D and 3D cocultures with LSEC. Endothelial cell viability was comparable for both cell lines for the same dimensionality; however, 3D cocultures yielded higher endothelial cell viability compared with 2D. Protein secretion was comparable for 2D and 3D in the respective cultures throughout culturing. 3D coculture with LSEC yielded an APAP conversion profile that closely matched simulation. The trend for APAP-sulfate production was observed in simulation and experimental metabolic profiles. APAP-glucuronide production in experimentation did not match well with simulation; however, production was increased compared with HepG2 profiles. Enzymatic activity for CYP3A4 was higher in coculture

with HUVEC for 2D and 3D cultures. HepaRG tissue culture models also demonstrated sensitivity to the endothelial cell line used.

1.4 Summary

The overall objective of this project was to create a drug development, tissue culture platform for which metabolic and hepatic function data could be validated by comparison against clinical data. A number of obstacles were addressed in order to create this method of validation. Numerous tissue culture techniques have been investigated, but with the abundance of cell lines and experimental conditions to choose from, cross-comparison testing and selection of the best predictive platform is difficult. A method of bridging the gap between experimental and clinical results was achieved through the creation of a computational model. The developed computational model allowed for scaling between high-throughput screening conditions to those more physiologically relevant. With a method for connecting experimental and clinical results in place, a tissue culture platform needed to be selected. Multiple tissue culture techniques were performed for comparison under similar conditions using the commonly used HepG2 cell line. Coculture experiments were performed with an endothelial cell line that was native to the liver, and one that was not, to determine if the source of the non-metabolizing cell line affected results. Metabolic distribution and liver specific function data were compared with clinical data to evaluate each tissue culture model's ability to predict clinical data. Investigation of a second hepatocyte cell line was performed to determine whether use of the terminally differentiated cell line (HepaRG), rather than an immortal one (HepG2), would impact results. Again, evaluation of the effect of a native versus non-native endothelial cell line for coculture was performed. The same metabolic and functional analyses performed for HepG2 models were repeated with HepaRG models. Further validation of this methodology using other drugs is necessary, and if successful, would indicate potential for use in predicting the human response to newly developed medications.

CHAPTER II

BACKGROUND

2.1 Drug Development Process Deficiencies

Medications and treatments are developed through a series of controlled trials in which the efficacy and toxicity of a drug are analyzed. The drug development process is comprised of two major components: preclinical testing and clinical trials (**Figure 2.1**). At the preclinical phase, laboratory and animal studies are used to assess drug safety and biological activity. In clinical trials the drug is introduced to humans for expansion of safety profiles, determination of dosing, and evaluation of efficacy - first in healthy individuals, followed by intended patient populations. There are two FDA "check points" prior to major advancement of the drug. Drugs that make it to market are still monitored for an additional 11 – 14 years for long-term adverse effects [7]. Though entities like the FDA perform rigorous analysis at major advancement points throughout the process, some unsafe drugs still make it to market.

The drug development process is incredibly time and cost intensive. Development of a successful drug takes an average of 12 years [7], reaching an estimated cost of $2.6 billion when considering

time costs (expected returns that investors forego while a drug is in development) and post approval study costs, in addition to average out-of-pocket expenditures [8]. Failures at later phases of the drug development process are extremely costly and contribute significantly to increasing the cost of successfully developed drugs. The process is also very inefficient, considering that only 8% of the drugs that enter the preclinical stage actually make it to market. Additionally, some medications are withdrawn from the market even after FDA approval.

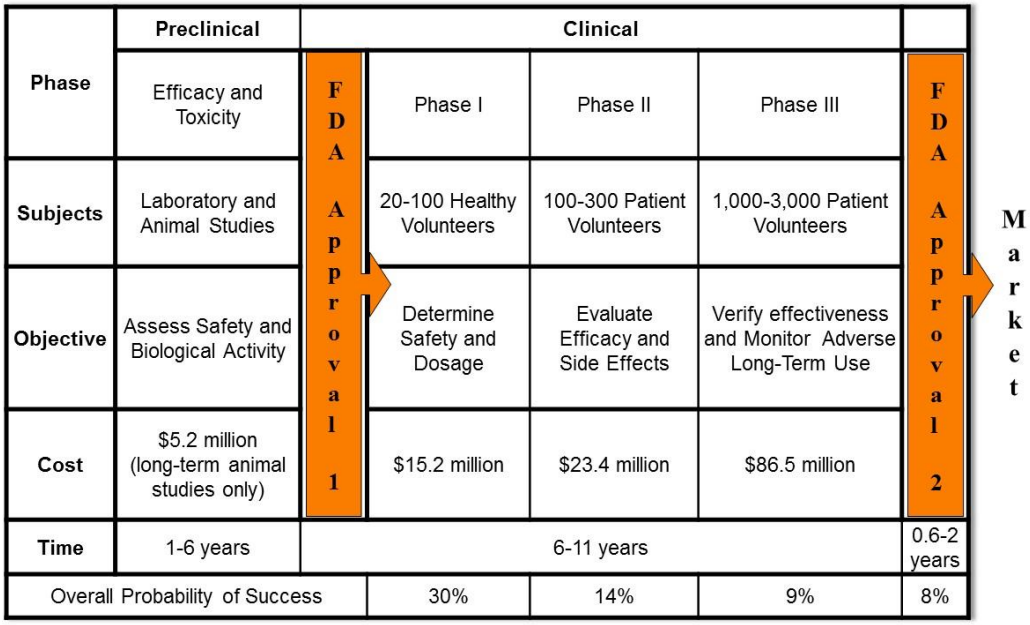

Figure 2.1: Drug development process timeline

Due to the inability to change clinical trial data acquisition methods, validation/alteration/optimization of preclinical testing methods provides the greatest potential for improving efficiency of the overall process. As evidence, out of all drugs studied at the preclinical level, approximately 70% fail to meet requirements to move on to human trials, and over half of those that make it to phase I clinical trials do not make it to phase II. The lack of accurate and predictive preclinical testing methods needs to be addressed. Improvement of knowledge and screening methods at the preclinical phase would increase safety in clinical trials

and efficiency of the entire process, decreasing industry and consumer expenses.

2.2 Preclinical Drug Screening

The primary goal of preclinical testing is to determine and evaluate human toxicity. One of the most important organ systems for determining toxicity is the liver, as it is the metabolic hub of the body. As further evidence, over 900 drugs, toxins, and herbs have been reported to cause hepatotoxicity. Drug-induced hepatic injury is the most common reason for withdrawal of a market-approved drug [9]. Preclinical hepatotoxicity is assessed *in vivo* using animal models and *in vitro*/*ex vivo* using human or animal organ slices or cell cultures.

2.2.1 Animal Models

Currently, the primary method for evaluating preclinical hepatotoxicity is animal testing [10]. Animal models are used to determine pharmacokinetic [11] and pharmacodynamics (PD) data for a specific drug. Animal models are advantageous in the fact that they provide results without harming patients and are readily available. The major issue with using animals in drug screening is cross species variation. Enzyme levels and activities differ from individual to individual and certainly differ between species. The argument over animal model predictability has gone on for decades. While animal models can be useful in gathering initial information, studies have shown that predictability is only around 50% [12-15]. The employment of animal models to determine drug safety and efficacy allows room for unsafe drugs to get to human trials, as well as eliminates drugs that could have possibly been safe and effective in treating human maladies. While animal models are necessary, models that more closely mimic the human body and improve prediction of human responses must be included in preclinical studies.

Methods circumventing primary dependence on cross species models would aide in increasing predictability of human response at the preclinical level. Use of human cells, tissue, or organ

slices for *in vitro* analysis of the human response would provide more accurate data without threatening human life.

2.2.2 Cell Culture Models

Due to the large expense of evaluating hepatotoxicity at the whole body level and the lack of readily available human organ slices, numerous less complex hepatocyte culture systems have been investigated [16, 17]. A wide assortment of devices and environments from static to flow-through, two-dimensional (2D) and three-dimensional (3D) cultures, and multiple culture techniques, including cell aggregation, cell suspension, and monolayer cultures have been investigated [18-23].

Three dimensional cell culture systems are preferred to 2D culture systems because 3D cultures require less area to seed more cells [17]. Also, 3D cultures provide necessary architectural structure, avoid exposure limitations due to cell-to-surface adhesion, and are shown to behave more organotypically, all of which cause major limitations for the application of 2D culturing systems in drug toxicity testing [24]. While 3D systems are preferred, they are not easy to maintain. Investigations of a variety of 3D systems have been performed. Cell suspension systems are not restricted to a flat surface and allow for an increase in cell count. However, the culture volume to surface area ratio is increased to a level at which adequate gas exchange is hindered (usually 0.2–0.5 mL/cm^2), and the medium requires agitation to adequately distribute nutrients throughout the system, which can result in cell death due to shear stress [25]. Aggregate systems or spheroids, a clump of many cells, encounter issues with uniform distribution of nutrients, where cells located closer to the center of the aggregate are deprived of the nutrient level necessary to survive [26, 27]. Recent advances in tissue culturing techniques have led to the development of porous structures from various sources, including Matrigel® obtained from a

mouse sarcoma [28]. Cell culture or tissue engineering using 3D porous, biodegradable scaffolds for use in drug development is an area with significant potential. This method provides results without causing harm to patients and could be made available on-demand, as a number of different cell lines have been immortalized, cryopreserved, and are commercially available.

Efforts to obtain more appropriate results, similar to the human body, in drug metabolism and toxicity studies, have led to investigation and development of multiple cell lines of the same cell type and environmental optimization. For example, there are many commercially available selections of human hepatocytes including primary, carcinogenic (i.e. HepG2), and terminally differentiated (HepaRG) cell lines. With so many choices available, one must consider which cell line will provide results that most closely mimic the human response for a particular study. Comparison of experimental results is often difficult due to setup and condition differences between laboratories. For example, analysis can be performed using whole liver cells or liver microsomes, subcellular fractions containing membrane bound drug metabolizing enzymes. As a result, numerous source and method combinations are available for hepatotoxicity assessment. Each preparation could yield different results, making cross-testing comparisons difficult.

2.3 Computational Modeling of Pharmacokinetics/Pharmacodynamics

There has been an immense interest in screening therapeutic agents *in silico* with the intent of reducing cost and time investments, while improving the success rate of candidate drugs. A variety of PKPD models and physiologically-based PK (PBPK) models have been developed using compartmental modeling and physiological observations at the whole body level. These models range from the molecular to whole body level. At the molecular level, significant research has been performed to investigate the effect of xenobiotic binding on cellular protein structures. PBPK models, such as SimCYP, MoBi, and GastroPlus, can be useful to predict the generic behavior of a drug *a prior* at the whole body-level, while providing the flexibility to

customize population distribution of factors like age and gender [29].

While these computational models characterize behavior at the smallest and largest levels, there is a need for intermediate mathematical models. Thus, interest in developing computational PKPD models for specific organ systems has increased in recent years. In terms of liver metabolism, many of these models employ grouped kinetics which ignore enzyme specific mechanisms which, in some cases, can yield very different results [30]. With the rise of tissue engineered constructs, there is a demand for data validation methods. These constructs can provide important PKPD data for a specific drug, but there is currently no method for determining the validity of that data by connecting to clinical data. Validation of a methodology using computational modeling to bridge the gap between tissue engineered constructs and the human response at the whole body-level would indicate potential predictive capabilities.

2.4 Employing a Cyclical Testing and Validation Approach

Data and information on metabolism and toxic pathways can be found in a number of published papers concerning clinical trials, animal work, cell culture, and simulation. Unfortunately, even with all of this data and information available, investigation of how the information from the three different prongs of drug research computational modeling, experimental work, and clinical data - have yet to all be compared and evaluated for appropriateness (**Figure 2.2**). There is also a lack of reliable parameters and validation experiments.

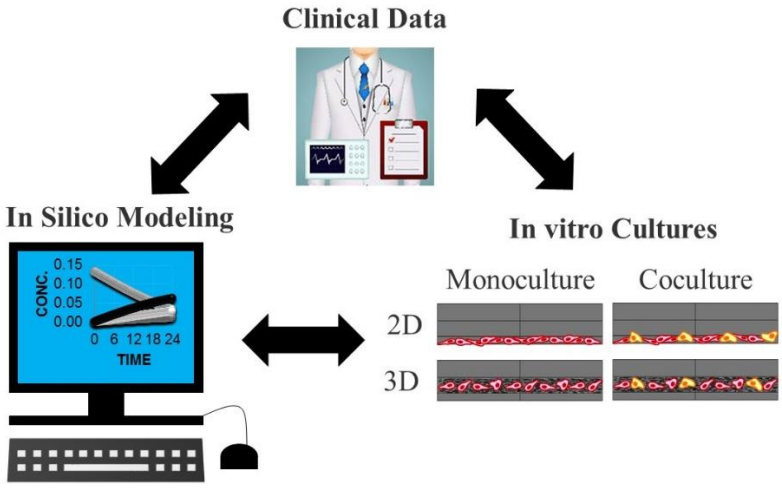

Figure 2.2: Cyclical testing and validation strategy to preclinical drug screening

Comparison of data from these different areas would help promote a "Learn and Confirm" testing methodology resulting in safer and more effective clinical trials.

2.5 Using Acetaminophen as a Case Study

APAP, an analgesic used to treat headaches, arthritis, and a wide assortment of other pain related ailments, as well as to reduce fever, is one the most widely used drugs in the world. Due to APAP's ability to treat a wide array of maladies and the ease of its acquisition, a high degree of misuse and overdose are associated with this drug. As a result, there is a significant amount of research and data pertaining to APAP metabolism. APAP is metabolized in the liver by hepatic enzymes via three different pathways (**Figure 2.3**). The bioactivation pathway is an oxidation pathway by which many toxic metabolites are produced. In the case of APAP, bioactivation produces N-acetyl-p-benzoquinone imine (NAPQI) via Cytochrome P450 (CYP) enzymes [31-33]. Normally, toxic NAPQI is quickly conjugated with glutathione, promoting bodily excretion. However, during APAP overdose, glutathione reserves in the body are depleted, leading to NAPQI buildup [34], which can cause hepatotoxicity.

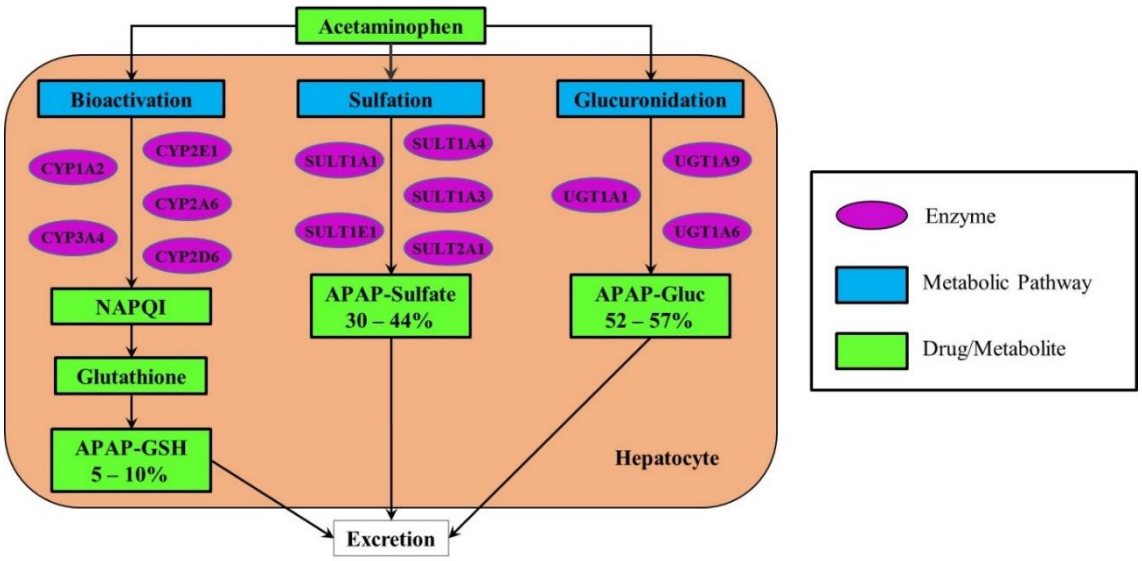

Figure 2.3: APAP hepatic metabolic pathways

The other two pathways, sulfation and glucuronidation, are detoxifying pathways. They produce self-named, conjugated metabolites that are easier to eliminate from the body. Glucuronidation produces APAP-Glucuronide via UDP-glucuronosyl transferase enzymes (UGT), and sulfation produces APAP-Sulfate via sulfotransferase enzymes (SULT) [35]. APAP and metabolites are eliminated from the body primarily via renal or urinary excretion.

Despite the clinical [36-39], experimental [40, 41], and simulation [11, 42, 43] research that has been performed, APAP overdose remains a leading cause of acute liver injury. APAP toxicities in the US alone have led to 56,000 emergency room visits, 26,000 hospital admissions, and nearly 500 deaths annually [44]. In fact, APAP would most likely not receive FDA approval by today's standards [45]. Understanding APAP metabolic events in vitro in less complex settings has not been possible due to i) the limitation of available organoid models, particularly 3D configuration mimicking *in vivo* architecture of the liver, and ii) lack of *in silico* comparable models for validation of *in vitro* synthetic tissues based on the available clinical data.

CHAPTER III

COMBINING PHARMACOKINETICS WITH ENZYME ISOFORM CONTRIBUTIONS IN 3D SYNTHETIC CULTURE SYSTEMS TO VALIDATE WITH CLINICAL DATA: USING ACETAMINOPHEN AS A CASE STUDY

3.1 INTRODUCTION

There has been an immense interest in screening therapeutic agents *in silico* with the intent of reducing the cost and time while improving the success rate of candidate drugs. A variety of pharmacokinetic and pharmacodynamics (PKPD) models and physiologically-based PK (PBPK) models have been developed using compartmental modeling and physiological observations at the whole body level. PBPK models, such as SimCYP, MoBi, and GastroPlus, can be useful to predict the generic behavior of a drug *a prior* at the whole body-level, while providing the flexibility to customize population distribution factors like age and gender [29]. However, drug-induced hepatotoxicity is the most common reason for the after-market withdrawal of a drug, despite effectiveness in treating a disease [46]. For example, acetaminophen overdose remains a leading cause of acute liver injury [47], despite many simulation studies using

SimCYP [42]. APAP toxicities in the US alone have led to 56,000 emergency room visits, 26,000 hospital admissions, and nearly 500 deaths annually [44]. Understanding APAP metabolic events in vitro in less complex settings has not been possible due to i) the limitation of available organoid models, particularly in 3D configuration mimicking in vivo architecture of the liver, and ii) in silico comparable models for validation of in vitro synthetic tissues based on the available clinical data.

There has been a significant development in generating 3D synthetic tissues using various techniques [48]. Three-dimensional systems provide a new integrative level, which is a complex environment where cells can interact, create cellular networks, and extend processes. Many synthetic tissues are developed based on the fundamental understanding that cell-cell and cell-matrix interactions in 3D systems are crucial to integrate the extensive signaling pathways, and the biophysics that regulate the development and regeneration of tissues. Cell-cell interactions between hepatocytes and non-parenchymal cells alter the functionality of hepatocytes [49], prolonging CYP-450 activity and albumin production. Novel bioprinting technology is emerging, allowing users to spatially locate multiple cell types in a desired configuration [50]. However, there is a lack of *in silico* models that help predict the overall metabolic product distribution within synthetic tissues.

In this regard, a computational fluid dynamic (CFD) approach was used to test APAP metabolism in configurations routinely used in 3D synthetic tissue cultures. A major advantage of CFD is that one could obtain concentration profiles across 3D structure in widely explored static cultures. This simulation approach has been extensively used in modeling fluid flow through porous medium, and validated using experimental results [51]. Our group has reported and validated various reactive systems by comparing CFD models with experimental results using HepG2 cells [52-54]. Here, the fact that drug metabolism within the whole liver tissue occurs simultaneously

was considered. Nearly 55% of APAP metabolism is formation of non-toxic APAP-Glucuronide (APAP-Gluc) via glucuronidation, which is mediated by UDP-glucuronosyltransferases (UGT's). Sulfation accounts for 30% of APAP metabolism into non-toxic APAP-Sulfate mediated by Sulfotransferases (SULT's). Remaining APAP is oxidized via bioactivation by the CYP450 family of enzymes to form the hepatotoxin, N-acetyl-p-benzoquinone imine (NAPQI). NAPQI is then conjugated glutathione (GSH) to form the nontoxic metabolite, APAP-GSH. Hepatotoxicity occurs when GSH is depleted and NAPQI builds up [34]. Abundance of these isoforms in hepatocytes has been analyzed, showing that some isoforms, such as CYP1A2, may be abundant, but their contribution to metabolism is low [55]. Also, some isoforms may be present in relatively small quantities, such as CYP2A6, but their contribution to metabolism is high [56]. In this study, static culture dimensions mimicking in vitro 3D cell culture experiments were simulated to show that this modeling approach is useful in linking pharmacokinetic parameters obtained *in vitro* to clinical metabolic profiles.

3.2 METHODOLOGY

3.2.1 Simulation Geometry

Using the dimensions of commercially available 24 and 96-well plates, a discoid-shaped, static culture was simulated (**Figure 3.1**). In order to incorporate the 3D configuration of cells in culture, a porous scaffold region was simulated. The scaffold region was given the same diameter as the culture plates and 1 mm thickness. The scaffold was elevated 0.5 mm above the bottom of the well, as previous simulations demonstrated physical diffusion limitations with scaffold placement directly on the well bottom [57].

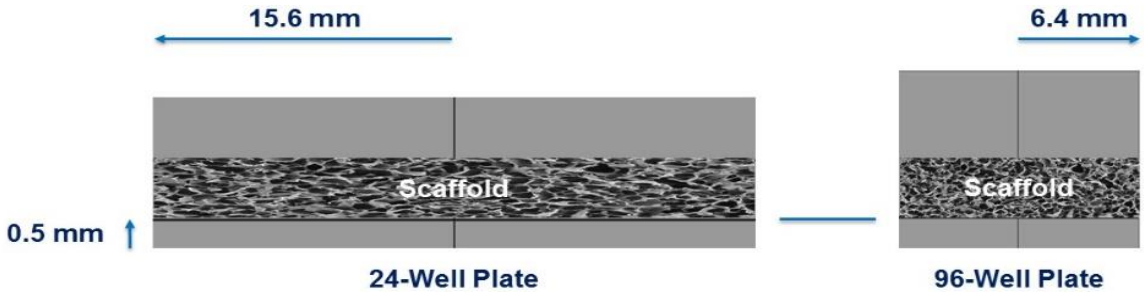

Figure 3.1: Schematic showing culture dimensions simulated in CFD. (Scaffold corresponds to the region where cells are assumed to be present)

The selection of 1 mm thick scaffolds was used for standardization and to ensure nutrient diffusion in and out of the porous scaffold was not a limitation. Working volumes of 500 µL for the 24-well plate and 100 µL for the 96-well plate were based on vendor suggested working volumes. These values were used to calculate the media height of 2.62 mm and 3.11 mm, respectively.

The 3D disc-shaped geometry was generated in COMSOL Multiphysics 5.2, (COMSOL, Inc., Burlington, MA) using 2D geometry and assuming axis symmetry, similar to previous publications [58]. A free tetrahedral mesh with a maximum element size of 0.5 mm and a minimum element size of 0.2 mm was used, resulting in a total of 260,731 nodes. A grid test was performed, decreasing the maximum element size by half and doubling the number of nodes. The percent difference in the volume average concentration was 0.016%, which indicated mesh quality to be sufficient so as not to affect results. A time step size of 120 seconds was used. Physical properties (density and viscosity) of the growth medium used for culturing cells were assumed to be that of water at 37°C. Scaffold porosity was assumed to remain constant at 85% based on the porosity of freeze-dried, chitosan-gelatin scaffolds which have been extensively evaluated in recreating 3D hepatic cultures [52, 53, 58]. Diffusivity values in both the porous and nonporous regions were assumed to be constant and isotropic. Free diffusivity of APAP through

the nonporous region was obtained from literature [59], while APAP's effective diffusivity through the porous region was calculated through interpolation, based on pore size of the scaffold, from literature [58].

3.2.2 Modeling Strategy

Mathematical equations were determined for characterization of APAP uptake, metabolite production, and molecular transport. A mass balance, Fick's law of diffusion, and a reaction rate term were combined to evaluate time dependent changes in concentration for the porous scaffold region in a constant volume, static bioreactor yielding

$$\frac{\partial C_i}{\partial t} = D_i \nabla^2 C_i + r_i \qquad (1)$$

where $\frac{\partial C_i}{\partial t}$ is the change in concentration of species *i* over time, D_i is the effective diffusivity constant for molecule *i* in water, $\nabla^2 C_i$ is the second order gradient along each of the major dimensions in the system, r_i is the rate of consumption or production depending on the species, and *i*, is the species being evaluated. In the non-porous region, the reaction rate term from Equation 1 is zero. An assumption of no mass flux occurring at the bottom (z = 0), walls (r =R), and atmosphere interface (z = 2.62 or 3.11 mm) was applied. The initial dose of APAP was used to set the initial condition for time dependent concentration. The interface between porous and non-porous regions was considered continuous. The COMSOL physics module, *Transport of a Diluted Species*, was selected to simulate Equation 1. The rate of APAP consumption and rate of production of APAP metabolites were assumed to be characterized by Michaelis-Menten kinetics [35, 60, 61]

$$\pm r_i = \frac{V_m C_i}{K_m + C_i} \tag{2}$$

where V_m is the maximum uptake or production rate of species i, C_i is the species concentration, and K_m is the Michaelis-Menten constant. Equations 1 and 2 were used due to previous success in characterizing urea production in HepG2 cell culture [57].

The rate of APAP bioactivation was input into simulation by two different methods: individually per CYP 450 enzyme, and as a grouped sum for K_m and V_m. Reaction rate constants employed are listed in **Table 3.1** by specific enzyme along with the reference. The reaction rate equation for individualized APAP bioactivation enzyme activity is

$$-r_i = \frac{V_{m1A2} C_i}{K_{m1A2} + C_i} + \frac{V_{m3A4} C_i}{K_{m3A4} + C_i} + \frac{V_{m2E`} C_i}{K_{m2E1} + C_i} + \frac{V_{m2A6} C_i}{K_{m2A6} + C_i} + \frac{V_{m2D6} C_i}{K_{m2D6} + C_i} \tag{3}$$

Where the subscripts for V_m and K_m identify kinetic constants related to specific CYP 450 enzymes (i.e. V_m for CYP3A4 is given as V_{m3A4}). Instead of assuming all CYP enzymes contribute to APAP metabolism completely, one could assume individual CYP enzymes contribute to metabolism partially, based on involvement in drug metabolism or abundance in the hepatocyte. Contribution probability of CYP enzymes based on their involvement in drug metabolism [55] was analyzed first.

Table 3.1: Kinetic constants and enzyme abundance and contribution data

Metabolic Pathway	Active Enzyme	K_m (µM)	x (% Contribution)	x (% abundance)	Vmax (pmol/min/mg microsomal protein)
Bioactivation	CYP 3A4/5 [31]	313	50.0 [55]	53.6 [62]	52
	CYP 2D6 [33]	1760	2.3 [55]	7.10 [62]	1298.6
	CYP 2A6 [32]	4600	34.9	3.60 [62]	3397
	CYP 2E1 [31]	1260	5.80	12.5 [62]	536
	CYP 1A2 [31]	3440	7.00	23.2 [62]	119
Glucuronidation	UGT 1A1 [63]	9400		18.6 [64]	1300
	UGT 1A6 [63]	2200		59.3 [64]	100
	UGT 1A9 [63]	20900		22.1 [64]	6300
					Vmax (mmol/h/kg body weight)
Sulfation	[35]	97		100	0.011
Glucuronidation	[35]	6890		100	0.968

Percentage contributions (x) were incorporated into the simulation using the equation

$$-r_i = x_1 \frac{V_{m1A2} C_i}{K_{m1A2} + C_i} + x_2 \frac{V_{m3A4} C_i}{K_{m3A4} + C_i} + x_3 \frac{V_{m2E} C_i}{K_{m2E1} + C_i} + x_4 \frac{V_{m2A6} C_i}{K_{m2A6} + C_i} + x_5 \frac{V_{m2D6} C_i}{K_{m2D6} + C_i} \quad (4)$$

where individual x_j values correspond to the activity contributions from that CYP isoform "*j*" from **Table 3.1**. Alternatively, analysis using the abundance of each CYP isoform and with Equation 4, but different values for x_j, shown in **Table 3.1** [50] was performed. Grouping constants and expressing as a single rate law was also considered

$$-r_i = \frac{\left(V_{m1A2} + V_{m3A4} + V_{m2E1} + V_{m2A6} + V_{m2D6}\right)C_i}{\left(K_{m1A2} + K_{m3A4} + K_{m2E1} + K_{m2A6} + K_{m2D6}\right) + C_i} \tag{5}$$

Initial APAP concentration was calculated based on the reported safe to toxic (commonly used in *in vitro* studies) range of adult doses [65] and the number of hepatocytes in an adult liver. The widely recommended, maximum clinical dose was 20 mg/kg [66]. For a 50 kg patient, the dose corresponds to a 1000 mg single dose, the most commonly recommended single, maximum APAP dose. Using the number of hepatocyte cells per gram of human liver, the average liver weight per kg body weight, and the cell density, the clinical dose was equivalent to 5.95 mg/L. Initial simulations were performed using this dosage. APAP was considered to be homogeneously distributed throughout the system at time t=0. The K_m and V_m values for each metabolic pathway were summed or "grouped" into one value to give a total contribution to metabolism. An initial cell density of 1.2×10^{12} cells/m^3 was used in simulation. To account for cell growth, a 24 hour doubling time was assumed, based on a broad range of reported average doubling times [67-69]. The following differential equation was used to determine the change in the number of cells, dN, in the scaffold over time,

$$\frac{dN}{dt} = \mu N_0 \tag{6}$$

where μ is the specific growth rate constant and N_0 represents the initial number of cells seeded in the scaffold. An analytic function was used to vary the kinetic constant V_m, with respect to the

increase in cell number over time. The initial number of cells in the scaffold was calculated based on the cell density and the calculated volume of the scaffold.

APAP metabolism was simulated for a 24 hour time period, for clinical data comparison purposes [70]. A time-dependent, fully-coupled, iterative, Generalized Minimal Residual solver (GMRES) [71] was used to simultaneously solve the governing equations at node points throughout the 3D geometry. The selected solver and method for determining mesh quality was used due to previous successful use in characterizing urea synthesis [57]. APAP conversion was calculated at various time points to create a transient profile using

$$\text{APAP Conversion} = 1 - \frac{C_{APAP} \text{ at time t}}{C_{APAP} \text{ at time t} = 0} \tag{7}$$

Generated profiles are independent of initial dosage and cell number, making them comparable with clinical data at any specific time. Further, concentration of each metabolite was used to calculate the yield using the expression

$$\%Yield = \frac{C_i}{\sum C_{\text{other metabolites}}} * 100 \tag{8}$$

where C_i is the concentration of the metabolite yield being calculated.

3.3 RESULTS

3.3.1 Converting the Kinetic Constants to a Standard Form

In order to understand the metabolism of therapeutic agents by hepatocytes, various techniques have been utilized. Specific pharmacokinetic constants involved in liver metabolism are determined using hepatocytes, although the origin of hepatocytes varies from primary cells to hepatocarcinoma cell lines. Some studies even utilize liver microsomes, particularly when the

primary metabolic enzymes of interest are CYPs. In order to compare various pathways, one has to express these constants on a basis that is convenient to relate to the total liver and to clinical data. In this regard, pharmacokinetic constants obtained using liver microsomes were converted to a per cell density used in the *in vitro* cell cultures basis. For this purpose, microsomally obtained kinetic constants (for V_{max} only, as K_m is not affected by cell count) were converted using the microsomal protein content per gram of human liver and the number of hepatocytes per gram of human liver (**Table 3.2**). Use of conversion parameters helped in comparing simulated results to clinical data.

Table 3.2: Parameters for the liver

Number of hepatocytes in adult human liver [72]	139×10^{6} cells/g liver
Mean liver weight	1561 g
Liver weight (males) [73]	20 g/kg body weight
Human microsomal protein [73]	45mg/g liver
Total P450 Concentration (Caucasians) [56]	0.43 nmol/mg protein
Diffusivity (D_e)	2.22×10^{-10} m^2/s
Partition Coefficient (P_A)	0.79
Hepatocyte Wall Thickness (δ)	4×10^{-9} m
Cell Radius (R)	11.2×10^{-6} m
Hepatocyte Volume (V_{cell})	5.88×10^{-15} m^3 *
Time Interval (Δt)	300 s

*Hepatocyte surface area and volume were calculated assuming spherical shape using the radius

3.3.2 Effect of Individualized Bioactivation Reaction Rate Constants

Many have reported various CYPs playing a role in bioactivation of APAP. APAP bioactivation reaction rate constants have been extensively characterized by isoform (**Table 3.1**), while APAP glucuronidation and APAP sulfation rate constants are more commonly reported on a grouped enzyme basis. In order to understand the effect of these rates on the total products formed, simulations were performed using individual rate constants and Equation 3 for each CYP isoform,

to obtain metabolic profiles. Individualized reaction rate results showed that nearly 93% of APAP was converted after 24 h, and the yield of APAP-GSH was 31% (**Figure 3.2**). Also, APAP-Sulfate comprised 19% of the distribution, while that of APAP-Gluc was 39%.

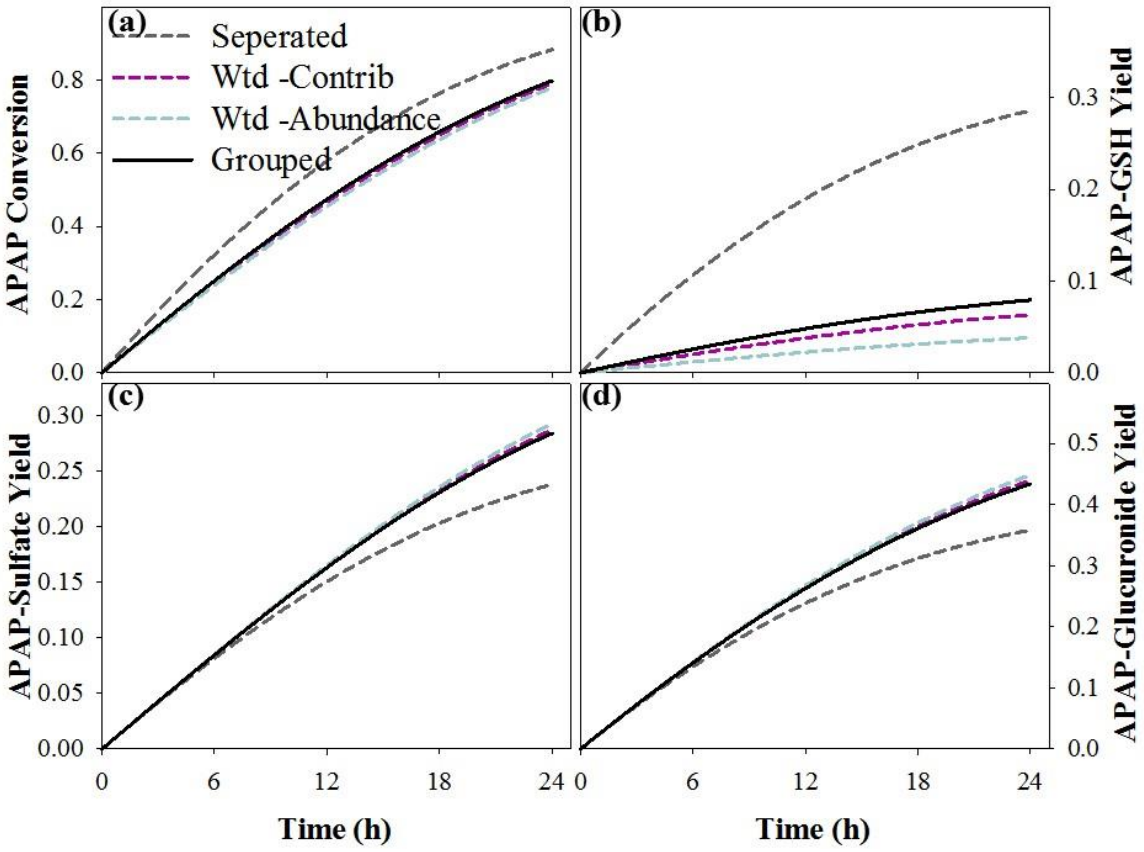

Figure 3.2: Effect of reaction rates on the metabolic profiles with a dosage of 5.95 mg/L in different well configurations: (a) APAP conversion, (b) yield of APAP-GSH, (c) yield of APAP-Sulfate, and (d) yield of APAP-Glucuronide

When percentage distribution of products and unchanged APAP were compared with clinical data [66] after 24 h (**Figure 3.3**), clinical data showed that only 8% of the metabolic distribution corresponded to APAP-GSH formation. Clinical data also showed APAP-Sulfate composition to be 30%, while that of APAP-Gluc was 55%. Since all reactions were simulated to occur at the

same time, the concentration of APAP-GSH was increasing faster. Further, the other two metabolites were smaller in comparison with clinical data. Distributions of APAP and metabolites at 24 h showed that consideration of APAP bioactivation (**Figure 3.3**) on an individual CYP isoform basis significantly over-predicted APAP-GSH formation when compared with clinical data.

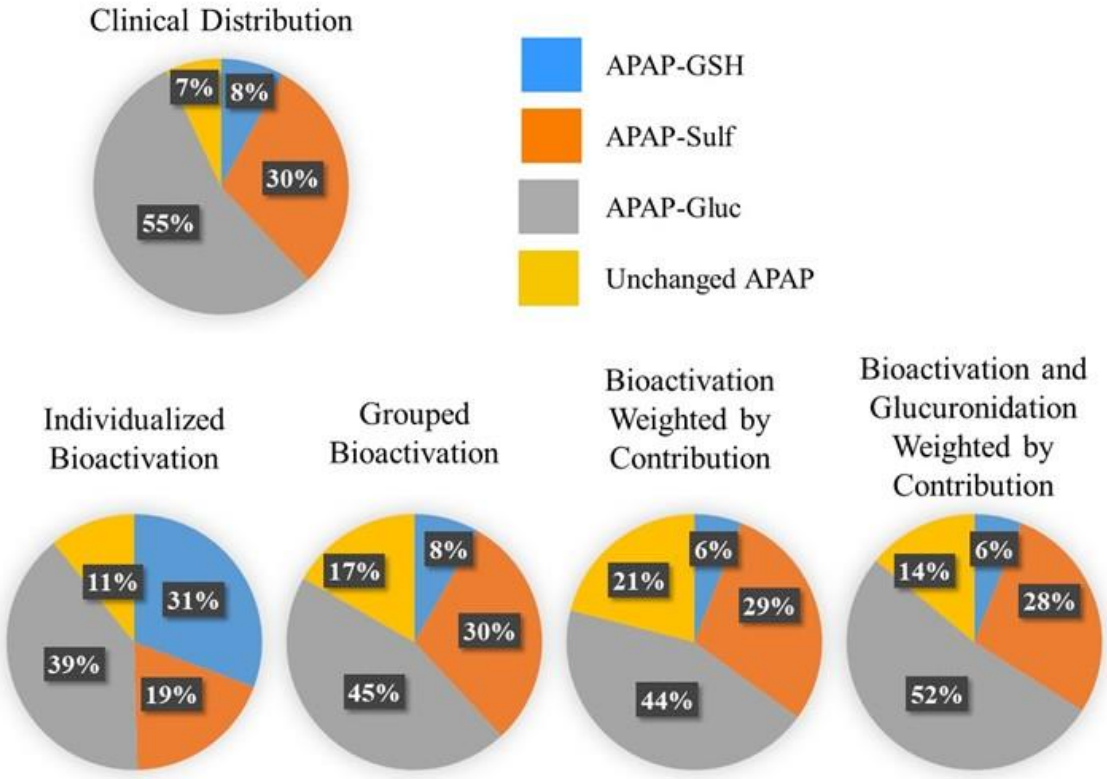

Figure 3.3: Comparison of APAP and metabolites distribution after 24 hours when simulated in a 24-well plate using 5.95 mg/L

This over-prediction may be due to the method by which CYP isoform parameters were obtained, or these pathways could be redundant and only one CYP isoform could be active. In order to test this possibility, one scenario is to consider the dominant CYP2E1 pathway. When simulations were performed with CYP2E1 reaction only, 20.7% APAP remained after 24 h, while the rest of

the distribution was 7% APAP-GSH, 28.6% APAP-Sulfate, and 43.7% APAP-Gluc. This suggested that other CYP isoforms are also contributing, although possibly not independently.

3.3.3 Effect of Incorporating Fractional Contributions

Alternatively, contribution of each CYP isoform could be regulated by the percentage of abundance within the hepatocyte or contribution to metabolic activity. In literature, many of these values have been extensively analyzed due to the critical role of CYP isoforms in drug metabolism. Using those values (**Table 3.1**), simulations were performed in conjunction with Equation 4. These results showed that incorporating the percentage of contribution to activity for each isoform provides a profile in agreement with that reported in the clinical data. This is in line with the understanding that it is not the enzyme abundance, but rather the enzyme activity that is more important in metabolism studies. In the case of activity-based simulation, 21% APAP remained after 24 h, while the rest of the distribution was 6% APAP-GSH, 29% APAP-Sulfate, and 44% APAP-Gluc. Hence, formed APAP-GSH and APAP-Sulfate were similar to clinical data [66]. However, when simulations were performed using CYP isoform abundance, there was an under prediction of APAP-GSH while the other components did not change significantly. Only 3.8% of the distribution was due to APAP-GSH formed, which suggests that CYP 2A6 isoform, which is less in abundance, contributes significantly to APAP-GSH formation. Further, other isoforms which are in abundance contribute less to the formation of APAP-GSH. Nevertheless, formed APAP-Gluc was consistently less than clinical data and corresponded to a greater amount of unconverted APAP. This suggested that the kinetic parameters used for APAP-Gluc could be underestimated by consideration on a total contribution to metabolism basis (**Figure 3.3**). Thus, the glucuronidation pathway was analyzed on an individual, UGT isoform and isoform abundance-weighted basis using the same methodology discussed for bioactivation by CYP isoforms. The kinetic constants for UGT isoforms 1A1, 1A6, and 1A9 as well as their

respective abundance in the liver (**Table 3.1**) were also used in conjunction with Equation 4 in simulation. The resulting metabolic profiles demonstrated complete conversion of APAP to APAP-Gluc within minutes for individualized UGT isoform activities. However, when abundance-weighted UGT isoform activities were used, the distribution of APAP-Gluc formation matched that of clinical results (**Figure 3.3**).

In order to understand whether an algebraic averaging of V_m and K_m for CYP isoforms would provide a reasonable estimate of APAP-GSH formation, simulations were performed using Equation 5. These results showed that formed APAP-GSH was in agreement with that reported in the clinical data (**Figure 3.3**). Since the rate of APAP-GSH formation decreased, compared with individualized reaction rate considerations, this showed improvements in the formation of APAP-Sulfate and APAP-Gluc (**Figure 3.2**).

3.3.4 Effect of Diffusion of Molecules

Since some enzyme activities were evaluated in isolated microsomes or purified form, differences between simulated and clinical data could be due to diffusion being the rate limiting step. In order to understand whether the phenomenon is diffusion limited at the cellular membrane, a material balance was performed around a single cell according to

$$\frac{D_e P_A}{\delta}\left(C_s - C_{cell}\right)A = \frac{C_{cell} V_{cell}}{\Delta t} \tag{9}$$

where D_e is the diffusivity, P_A is the partition coefficient, δ is the cell wall thickness, C_s is the surface concentration of APAP, C_{cell} is the concentration of APAP inside of the cell, A is the surface area of a hepatocyte, V_{cell} is the volume of the cell, and Δt is the time interval for evaluation. Equation 9 was rearranged to solve for C_{cell} yielding

$$C_{cell} = \frac{D_e P_A A C_s}{\delta\left(\frac{V_{cell}}{\Delta t} + \frac{D P_A A}{\delta}\right)} \quad (10)$$

C_{cell} was determined in terms of fraction of C_s. The values listed in **Table 3.2** were used to determine that C_{cell} was $0.999C_s$, indicating that the vast majority of APAP at the cell surface enters the cytoplasm, indicating that APAP metabolism is a reaction rate limited process.

An additional method for determining reaction or diffusion limitation employs the Thiele modulus. For a reaction that follows Michaelis-Menten kinetics, such as those involved in APAP metabolism, the Thiele modulus (φ) is defined as

$$\varphi = \frac{R}{3}\sqrt{\frac{V_{\max}}{K_m D_e}} \quad (11)$$

where R represents the particle or cell radius. The calculated Thiele modulus was significantly less than 1, again suggesting that the process is reaction limited. Hence, the observed difference in the formation of metabolic products and APAP conversion is not due to diffusional limitation. Thus the observed variation in the product formation is attributed to the difference in kinetic parameters.

3.3.5 Effect of Cell Density

While converting many of the kinetic parameters, generalized liver parameters (**Table 3.2**) were used. Also, when individual components of tissue or cells are harvested, there could be loss of some components during the isolation process. Thus, there could be discrepancy in scaling the V_m values to per cell basis. Alterations in cell density also alter V_m for all metabolites, but the K_m value is independent of cell density. In order to understand the effect of cell density on APAP metabolic profiles, simulations were performed a 4, 2, and 0.5 times the initial cell density

(**Figure 3.4**) using "grouped" pharmacokinetic parameters. As expected, increased cell density increased APAP conversion and formation of all metabolites. With 4 times the cell density, less than 1% of APAP remained, with an increase in metabolites; nearly 11% of the distribution was APAP-GSH, while 30% was APAP-Sulfate and 59% was APAP-Gluc. Formation of APAP-Sulfate seemed to be less dependent on the increased cell number compared to the other two metabolites. However, when cell numbers were decreased by one half, 51% of APAP remained, and nearly 6% of the distribution was APAP-GSH, 13% was APAP-Sulfate, and 31% was APAP-Gluc.

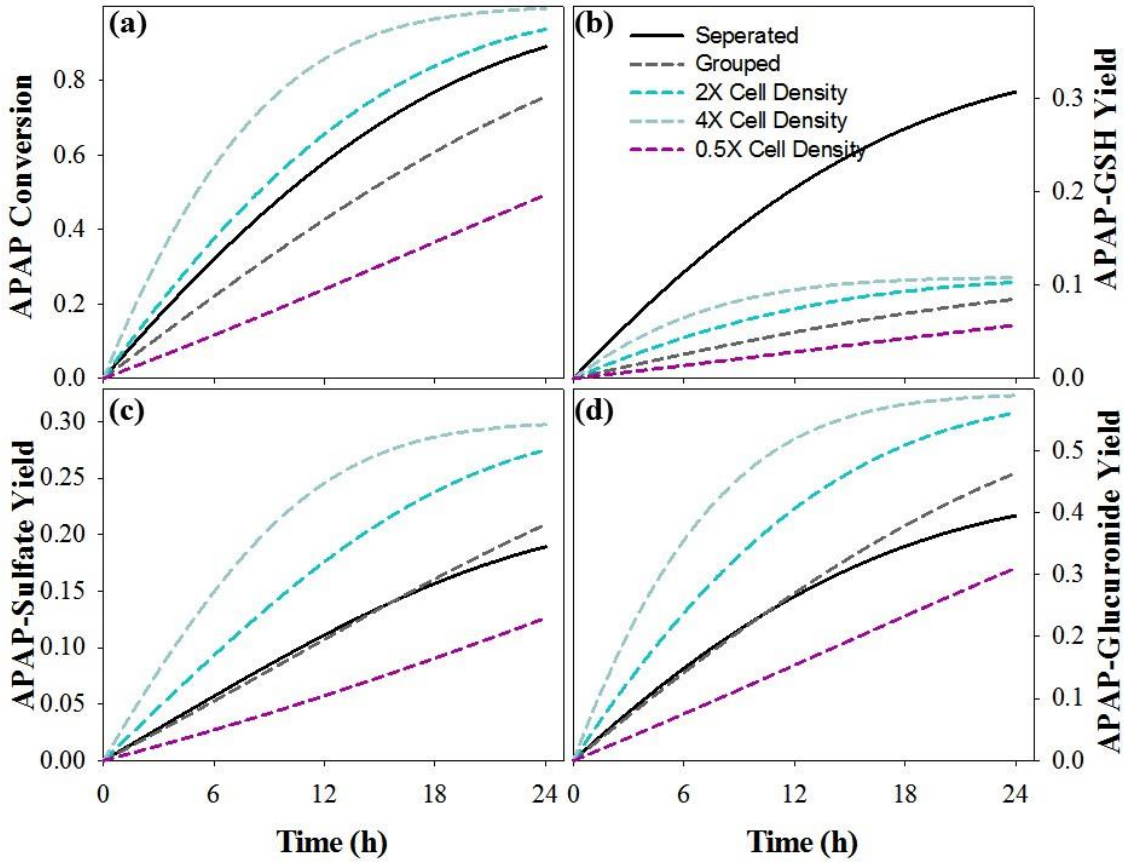

Figure 3.4: Effect of cell density and the reaction rates on the metabolic profiles with a dosage of 20mg/L in a 24-well configuration: (a) APAP conversion, (b) yield of APAP-GSH, (c) yield of APAP-Sulfate, and (d) yield of APAP-Glucuronide

This suggested that reduction in cell number affects the overall conversion of all components, including APAP-Sulfate (**Figure 3.4c**). Cell number to dosage needs to be appropriately accounted for in order to understand the formed metabolic profiles, as some pathways may show dependency at lower cell density. Thus, a higher cell number could account for such variation in the simulation.

3.3.6 Effect of APAP Dosage

Many dosages are used and evaluated in the clinical setting. Hence, observed differences could be attributed to the dosage. In this regard, the sensitivity of product distribution to initial dosage was evaluated. In order to test the effect of initial APAP concentration on metabolic products, simulations were performed and metabolic profiles were examined (**Figure 3.5**). Initial concentrations of 5.95 mg/L and 50 mg/L, equivalent to a highly toxic adult dose, were simulated in a 24-well plate.

With 50 mg/L dosage, nearly 29% of APAP remained, and the rest of the distribution was 9% APAP-GSH, 13% APAP-Sulfate, and 49% APAP-Gluc. At 5 mg/L dosage, less than 20% of APAP remained, and nearly 8% of the remaining distribution was APAP-GSH, while 29% was APAP-Sulfate and 43% was APAP-Gluc. Initial concentration was observed to only effect APAP-Sulfate production.

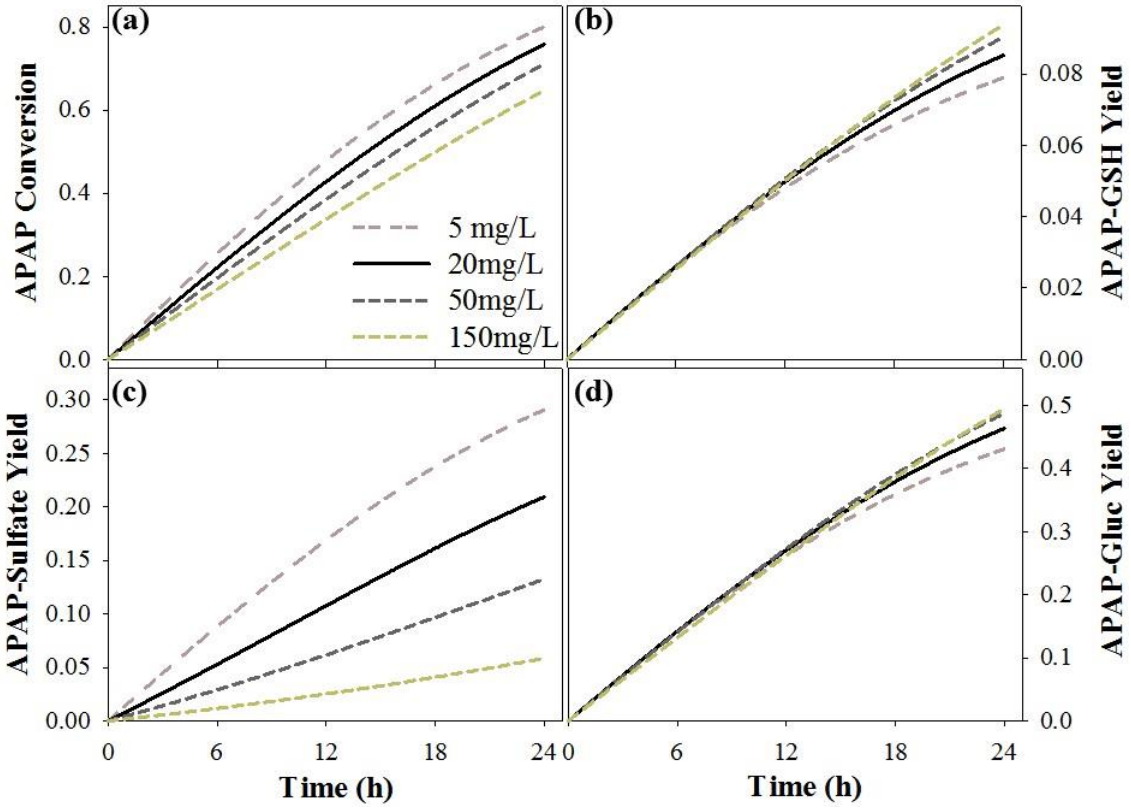

Figure 3.5: Effect of APAP dosage in a 24-well configuration: (a) APAP conversion, (b) yield of APAP-GSH, (c) yield of APAP-Sulfate, and (d) yield of APAP-Glucuronide

When cell cultures are performed, even higher doses were reportedly used due to low metabolism of APAP. In order to test the effect of higher dosage, a 150 mg/L APAP dosage was simulated. Increasing the APAP dosage decreased the conversion (**Figure 3.6a**). Nearly 35% of APAP remained unchanged, while 9% APAP-GSH, 6% APAP-Sulfate, and 49% APAP- Gluc was present at 24 h. This suggests that APAP-Sulfate is very sensitive to initial concentration of APAP relative to the other two metabolites (**Figure 3.6b**). While both APAP-GSH and APAP-Gluc yield increased with dosage, APAP-Sulfate decreased.

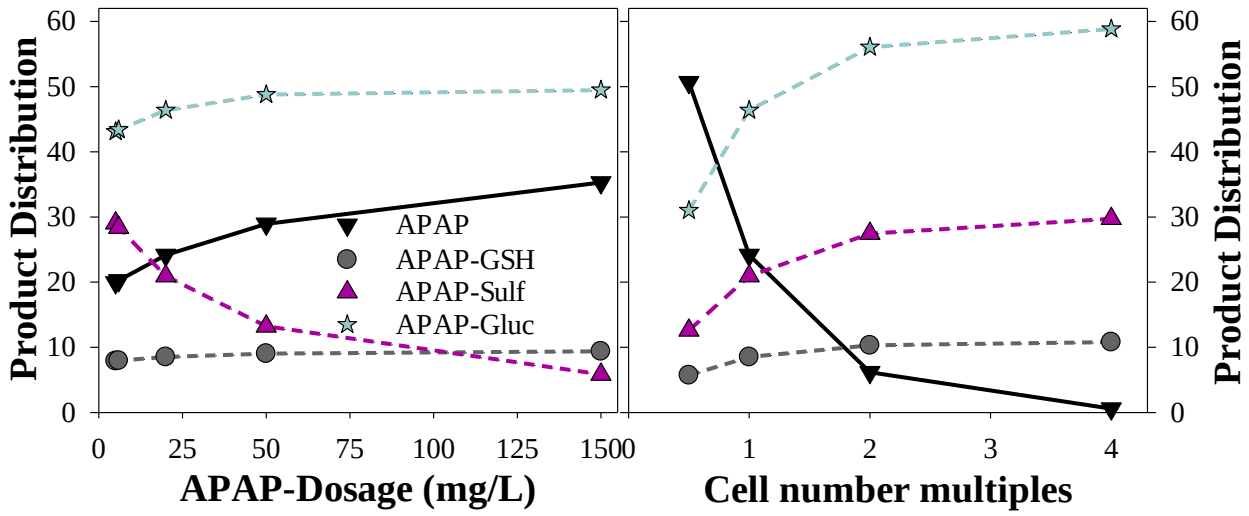

Figure 3.6: Product Distribution at 24-hr in various conditions on different products formed: (a) effect of APAP dosage and (b) cell number effect

Thus when different dosages are used to evaluate the metabolic profiles, different rates than *in vivo* conditions may be observed. APAP-sulfate yield decreased significantly with increased substrate concentration.

There was no significant increase observed for APAP-Gluc or APAP-GSH yield, indicating APAP-sulfate yield decrease was not attributed to increases in the yield of these other two metabolites. APAP-sulfate results are in agreement with previous studies [74-76] demonstrating that the sulfate pathway employs high affinity, not high capacity, enzymes and experiences uncompetitive inhibition resulting in a bypass ordered mechanism.

3.3.7 Effect of Well Size

There is increasing need to develop high throughput screening technologies in drug development. In order to understand how reduced size would affect the metabolic profiles, the same

configuration was tested in a 96-well plate (**Figure 3.7**). Change in well size from that of a 24-well plate to a 96-well plate demonstrated no discernable impact on metabolism of APAP.

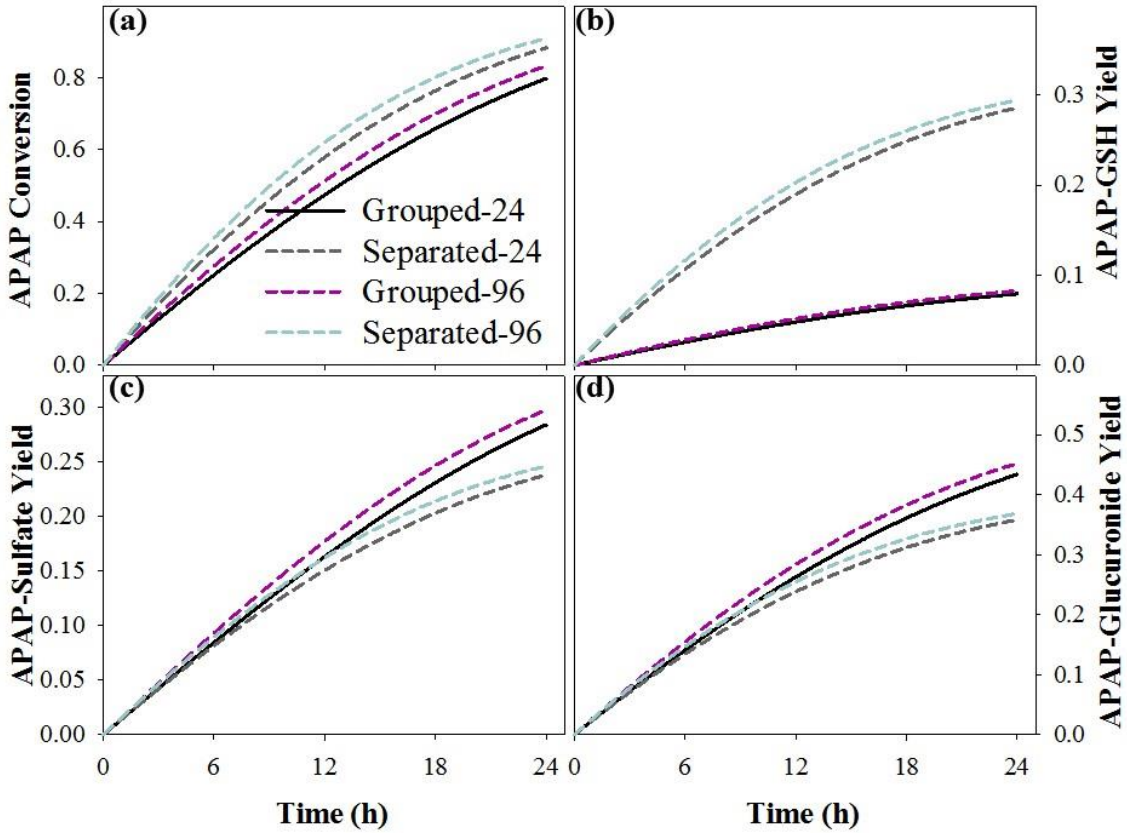

Figure 3.7: Effect of reaction rates on the metabolic profiles with a dosage of 5.95 mg/L in different well configurations: (a) APAP conversion, (b) yield of APAP-GSH, (c) yield of APAP-Sulfate, and (d) yield of APAP-Glucuronide

Hence, one could use small well sizes, but the formed product quantity is significantly smaller. In order to detect and validate those results, one has to have sensitive techniques to detect the formed metabolites. Typically used techniques, such as HPLC and ELISA, may not be sensitive in such low ranges, thus requiring the determination of alternative techniques.

3.4 DISCUSSION

Development of *in silico* approaches for use in drug discovery are important as simulation plays a vital role in reducing drug development costs and increasing drug screening throughput relative to *in vitro* and *in vivo* methods. Hence, PBPK and pharmacodynamics methods are used in drug development as a cost effective tool for analyzing various aspects of drug and body interactions [77]. Simulation allows evaluation of numerous kinetic parameters quickly and at low cost. Models range from whole body [78] to compartmental [79] to cellular [80] levels, and even nanoscale. Although these models rely on literature data for model constants or parameters, one has to choose various compartments and regress the obtained data. Further, these tools have to be adapted to conditions that mimic *in vitro* 3D tissue culture conditions that are becoming the next stage of drug screening. In this study, we evaluated a novel, *in silico* approach, predicting metabolic profiles for comparison of 3D culture conditions with clinical data.

Time dependent changes obtained for the various metabolites of a drug can be used to test *in vitro* results by plotting them in tandem with experimental results. Data obtained from *in vitro* experiments using synthetic tissues at various times can be compared to the simulation data. Experimental, simulated, and clinical data values should be non-dimensionalized to ease cross-testing comparison. This helps in understanding whether the developed *in vitro* model(s) mimic whole liver metabolism. These comparisons would help validate the 3D models whether further modifications, such as adding another cell type, changing cell density ratios, altering the porosity of the porous structure, incorporating fluid flow to induce shear stress, and/or recreating zonation observed in the liver [81], are required. There is also an increasing need to develop high throughput, 3D, synthetic tissue screening technologies in the discovery and development of new drugs. Product profiles from 96-well cultures evaluated similar to 24-well configuration or other well sizes could be scaled to the requirement. Also, simulation aides in understanding the

sensitivity of various parameters while developing synthetic cell cultures. We have shown that one could test the effects of drug dosage, cell number, and sizes of 3D cultures on the metabolic profiles. Further, CFD can be extended to understand zonal variations in metabolic activity.

Well-investigated APAP was used as a case study to evaluate the utility of such 3D structures. Evaluation of these 3D cultures is critical, as there is currently no FDA-approved tissue culture method for drug development, due to the vast number of differences in culturing conditions and techniques observed in cross-laboratory comparisons. Using various hepatocyte cultures, differing results are often reported with little overlapping information. Some differences could be due to varying experimental setup, cross species comparisons, or comparison of data from different cell lines. The lack of methods capable of connecting and validating data across laboratories to clinical data indicate great need for technologies that can close this gap. There are many biochemical assays for evaluating enzymatic activity which can be compared to determine the effect of various culture conditions on specific enzymatic activity. For example, if activity of one CYP isoform is increased without changing the other two pathways in APAP metabolism and other CYP isoforms, an increase in APAP-GSH concentration and yield would be observed. However, if all three pathways show a reduction, then APAP conversion would decrease. We need to extend these analyses to other drugs and establish whether the pharmacokinetic parameters mimic clinical data. Further, databases utilized in various PBPK models could be refined to improve the prediction capabilities. Comparison of data from these different areas would help extend "Learn and Confirm" testing methodology resulting in safer and more effective clinical trials.

This study demonstrated that when CYP isoforms are simulated with individual rate parameters, there is an increased amount of the bioactivated product, leading to over prediction of APAP-GSH formation. When each isoform was coupled with its relative contribution based on activity,

the overall product distribution was similar to that observed in clinical data. Similarly, "grouped" averages of those rate constants showed similar results. Further evaluation of these pharmacokinetic equations using different drugs could help in determining whether a "grouped" or contribution based activity is more appropriate for consideration when evaluating bioactivation. The pharmacokinetic parameter values for APAP-sulfation and APAP-glucuronidation were not listed by individual transferases in the initial resource used. Unfortunately, UGT isoform pharmacokinetic data is sparse relative to CYP isoforms, making value selectivity difficult. SULT isoform pharmacokinetic data is not currently obtainable. Investigation of different individual kinetic constants as well as activity-weighted UGT isoform kinetics needs to be further investigated. Verifying whether the pharmacokinetic parameters provide comparable metabolic profiles with respect to clinical data is vital for validity evaluation.

CHAPTER IV

EVALUATION OF THE IINFLUENCE OF ENDOTHELIAL CELL TYPE ON HEPG2 CELL FUNCTION IN CO-CULTURE AND 3D SCAFFOLDS ON ACETAMINOPHEN METABOLISM

4.1 INTRODUCTION

The liver is a multifunctional organ involved in the metabolism, detoxification, excretion of substances, and maintenance of appropriate levels of circulating proteins essential for homeostasis. Liver is uniquely organized with a high density of hepatocytes (~70%) aligned along liver sinusoids comprised of endothelial cells (<20%), ensuring many interactions [82]. Liver sinusoidal endothelial cells (LSEC) are strategically located between the blood stream and hepatocytes, and play vital roles in waste clearance [83]. Hence, numerous cell culture methods have been investigated to predict metabolism and toxicity of a drug prior to animal studies in the preclinical phase [84]. The shortage of readily available primary human hepatocytes and limitations for long term storage present a primary obstacle. As a result, many studies pertaining to hepatic drug metabolism/toxicity employ HepG2 heaptocarcinoma cell line, [85-87]. HepG2 cells are highly proliferative, easy to culture, and many molecular mechanisms and drug interactions are well documented. While 2D monolayer or sandwich cultures are often explored, they do not provide

the high cell density and cell-cell communication necessary to mimic *in vivo* functions.

With the introduction 3D culture techniques as early as 1912 [88], cells were shown to behave more organotypicly when cultured in higher density [89]. Owing to a unique architecture which dictates complex interactions between cell-types, indicating that mimicking liver architecture is vital to maintaining hepatocyte function [90]. Three dimensional systems provide a new integrative level, where cells can interact, create cellular networks, and extend processes. Developing liver cultures using 3D porous scaffolds have shown significant promise [91]. Porous scaffolds provide a surface for cell attachment allowing for a homogeneous cell distribution across the scaffold, resulting in homogeneous distribution of nutrients/drugs to all cells in the culture. In this study, chitosan-based scaffolds formed by lyophilization based on their unique advantage of mechanical property and chemical properties were used. Chitosan is a polysaccharide, similar to heparan sulfate [92] richly present in the extracellular environment of the liver and sharing many features [93]. Various molecules can be blended through electrostatic interactions to modulate biochemical and mechanical signals, including gelatin [94-96] and heparin sulfate and dextran sulfate [97]. Due to the absence of a cell binding domain in chitosan, gelatin was blended, as gelatin has been shown to promote adhesion and spreading of endothelial cells (EC) in the absence of serum proteins [94] and promote matrix synthesis [98].

An additional consideration in 3D liver culturing to promote *in vivo* functionality is co-culturing. The addition of LSEC to primary hepatocytes has been shown to stabilize hepatic urea and albumin secretion *in vitro* [99, 100]. LSEC promote hepatocyte proliferation via secretion of HGF in co-culture systems or after partial hepatectomy [101]. LSEC are morphologically different from other EC present in other organs. LSEC possess non-diaphragmed fenestrae and are distributed on an ill-organized basement membrane [102]. However, LSEC are very sensitive to environmental conditions and changes. As a result, HepG2 cells have been co-cultured with

established human umbilical vein endothelial cells (HUVEC), which can be maintained and proliferated. Studies have shown restoration of some HepG2 cell functions when co-cultured with HUVEC [103]. However, effects of co-culturing with different cell types have not been investigated. In this regard, the effect of pairing HepG2 with primary LSEC or HUVEC on hepatic function was questioned. Further, the effect of culturing cells in 3D porous structures made of chitosan and gelatin in comparison with 2D configurations as a reference was investigated. Using these cultures, the effect of 2D and 3D configurations on APAP metabolism as a model to understand hepatic function was evaluated. These results show discernable culturing effects on APAP metabolism and influence on all three pathways. Further, there are differences in the activity of CYP3A4 enzyme.

4.2 MATERIALS AND METHODS

4.2.1 Chemicals

Chitosan (190–310 kDa MW and 85% degree of deacetylation, Catalog # 448877), gelatin type-A from porcine skin (Bloom300, Catalog # G2500), acetaminophen (Catalog # A3035), acetaminophen-sulfate (Catalog #UC448), acetaminophen-gluconuride (Catalog # 43073), perchloric acid solution (Catalog # 311413), theophylline (Catalog # T1633), and sodium sulfate (Catalog # 71729) were all purchased from Sigma Aldrich Chemical Co. (St. Louis, MO). Absolute Ethanol (ACS grade, Catalog # 111000200), glacial acetic acid (ACS grade, Catalog # 281000ACS), and acetonitrile (Distilled/HPLC grade, Catalog # 300000DIS) were purchased from Pharmco-AAper (Shelbyville, KY). Phosphoric acid (85%, certified ACS Catalog # A242-212) was purchased from Fisher Scientific (Hampton, NH). Carboxyfluorescein diacetate succinimidyl ester (CFDA-SE) and live/dead cell viability assay kit (Catalog # L34951) were purchased from Invitrogen Corp. (Carlsbad, CA). eFluor® 670 (Catalog #) was purchased

from eBioscience (San Diego, CA). Pierce™ BCA (bicinchoninic acid) Protein Assay Kit (Catalog # 23227) was purchased from Thermo Fisher Scientific (Waltham, MA).

4.2.2 Cells and Media

HepG2 cells (hepatocellular carcinoma line, Catalog # HB-8065), Eagles Minimum Essential Medium (EMEM Catalog # 30-2003), Fetal Bovine Serum (FBS Catalog # 30-2020), and Trypsin-EDTA Solution (Catalog # 30-2101) were purchased from American Type Culture Collection (ATCC, Manassas, VA). Maintenance and subculture processes for all cell lines is given in **Table 4.**2. Liver sinusoidal endothelial cells (LSEC, Catalog # ACBRI 566), CSC Complete Medium with 10% serum (Catalog # 4Z0-500), CSC Passage Reagent Group (includes PRG1: an EDTA/dPBS solution, PRG2: a Trypsin/EDTA/dPBS solution, and PRG3: a Trypsin Inhibitor/PBS solution, Catalog # 4Z0-800) were all purchased from Cell Systems Corp. (Kirkland, WA).

Table 4.1: Cell sources and maintenance/subculture procedures and chemical requirements

Cells	Source	Maintenance medium	Centrifuge	Subculture process
HepaRG	Lonza	Base Medium with 12% Plated Metabolism Additive	100×g	Not subcultured. Plated using Base Medium with 12% Thawing and Plating Additive
LSEC	Cell Systems	CSC Complete Medium with 10% serum	150×g	Washed with EDTA/dPBS, detached using Trypsin/EDTA/dPBS, and neutralized with Trypsin Inhibitor Solution/PBS
HUVEC	BD Biosciences	200PRF Medium with 10% LSGS	125×g	Detached using trypsin/EDTA, and neutralized with trypsin neutralizer solution

Human umbilical vein endothelial cells (HUVEC-2) derived from single donors were purchased from BD Biosciences (San Jose, CA). Medium 200 phenol red free (PRF, Catalog # M-200PRF-500), low serum growth supplement (LSGS, Catalog # S-003-10), trypsin/EDTA (Catalog # R001100), trypsin neutralizer solution (Catalog # R002100) were all purchased from Life Technologies Corporation (Carlsbad, CA). Cell combinations for experiments are shown in **Table 4.2**.

Table 4.2: Cell culture combinations explored

Cell Culture Combinations		
HepG2	**LSEC**	**HUVEC**
X		
X	X	
X		X

4.2.3 Porous Chitosan-Gelatin Scaffold Preparation

Discoid-shaped, chitosan-gelatin (CG) scaffolds of 10 cm diameter with 1 mm thickness were prepared by previously reported methods with minor modifications [54]. In brief, 2% chitosan and 2% gelatin were mixed and sterilized using a benchtop oven set at 148 °C. Under sterile conditions, powder was dissolved in a 0.5 M acetic acid solution. The CG solution was then poured into 10 cm diameter circular molds on a Teflon sheet (US Plastics Co.) and frozen overnight at -80 °C, then freeze-dried overnight in a Virtis freeze dryer (Gardiner, NY). Dry CG scaffolds were sealed in petri dishes, wrapped in aluminum foil, and stored in a desiccator until time of use. The day prior to cell culture, CG scaffolds were cut to 34 mm diameter discs using a stencil to fit into the well of a 6-well plate (**Figure 4.1a**). CG scaffolds were neutralized in absolute ethanol (pH 7.4) for 24 hours at room temperature.

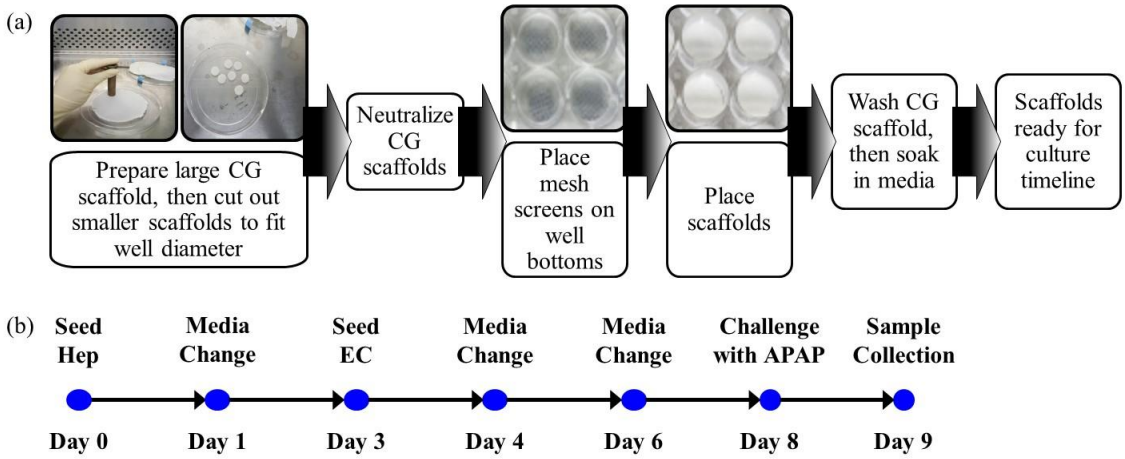

Figure 4.1: The basic steps for (a) preparation of chitosan-gelatin porous scaffolds and (b) the culturing timeline followed for all conditions

A wear-resistant, 8×8 nylon mesh with an opening size of 0.0944" (McMaster-Carr, Atlanta, GA) cut to the diameter of the well was sterilized via autoclave, and then placed on the bottom of each well i) to elevate the CG scaffold from the bottom of the tissue culture plate to avoid diffusion limitations along the bottom, and ii) to provide support while removing scaffolds for analysis post-experiment. The neutralized, CG scaffolds were placed on top of the mesh and rinsed with sterile PBS to remove trace ethanol, and ten soaked in HepG2 media for 2 hours prior to cell seeding.

4.2.4 Establishing Co-cultures

Cell culture experiments were performed in triplicate for each condition (2D, 3D, Mono, and Coculture) in two formats: i) seeding pre-stained cells for imaging and viability analysis, and ii) seeding non-stained cells for enzyme activity analysis. HepG2 cells were pre-stained with eFluor® 670 and EC were stained with CFDA-SE following the vendor's protocol. In brief, a 10 µM solution of eFluor® 670 in PBS was mixed in equal parts with a hepatocyte cell

suspension. The mixture was then incubated for 10 minutes at 37°C in the dark. Cells were washed twice with media prior to seeding. For EC staining, a 1 μM CFDA-SE stain solution was added to cell suspension and incubated at 37 °C for 20 min, followed by washing with PBS and then cell seeding.

The timeline shown in **Figure 4.1b** was used for all cell culture experiments. On Day 0, 0.5×10^6 viable HepG2 cells were seeded and allowed to attach on the CG scaffold for one hour prior to the addition of 2 mL media per well. After the first day, spent medium was collected and replaced with fresh media. On day 3, the media was changed and, in the case of co-culture experiments, EC were added. Considering the physiological ratio of hepatocytes to EC in an adult liver, 0.1×10^6 LSEC or HUVEC were seeded. One day was allowed for EC attachment prior to aspiration of spent media followed by the addition of 2 mL of fresh media. A ½ and ½ mixture of hepatocyte (Hep) and respective EC medium was used from day 3 through the rest of the co-culturing timeline.

For 2D experiments, digital fluorescent and phase contrast micrographs were taken at random locations on days 1, 3, 4, 6, and 8 for stained and unstained cells using an inverted fluorescent microscope (Nikon Eclipse TE 2000-U, Melville, NY) equipped with a CCD camera, similar to previous publications [104].

4.2.5 Challenging with APAP

After 8 days of culture, each condition was randomly assigned to one of the two groups:

Group 1: Controls: no APAP was added and cultured by adding medium, as before.

Group 2: Treated: Cells were challenged with APAP at a concentration of 150 μg/mL.

A 5 mg/mL stock solution of APAP was prepared by dissolving 50 mg of APAP powder in 10 mL of sterile, deionized water. The solution was mixed on a temperature controlled stir plate at 25 ºC. The solution was syringe filtered with a 0.2 µm nylon filter.

From both groups, a 25 µL sample was retrieved from each well every six hours for 24 hours, including a sample at the zero time point. All samples were stored at -20 °C until time of analysis.

4.2.6 Cell Distribution in 3D Culture

Upon completion of the 24 hours of APAP challenge, the scaffolds (treated and control) were divided into 3 parts (**Figure 4.2**) for use in the following analyses:

- Viability by freeze-thaw using a spectrofluorometer
- Cell distribution through the scaffold thickness by H&E staining
- Cell distribution in the radial direction by confocal imaging

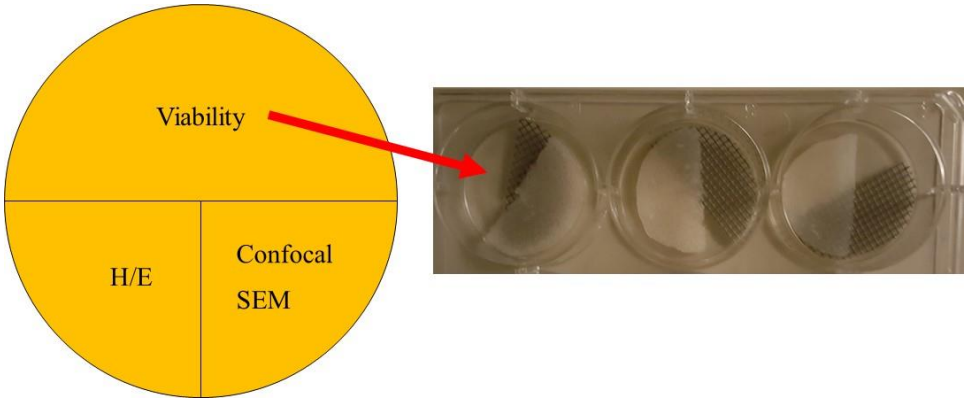

Figure 4.2: Scaffolds were split post-experimentation for performing multiple analyses

Initially, all treated and non-treated CG scaffolds were split into two parts. One half was used in fluorescence imaging, while the other half was stored in 1 mL of PBS and frozen until used to

determine viability via methodology described in the section below. For 3D experimental configurations, confocal images were collected using Leica TCS SP II (Heidelberg, Germany). Images were captured at various depths for both HepG2 and EC. Obtained images were overlapped to obtain a single image at each depth and location.

One portion of the harvested CG scaffolds was fixed after 9 days in culture according to previously reported methods [105]. In brief, half of the CG scaffold was washed with PBS, then fixed in a 3.7% formalin solution for 45 minutes at room temperature, washed with PBS (×2), and submerged in 2 mL of absolute ethanol. The 6-well plates in which the CG scaffolds were housed were tightly sealed using paraffin film and stored at 4 °C. From each CG scaffold, 4 µm thick sections were cut and processed according to standard haematoxylin and eosin (H/E) staining protocols. Bright field micrographs were obtained at random locations using an Evos™ AME-i2111 Digital Inverted Microscope.

Cell morphology and distribution were analyzed using a JOEL 6360 electron microscope (Joel USA Inc., Peabody, MA) at an accelerated voltage of 8 kV, similar to previous methods [97]. Twenty-four hours prior to SEM analysis, a portion of the fixed CG scaffolds was vacuum dried in a Virtis freeze dryer (Gardiner, NY). Dry samples were attached to 10 mm diameter aluminum stubs (Electron Microscopy Sciences, Hatfield, PA) using a conductive graphite glue (Ted Pella, Redding, CA), and sputter-coated with gold for 1 minute.

4.2.7 Determining cell Viability

Cell viability was analyzed, using a fluorescence method previously described [105]. After 9 days, media was aspirated, wells were filled with 1 mL of PBS, then frozen at -80 ºC. The number of viable cells per well for each condition was determined by lysing cells via four repeats of a freeze-thaw cycle and measuring fluorescence released from pre-stained cells. The freeze-

thaw cycle involved freezing at -80 ºC for 30 min and thawing at room temperature for 30 min. After the final thaw, 150 µL were taken from each well and pipetted into a black, 96-well plate. Fluorescence was measured using a Spectramax GeminiXS spectrophotometer (Molecular Devices Sunnyvale CA) with excitation wavelengths of 485 nm and 615 nm and emission wavelengths of 538 nm and 660 nm for EC and hepatocytes respectively.

Fluorescence intensity was converted to cell number using a calibration curve developed using corresponding cell types and respective fluorescence stains. For this purpose, cells were harvested from T-75 plates, and counted using a trypan blue dye exclusion assay. Hepatocytes were stained with eFluor® 670 and EC with CFDA-SE, using the protocol described above. Cells ranging from 250,000 to 1,500,000 for HepG2 cells and 25,000 to 200,000 for ECs were deposited into separate wells, sterile PBS was added to bring the total volume to 1 mL, and plates were then frozen at -80 ºC. Using the four freeze-thaw cycles, cells were lysed. Fluorescence was measured using respective excitation and emission wavelengths. Relative fluorescence to a known number of cells was prepared for each cell type. The linear regression equation from each calibration line was used to calculate the number of given cells in experimental wells and scaffolds.

4.2.8 Protein Content Analysis

Protein content in the media was evaluated using a BCA assay, according to the vendor's protocol. In brief, standards and samples were diluted 1:5 by mixing 25 µL of sample/standard with PBS. Twenty-five µL of the diluted standard/sample followed by 200 µL of working reagent were mixed in a 96-well plate on a plate shaker for 30 seconds, and incubated at 37 °C for 30 minutes. Absorbance was measured at 490 nm using Emax spectrophotometer (Molecular Devices Sunnyvale, CA).

Blood urea nitrogen content (BUN) was analyzed using QuantiChrom™ Urea Assay Kit (BioAssay System, Hayward, CA) following the vendor's protocol. In brief, 50 µL samples were added to a 96-well plate along with 200 µL of reagent. After 20 min of incubation at room temperature, absorption was measured using a Emax spectrophotometer at 490 nm.

4.2.9 APAP and Metabolite Analysis

APAP and its formed metabolites were analyzed using a Dionex HPLC system (Dionex Sunnyvale, CA), similar to previously reported methods, with minor modifications [106]. In brief, a 25 µL sample from each time point was deproteinated using a 6% perchloric acid solution, containing 10 mg/mL of theophylline (the internal standard), at twice the sample volume. Samples were mixed on a mini vortex for 5 s and centrifuged at 14,000 g for 6 min. Supernatant was aspirated and placed into a glass vial for analysis. An injection volume of 10 µL was delivered to the HPLC column via the autosampler (Model ASI-100). APAP and metabolites were resolved using a 4.6 ×150 mm C18 column (Acclaim, National Scientific Rockwood, TN) with a 5 µm particle diameter and a 120 Å pore size. A 4.6 × 10 mm C18 guard column with a 5 µm particle diameter (Acclaim, National Scientific Rockwood, TN Guard Cartridge and Cartridge Holder) was included in line for column protedtion. The HPLC system was controlled using Chromeleon software (version 6.8 Dionex Sunnyvale, CA). An isocratic mobile phase consisting of 93% 0.05 mM sodium sulfate solution and 7% acetonitrile was used. Mobile phase pH was decreased to 2.2 using phosphoric acid (85%). Samples were eluted employing a 1.5 mL/min flowrate, column oven temperature of 30 °C, and UV absorbance was detection wavelength of 254 nm.

Standards were prepared using a 12 to 159 µg/mL concentration range for APAP, and 9 to 100 µg/mL range for APAP-sulfate and APAP-gluc. Two combination standards were prepared for

quality control, where i) APAP and metabolite concentrations were equal at 60 µg/mL and ii) APAP concentration was 81 µg/mL and APAP-sulfate and APAP-glucuronide concentrations were 24 µg/mL concentrations. APAP concentrations from HPLC analysis were converted to conversion values by,

$$\text{APAP Conversion} = 1 - \frac{C}{C_0}$$

where C is the APAP concentration at any given time, and C_0 is the initial APAP concentration.

4.2.10 Enzymatic Activity Analysis

A CYP 3A4 assay kit with Luciferin-IPA (Promega Corp. Madison, WI Catalog # V9002) was used to quantify changes in the activity of that enzyme, following vendor's protocol. In brief, cells were washed with medium prior to the addition of the substrate, luciferin-IPA, and then incubated at 37 ºC for 50 minutes. Twenty-five µL of culture medium from each experiment was transferred into a 96-well, opaque, white plate (Thermo Fisher Scientific Waltham, MA Catalog # 15042) at room temperature, followed by the addition of 25 µL of luciferin detection agent for reaction initiation. Plates were incubated for 20 minutes at room temperature. A DTX 880 Multimode Detector and Multimode Analysis software (Beckman Coulter, Brea, CA) was used to quantify luminescence and enzymatic activity.

4.2.11 Statistical Analysis

Each experiment was performed in triplicate for each condition. Viability and CYP 3A4 activity averages are based on results from non-stained and stained sets respectively. Total protein content and metabolism averages are based on data from both stained and non-stained experiments, with n = 6. In order to determine significance of variance, ANOVA analysis was performed in MS Excel between groups.

4.3. RESULTS

4.3.1 Morphological Changes in Cell Culture

In this study, porous CG scaffolds prepared using freeze-drying were used to develop 3D cultures where cells can be uniformly distributed throughout the structure. This study did not employ spheroid culture, though also referred to as 3D cultures [107]. The 3D porous scaffolds were first examined in dry and hydrated conditions in order to confirm pore openness and stability of pores to ensure that cells could infiltrate uniformly, similar to previous results [98]. Scanning electron micrographs showed that the dry surface (**Figure 4.3b**) possessed an open pore architecture which would allow cell infiltration when seeded. Hydrated scaffolds were semi-transparent (**Figure 4.3a**), which allowed visualization of internal pore architecture via light microscopy. Pores appeared intact even after hydration.

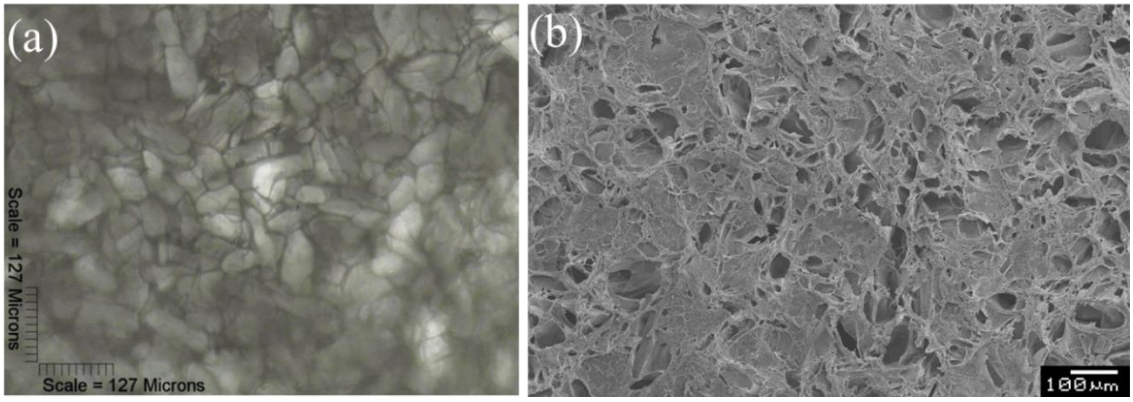

Figure 4. 3: Chitosan-gelatin 3D scaffold showing porous structure. (a) Digital phase contrast micrograph in hydrated condition and (b) SEM micrograph in dry condition. The SEM micrograph shows that pores at the surface are open to allow for cell infiltration

Next, many experiments were performed to develop a protocol for testing the co-culture system. Initially, when 1×10^6 HepG2 cells were seeded per well, there was limited space for the

organization of cells, even without the addition of EC for co-cultures. Alternatively, seeding at lower than 0.5×10^6 HepG2 cells was explored; however, metabolite production was undetectable. For co-cultures, seeding of HepG2 cells and EC simultaneously was also explored. Simultaneous seeding led to cultures that appeared disorganized after allowing 2 to 3 days for reorganization of cells. Seeding separately allowed establishment of HepG2 cell colonies, around and among which EC preferred to attach (**Figure 4.4**), more similar to the configuration of these cell types *in vivo*. On Day 1, HepG2 cells were uniformly distributed throughout the culture, and more as individual cells (**Figure 4.4**). After 3 days, small colonies of HepG2 cells were observed with an increase in number of cells with time progression for all cultures. Increases in cell number were particularly significant in 2D cultures with HUVEC. No changes in morphology of any cell line were observed. Hence, after allowing for HepG2 cells to attach and reorganize, EC were added. Comparison of fluorescent micrographs in the same location allowed for distinction of cell type. CFDA-stained EC attached in and around hepatocyte colonies (**Figure 4.5**). These analyses confirmed that seeding HepG2 cells first followed by EC seeding after 3 days helped in promoting organizational changes and aided in the elimination of issues due to space limitation. Challenging the cell cultures on day 8 with APAP, also helped minimize the effects of proteases used during subculturing.

4.3.2 Evaluating the Distribution of Cells in 3D Cultures

In order to evaluate the distribution of cells in 3D cultures, confocal images were taken at various depths through the scaffold thickness.

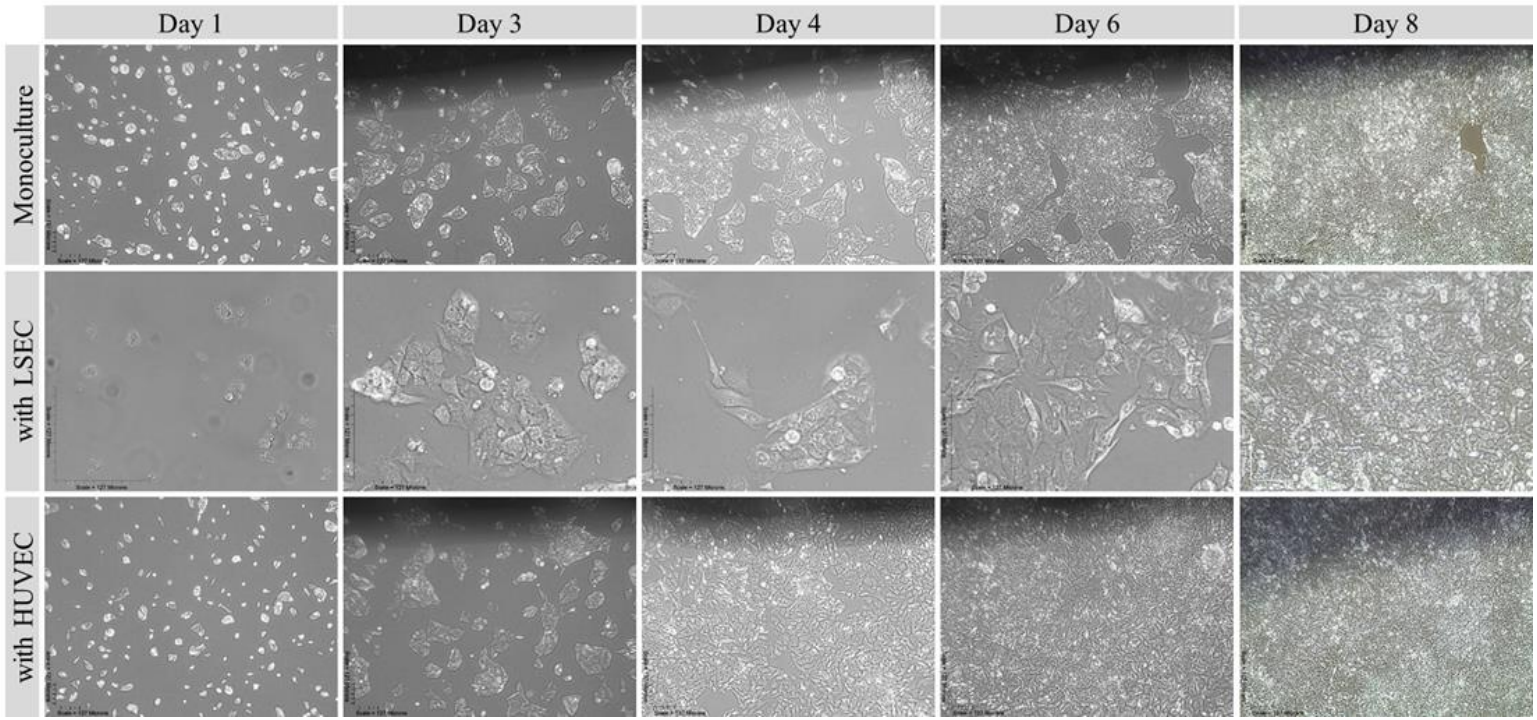

Figure 4.4: Digital micrographs of 2D cultures for observation of morphology and distribution. Proliferation of cells was observed in all cases, particularly for HepG2 cells

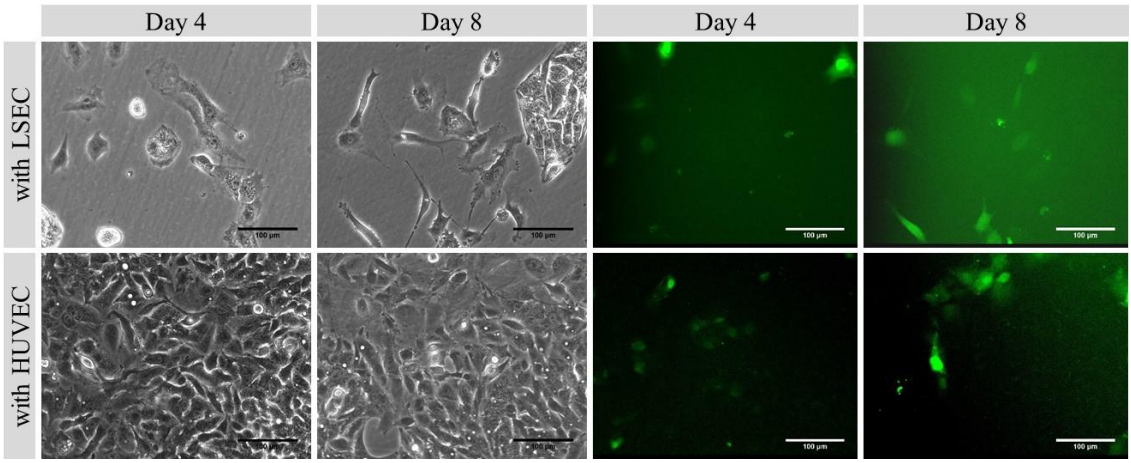

Figure 4.5: Digital and fluorescent micrographs show cell distribution in coculture with respect to time. The fluorescent images make HUVEC/LSEC (-green) discernable from HepG2

The collection of confocal images demonstrated that both efluor-stained HepG2 and CFDA-stained LSEC or HUVEC were distributed in the scaffold (**Figure 4.6**). A considerably larger number of hepatocytes were observed compared to EC, in agreement with the seeding ratio of 5:1. This suggested the presence of both the cell types in co-cultures. However, hepatocytes appeared in greater number in 3D cocultures compared to 3D monocultures.

Additional analyses were performed to confirm cell distribution in 3D i) at the surface and ii) in the open pore architecture. SEM images of the scaffold surface demonstrated cell attachment of all cell lines (**Figure 4.7**). HepG2 cells appeared as rough, spheres approximately 7 µm in diameter, while both EC lines were more elongated, approximately 50 µm in length. EC were observed in smaller numbers relative to HepG2, in agreement with the seeding ratio.

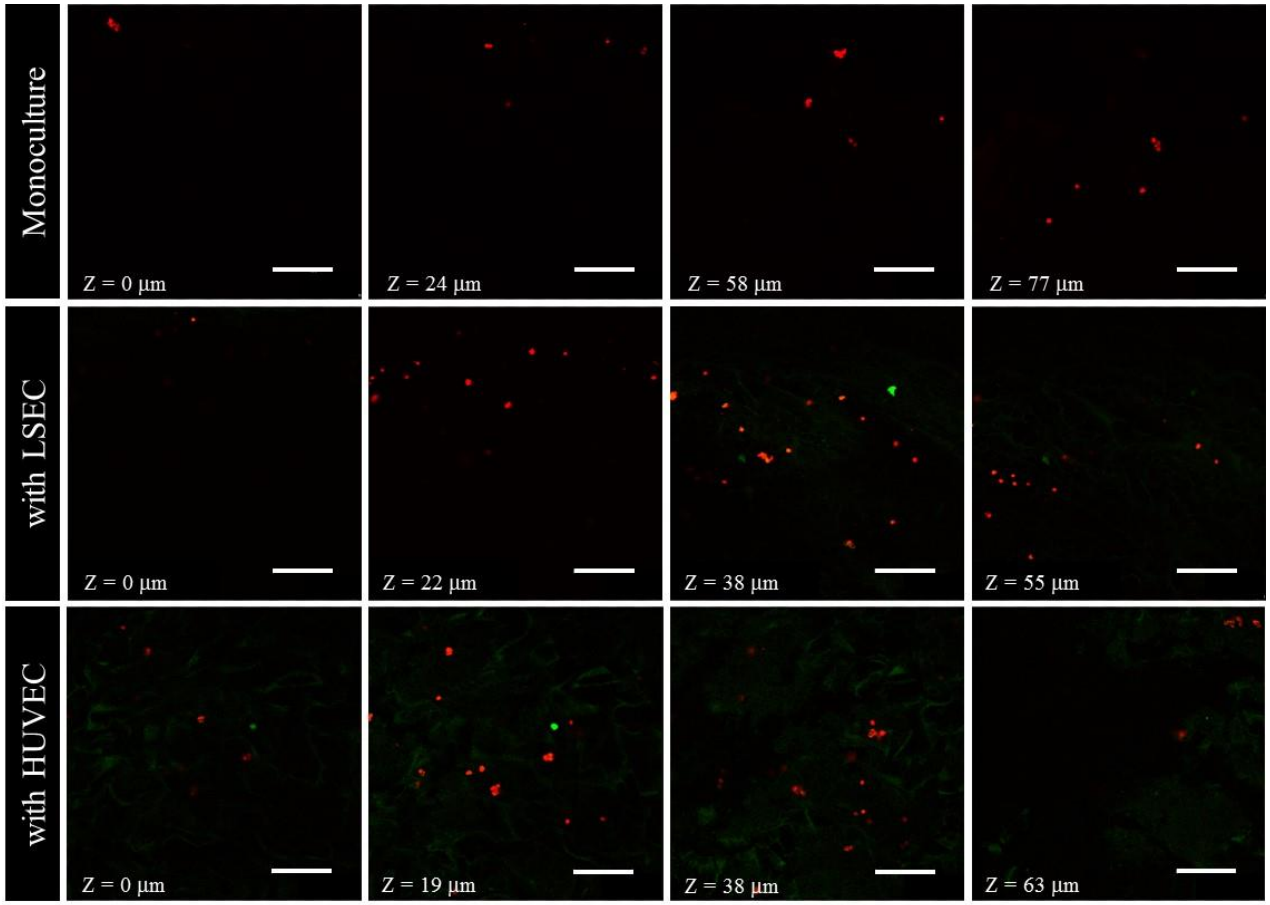

Figure 4.6: Confocal images of 3D cultures with HepG2 cells (red) and LSEC/HUVEC (-green) at different depths confirming 3D configuration. (scale = 100 µm)

HepG2 cells were observed in clusters as well as independently. Micrographs obtained after H&E staining from cross-sections of the thickness of the scaffold showed HepG2 cells in clusters and individually distributed (**Figure 4.8**). HepG2 were identified by high nuclear to cytoplasmic ratio.

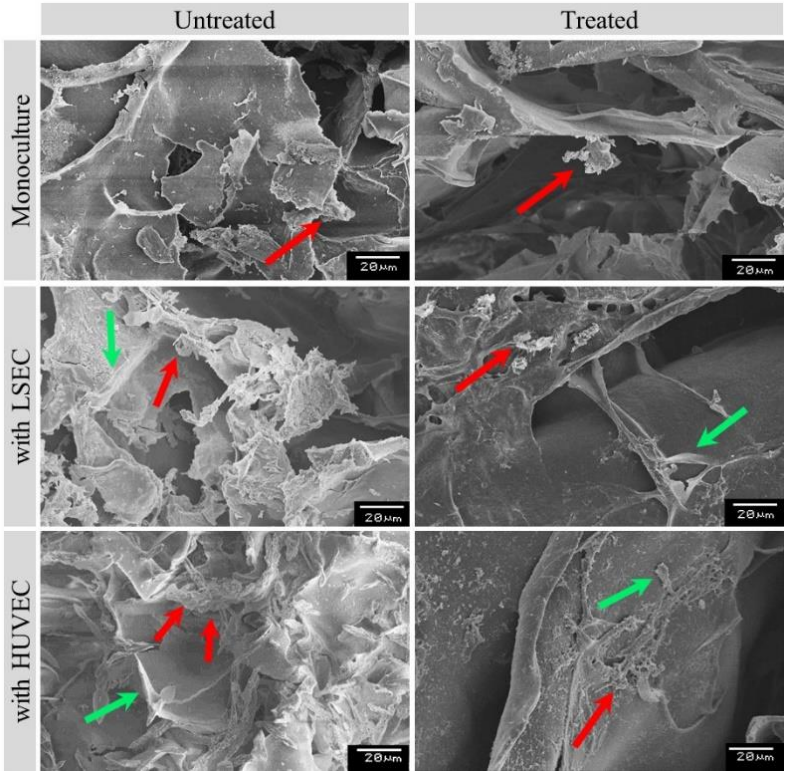

Figure 4.7: SEM micrographs show attachment of HepG2 cells (red) and LSEC/HUVEC (-green) on the surface of the scaffold. HepG2 were observed to grow individually and in clusters

This confirmed the presence of cells in the interior of the scaffolds. The combination of confocal imaging, SEM, and H&E staining confirmed that cells were distributed in 3D and present both i) on the surface and ii) within the porous structure.

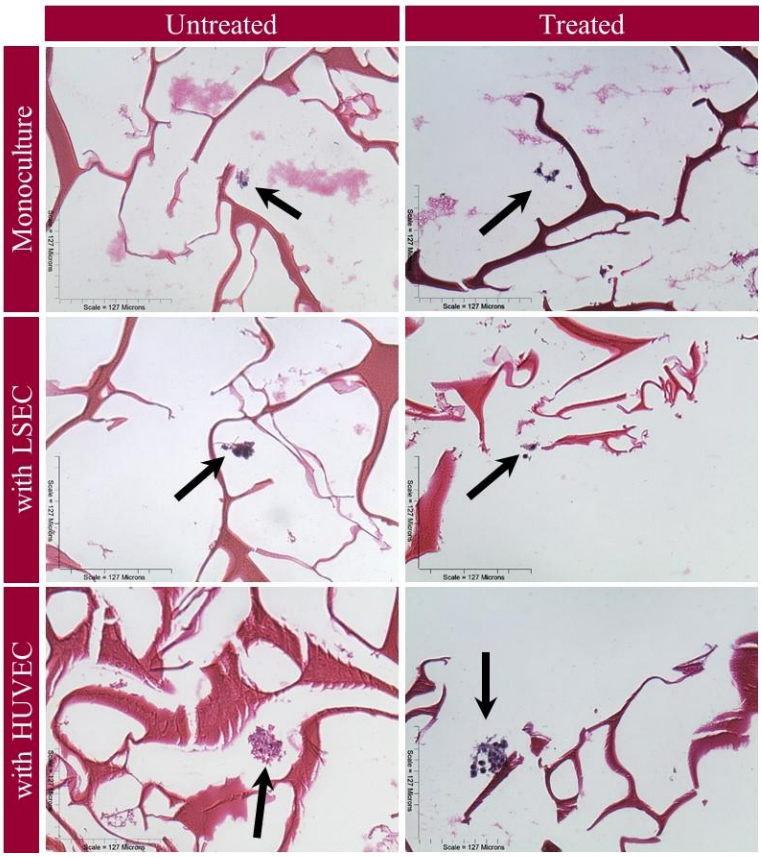

Figure 4.8: H&E treated scaffold slices of the cross sectional view of the thickness. HepG2 cells were observed as individual cells and as clusters

4.3.3 Evaluation of Cell Viability

While the various imaging techniques qualitatively confirmed 3D distribution of cells, a quantitative analysis was also performed using pre-stained cells and lysing hem by use of a freeze-thaw cycle. Initial calibration plots prepared with varying cell numbers demonstrated a linear increase in fluorescence with increased cell number, suggesting the possibility of using such a technique. The ratio of the fluorescent signal to the number of cells was much lower for HepG2 cells (**Figure 4.9a**) compared to both EC lines (**Figure 4.9b**), indicating an increased cytoplasmic content in ECs relative to HepG2, in agreement with known cell morphologies.

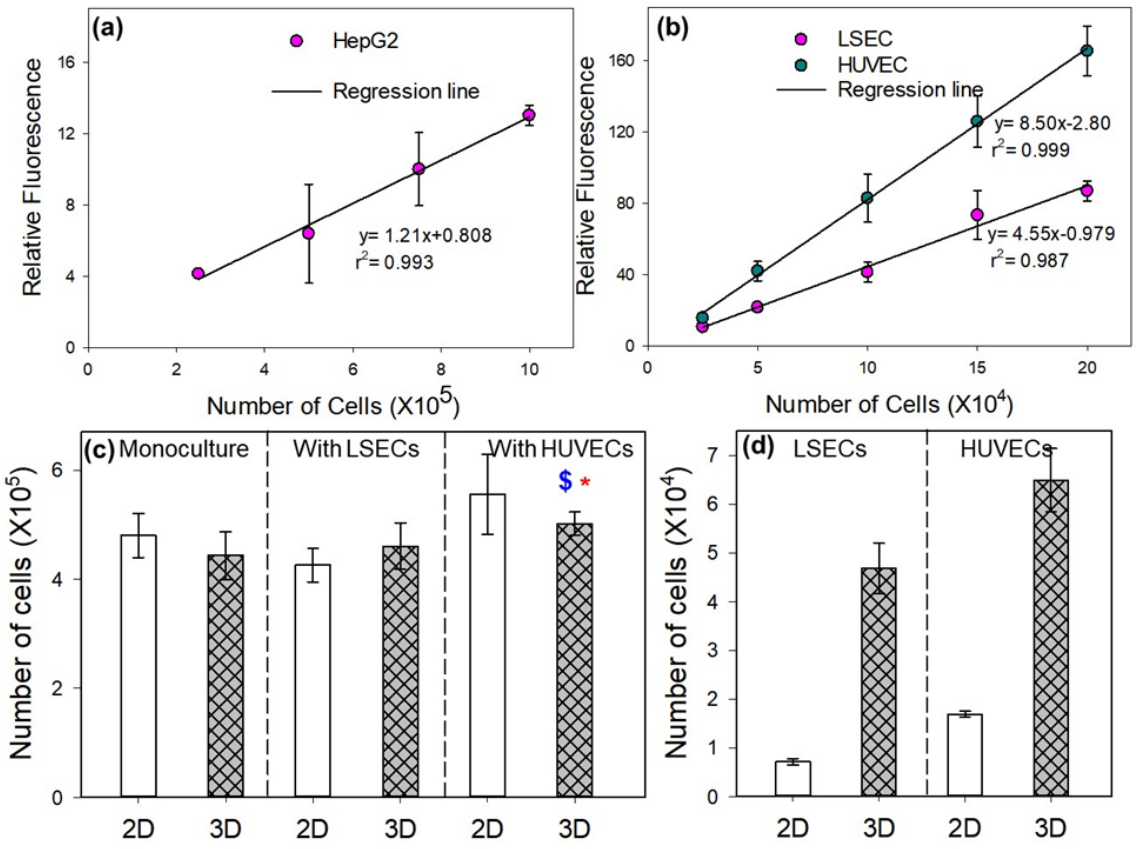

Figure 4.9: Cell viability analysis during cell culture. Calibration curves for a) HepG2 cells and b) LSEC and HUVEC were prepared over a range of relevant cell totals for each cell line. The regression line equations were used to obtain the relative viability for c) HepG2 cells in monoculture and co-culture with LSEC or HUVEC and d) LSEC and HUVEC in co-culture. * represents statistically significance between 2D and 3D HUVEC co-cultures with $p<0.01$. $ represents statistically significance between 3D monoculture and 3D HUVEC co-culture with $p<0.01$. There was statistically significant difference between each group of EC and not shown to reduce cluttering of the figure.

Also, LSEC has less cytoplasmic content relative to HUVEC, suggesting LSEC are smaller in cell size.

When viability was assessed using respective fluorescent signals, HepG2 cell viability on Day 9 was comparable to the initial 0.5×10^6 cells per well seeding (**Figure 4.9c**) across most cultures. ANOVA analysis demonstrated significant differences between 2D and 3D co-cultures with HUVEC, and a significant difference between 3D monoculture and 3D co-culture with HUVEC. Viability results confirmed that the majority of the initial HepG2 cells survived, unlike EC viability, which varied significantly according to dimensionality and cell line (**Figure 9d**), as indicated by ANOVA analyses. EC demonstrated higher viability in 3D cultures compared with 2D cultures for both cell lines. LSEC's were observed to be less viable than HUVEC, confirming increased sensitivity of LSEC compared with HUVEC. However, HepG2 cell viability was not significantly affected by culturing in 2D or 3D and in presence of LSEC, but HUVEC co-cultures affected viability.

The effect of 1 μM APAP concentration on viability was also compared. Comparison between APAP treated and untreated viability showed no significant difference in viability in all cultures. Hence, that data is not shown.

4.3.4 Assessment of Total Protein Content

In order to better understand the viable cell population and the effect of co-culture on hepatocytes, total protein content was evaluated during nine day culture. First, differences in total protein content were observed for three media mixtures (pure HepG2 media, ½ and ½ HepG2 and LSEC medium, and ½ and ½ HepG2 and HUVEC medium). When fresh media was analyzed, the protein content of the HepG2 and LSEC mixture had the highest protein content, followed by pure HepG2 media and then the HepG2 and HUVEC mixture. The protein content for the EC and HepG2 mixtures were normalized for total protein content to pure HepG2 media. An increase in the total protein content was observed in media for all APAP treated cultures at

Day 9 (**Figure 10a**). Otherwise, the protein content remained constant (from Day 1 to Day 8). Dimensionality did not greatly affect protein content; however, a trend of increased protein content was noticeable in co-cultures compared with monoculture.

In order to understand HepG2 cell specific functionality, urea content was analyzed in the retrieved media. These results showed (**Figure 10b**) trends similar to the total protein content, except 3D configuration, which showed increased urea production relative to corresponding 2D cultures. Co-cultures with HUVEC seemed to have higher urea production during day 4 but 3D configuration had more effect. Previously, increased matrix synthesis by fibroblasts in CG scaffolds while cell proliferation was minimal has been shown [98]. Similar behavior with HepG2 cells and EC were expected, given the ratio of HepG2 cells to EC in co-cultures. This suggested that protein content variations mimic HepG2 cell function and there may lead to increased urea production. Dimensionality did not appear to greatly affect protein content; however, co-culture trends demonstrated increased protein content compared with monoculture.

4.3.6 APAP Metabolism

The primary focus was to evaluate the effect of various cell culture conditions on hepatocellular metabolism with APAP as a model. First, the detection system was established using HPLC and obtaining calibrations prepared for APAP and the associated metabolites. All calibrations (**Figure 11**) demonstrated high linearity as evidenced by the r-squared (r^2) values for the respective regression lines. As the theophylline concentration remained the same throughout all preparations, the standard curves also indicated that for the same concentration, APAP yielded a higher area under the curve in HPLC analysis, compared to metabolites (**Figure 4.11a**); while APAP-sulfate and APAP-glucuronide areas under the curve were comparable (**Figure 4.11b and 4.11c**).

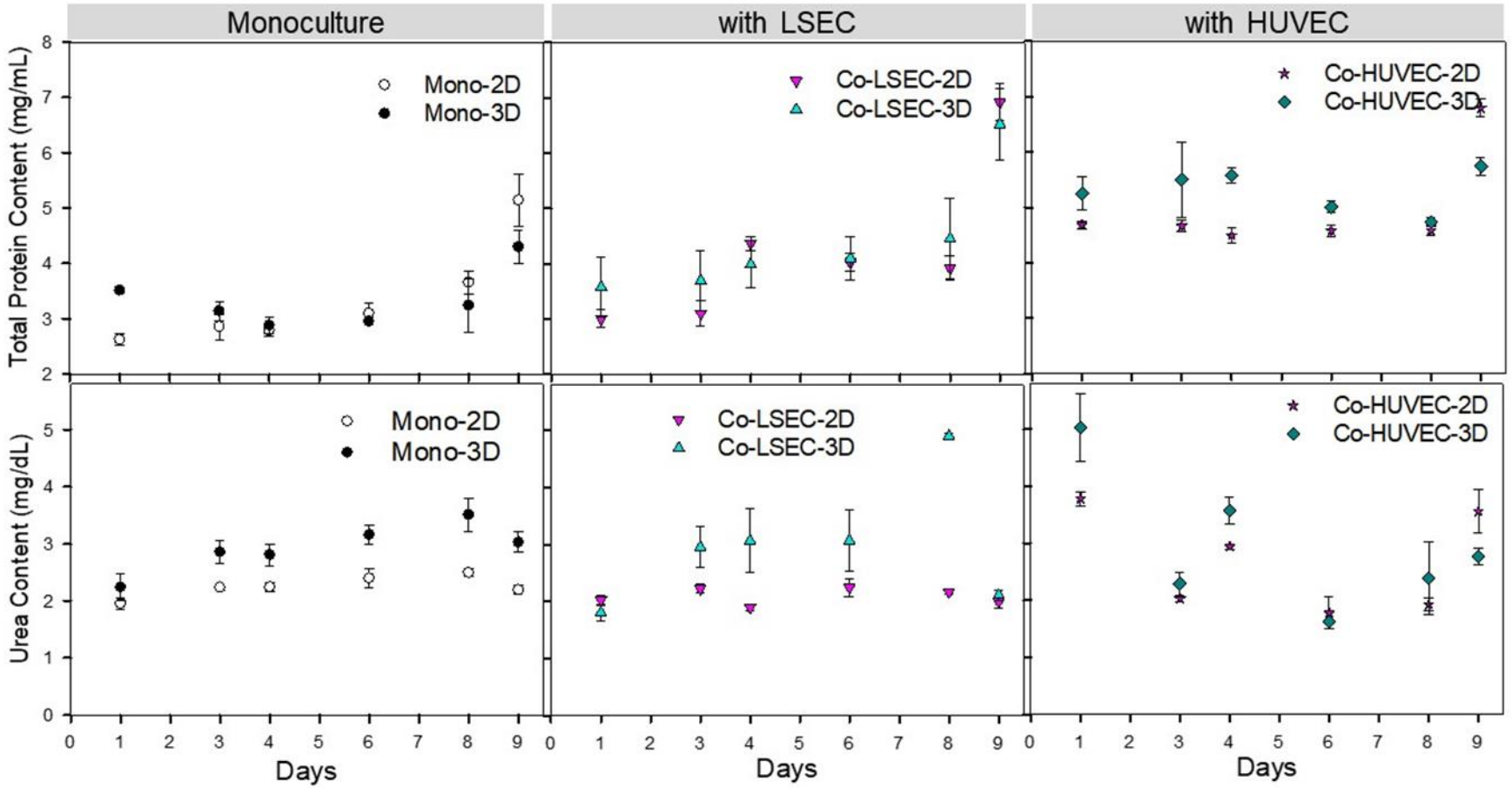

Figure 4.10: Changes in the total protein content and urea concentration during the culture period

Comparison of metabolite data from *in vitro* cultures with clinical data is important for understanding whether the integrity of metabolic processes is maintained in *in vitro* culture settings. Experimental metabolic data was compared to clinical data by use of the computational model discussed in Chapter III. In experiments, APAP conversion was highest in 3D co-cultures containing HUVEC (**Figure 10d**). Other cultures also showed similar increases. Production of the APAP-sulfate conjugate followed a general increasing trend for most cultures, but 2D co-cultures yielded results with the highest product formation matching that of the clinical scenario (**Figure 10e**). Three-dimensional monoculture and co-culture with LSEC gave the better results, with significantly higher distribution of APAP-sulfate. However, production of the APAP-glucuronide metabolite (**Figure 10f**) was lower compared with APAP-sulfate production, which is in contradiction to clinical results reported by others [66]. APAP-sulfate distribution was higher than that of APAP-glucuronide in 2D monoculture, 2D co-culture with LSEC, and 3D co-culture with HUVEC. Three dimensional co-cultures yielded lower production values relative to 2D cultures, unlike urea production. Although diffusion and distribution may not be significantly different between urea (molecular weight is 60 Da) and APAP (molecular weight is 151 Da) and its metabolites, the possibility of non-specific binding of APAP, which could lower the concentration of APAP, is suspected. In this regard, additional experiments where APAP was loaded directly on to CG porous scaffolds without cells were performed. However, no significant variation was observed. With the observation of higher APAP conversion in 3D structures and no binding, it is possible that metabolites could bind to the structures or the cell phenotype in these pathways are not affected. Thus, phenotypic changes have to be further investigated.

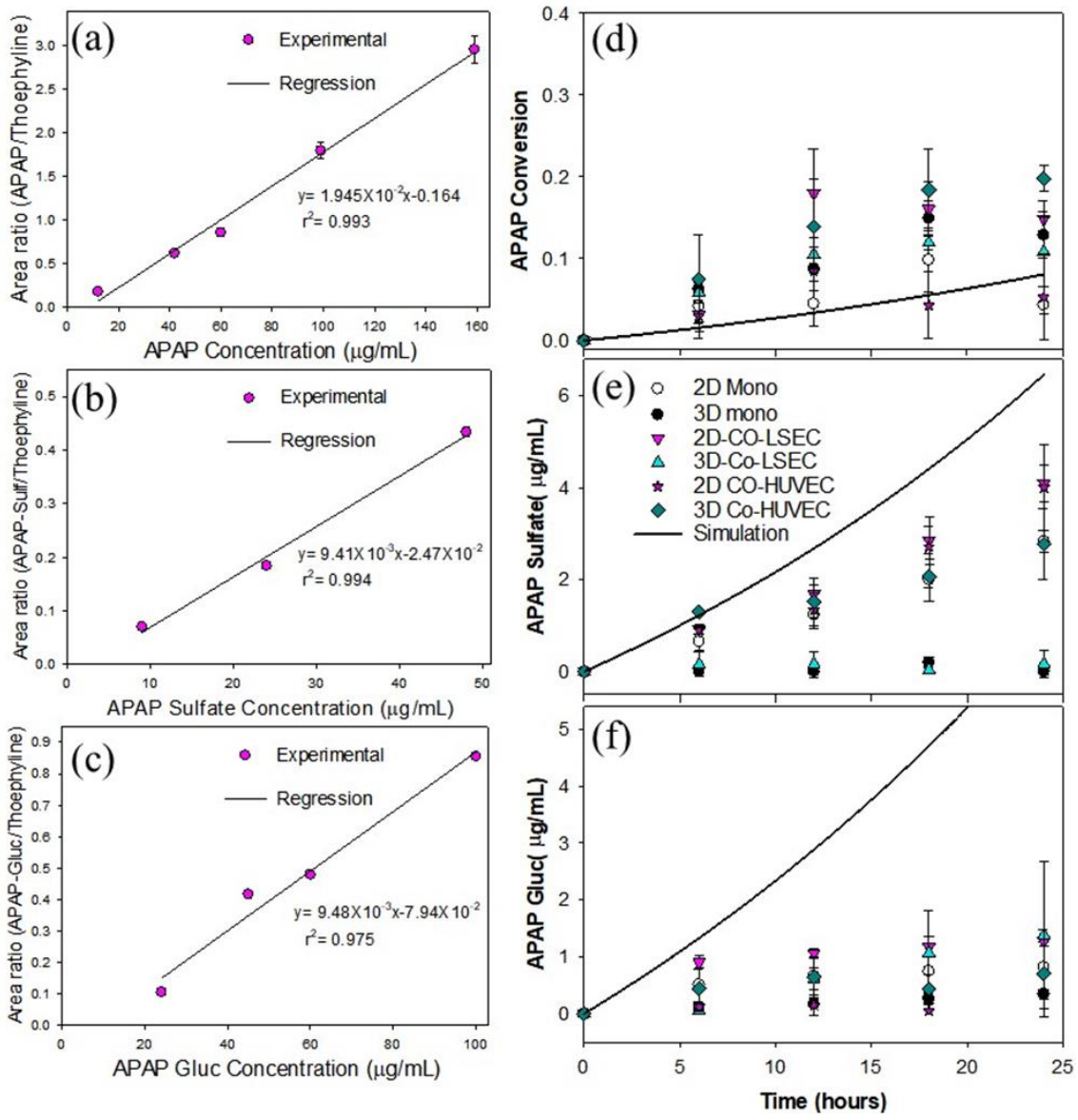

Figure 4.11: Calibration curves for APAP and metabolites (left column) were prepared over a relevant concentration range. The regression line equations were used to determine experimental concentrations with respect to line (right column)

4.3.6 Changes in CYP Enzyme Activity

When metabolite analyses were performed, APAP-GSH metabolite was not detectable using these HPLC methods. As a result, CYP3A4 activity was evaluated on Day 9 (**Figure 4.12**) in

separate cultures. CYP 3A4 activity was significantly higher in all 2D cultures when compared with 3D counterparts. CYP 3A4 activity was significantly higher in all 2D cultures when compared with 3D counterparts. Significantly higher CYP3A4 activity was observed in co-culture with HUVEC for both 2D and 3D conditions in untreated and treated cultures, when compared with monoculture. ANOVA analyses indicated differences in CYP3A4 activity between treated and control cultures for 2D experiments were significant. Others have shown similar increase in CYP3A4 activity when primary human hepatocytes are co-cultured with adipocyte stem cells in spheroid cultures [108]. Further, the location of increased expression is shown to exist at the periphery of the cell. Monoculture and co-culture with LSEC demonstrated higher activity under treated conditions compared with controls for both 2D and 3D; however, the opposite was observed when evaluated in 2D co-cultures with HUVEC, and activity was comparable for treated and controls in 3D co-cultures with HUVEC.

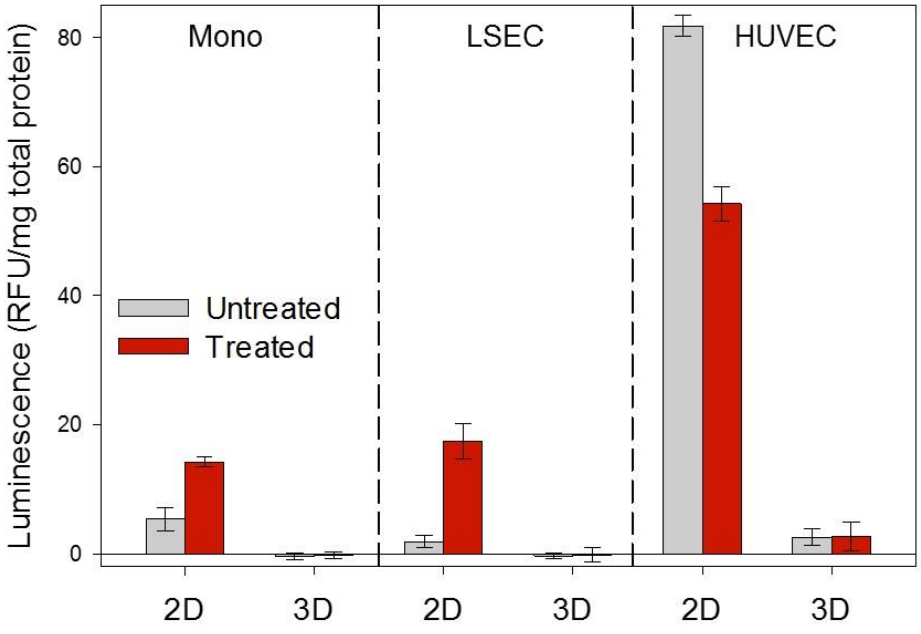

Figure 4.12: The CYP450 enzyme activity for isoform 3A4 was measured at the end of experiments on Day 9 via a luminescent assay

As the protocol for the assay and others have reported, CYP3A4 activity increases in hepatocytes when challenged with a drug. Observance of the activation of CYP3A4 activity in untreated co-cultures with HUVEC indicates that co-culture of hepatocytes with a non-native liver cell line could cause changes in behavior. Hence, not all co-cultures are similar. Further, analyses of other enzymes should be performed to better understand the effect of these configurations and observed changes in APAP metabolic products.

4.3.7. Comparison to Clinical Data

Comparison of the metabolic distribution of the parent drug and metabolites from cell culture experiments to clinical data is challenging, as changes in parameters, such as the cell density, can alter the distribution. Computational modeling was used to evaluate APAP metabolism over a 24 h period under identical conditions. Pi charts (**Figure 4.13**) representing the metabolic distribution results from the 6 experimental setups were compared with computational results previously validated by clinical comparison. APAP-glucuronide distribution was higher than simulation predictions by at least 1% in all 3D cultures as well as 2D co-cultures with LSEC. APAP-glucuronide production was less than that predicted by simulation by 1% in 2D monocultures. Two dimensional cocultures with HUVEC appeared to more closely match the metabolic distribution of APAP from simulation than any other experimental set up.

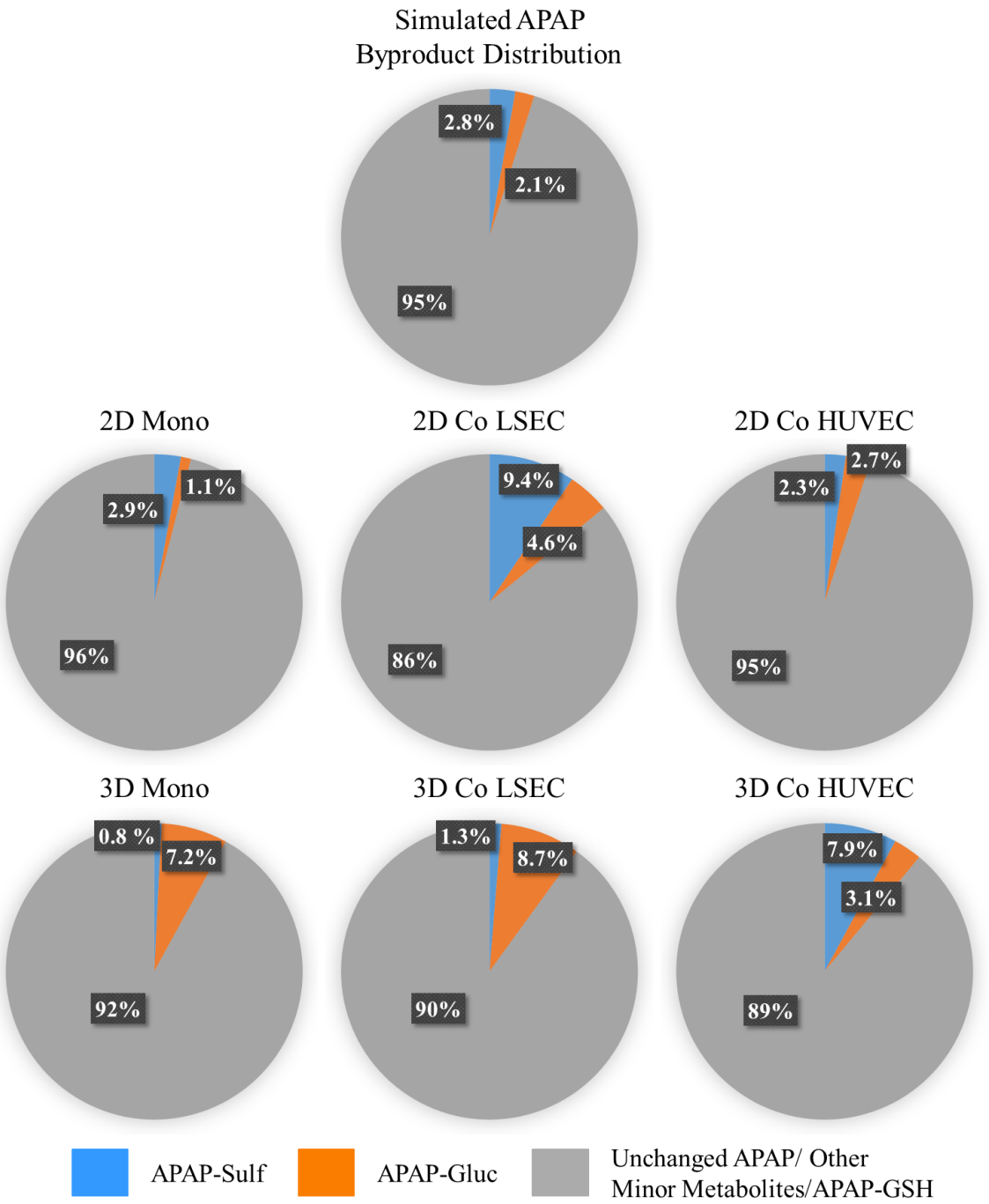

Figure 4.13: Metabolic distribution comparison with simulated data with APAP-GSH and APAP-glucuronide metabolism individualized and weighted. Simulation was performed under the same conditions as experiments: 150 mg/L dose, 6-well plate, and 0.5×10^6 HepG2

4.4 DISCUSSION

In this study, extensively explored CG porous structures were used to evaluate the effect of co-culturing HepG2 cells with ECs from two origins. First, the integrity of the porous structure was maintained in these experiments, as evidenced by SEM and bright light microscope imaging. Many 3D systems employ the development of cell aggregates or spheroids [109]. While spheroids provide increased, appropriate cell-cell communication and development of the extracellular matrix, diffusion limitation issues in such 3D systems lead to cell death at the core of the aggregates, as well as heterogeneous distribution of substrates. In addition, drugs to be tested are not uniformly exposed to all cells.

Similar to our results, others show using micro-patterned cultures that hepatocytes reorganize with time [110]. In addition, our study demonstrated that delayed EC seeding allowed the formation of hepatocyte colonies and EC to orient themselves around the hepatocyte colonies on their own. Hence hepatocytes self-organize and move toward each other into small colonies, while the delay in seeding EC allowed their organization around the established hepatocyte colonies. Others show similar benefit of delaying the culture time as HUVEC need three days for formation of tubular networks [111]. Also, CYP450 enzymes have shown alterations in isoform activity with respect to time in culture [110, 112, 113]. Where urea production [110] and albumin secretion [110, 114] are stable for a longer period of time. For these reasons, the culture timeline was increased to 8 days prior to challenging with APAP, unlike other studies that challenge cells with a drug 24 hours after plating [115, 116].

Both 2D and 3D fluorescent imaging showed opportunities for cell-cell communication between the same cell types and across cell types. Our cell viability analysis used cytoplasmic stain, and calibration comparison between LSEC and HUVEC showed that HUVEC are nearly twice the

size relative to LSEC. Viability comparison of HUVEC and LSEC co-cultures indicated that LSEC were more sensitive to change from a monoculture condition, with a significant decrease in viability relative to HUVEC. Several factors, including hormones, cytokines, and alcohol influence the porosity and filtering function of LSEC. In chronic liver disease and aging, morphological changes in LSEC, including capillarization, the loss of LSEC fenestration with formation of organized basement membrane, have been observed [117]. Thus, one has to evaluate such changes in order to better understand the co-culturing effect on LSEC. Differences in CYP3A4 activity were observed in response to being challenged with APAP. Co-culture with LSEC demonstrated typical response with an increase in CYP3A4 activity when challenged with APAP; however, co-culture with HUVEC had the opposite response. Others have seeded at a higher ratio of HepG2 to HUVEC and shown altered activity [103]. Although the physiological ratio of hepatocytes to ECs was used, one has to test other ratios to fully understand these effects. Further, one could compare the effect of HepaRG cells, which show different CYP450 enzyme activity [107] in similar settings and evaluate the effect of 3D and co-cultures of EC [118].

Hepatocellular metabolism of drugs is a well-orchestrated process with multiple pathways. In order to obtain detectable results in metabolic studies *in vitro*, high doses of APAP have been used which are toxic to humans [60, 63, 119]. For example, using 10 to 50 μM APAP concentration, which is equivalent to a 755 to 75,550 mg/L single dose. Nevertheless, using 10 to 40 μM APAP concentration on rat primary cells, effect of co-culturing LSEC, Kupffer cells, and hepatocytes in sandwich cultures was recently reported [120]. Effect on cell viability demonstrated reduction at 20 to 40 μM concentration in sandwich cultures. They also observed reduction in LSEC viability. However, no direct metabolic product analysis was performed. While high doses facilitate sensitive detection of metabolites and molecular mechanisms, toxic doses can lead to downregulation of enzymes as cells adapt to high drug concentrations by

desensitizing, internalizing, and then down regulating enzyme expression [121-123]. A dose of 1 μM was used, one of the lowest previously explored that also facilitated detection of three different metabolites formed via CYP450, UGT, and SULT enzymes.

Metabolism along these different pathways can be affected by many factors [124]. Interactions between pathways can play an important role in the metabolic outcome. Inhibiting or inducing enzyme activity along any of the pathways, in order to study one isoform or one pathway can skew results by the way cells compensate [125, 126]. Compensation can occur in the form of "metabolic switching, a phenomenon in which a change in metabolic pathway occurs either to the same enzyme family or to a different one [127]. While whole cells were used, many studies using isolated, microsomal isoforms may be able to avoid metabolic switching issues; however, one must consider that microsomes are not present in healthy, living cells [128].

Modeling biological liver tissue is complex as (1) precisely controlling the seeding and distribution of multiple cell types, (2) the challenge to achieve high cell density comparable to native tissues, and (3) difficulty in organizing 3D architecture of native tissue to mimic its accompanying microenvironmental cellular interactions are extremely difficult to incorporate [129-131]. However, seeding cells in pre-formed porous scaffolds depends on random distribution of cells in the pores. In order to develop highly structured organs with many distinct cell sub-populations [132-137], using novel technologies such as bioprinting would add value. Further, a physiologically relevant seeding ratio was used, but viability analysis of ECs showed a reduction relative to HepG2. At day 8, the ratio of ECs to HepG2 was nearly 1:10 instead of 1:5. Hence, seeding at a higher ratio would help in understanding the effect better. However, one must consider optimizing the culture medium that could equally support both the cell types.

CHAPTER V

EVALUATION OF THE METABOLIC FUNCTIONS OF MULTIPLE HEPARG TISSUE CULTURE PLATFORMS FOR USE IN DRUG SCREENING

5.1 INTRODUCTION

Drug-induced liver injury, termed hepatotoxicity, is the most common reason for the after-market withdrawal of a drug, despite effectiveness in treating a disease [138]. Currently available *in vitro* models do not mimic the *in vivo* performance of the liver thereby explaining shortcomings in predicting hepatotoxicity. HepG2 cells, frequently used to study the general cytotoxic potential of drugs, express very low levels of phase I drug-metabolizing enzymes such as cytochrome P450s [107, 139]. A more recently developed hepatic cell line differentiated from a hepatoma line is HepaRG, which have shown higher expression of P450 enzymes [140], comparable to primary human hepatocytes [141]. Increases in gene expression, enzymes, and transporters have been reported, relative to HepG2 [142, 143]. With the introduction of 3D culture techniques as early as 1912 [88], cells were shown to behave more organotypic when cultured in higher density [89]. Some have explored forming HepaRG spheroid cultures to

perform drug metabolic studies in 3D [109] and investigate alterations in enzyme expression/activity [144]. Although these results show differences in enzymatic activity, they suffer from two limitations: 1) non-uniformity in added drug and 2) difficulty in co-culturing other cells.

First, when cells are cultured in spheroids [140], addition of factors to medium is hindered by the creation of a concentration gradient across the spheroid. Typically, cells located in the periphery are exposed to higher concentration while those in the interior of the spheroid are exposed to lower concentration of the drug. Components added in the medium need to diffuse through freely via cells or cell-cell junctions [145]. Based on the organization of human liver which contains nearly 60 -70% hepatocytes and 30-40% nonparanchymal cells (<20% liver sinusoidal endothelial cells (LSEC) [82], and Kupffer cells), some have shown the importance of heterotypic cell-cell interactions. For example, co-culturing HUVEC and HepG2 cells is shown to restore some HepG2 cell function [103]. LSEC co-cultures have been shown to promote hepatocyte proliferation in co-culture systems or after partial hepatectomy [101]. Co-culturing with Kupffer cells to mimic inflammatory responses has also been investigated [146]. An alternative in developing 3D cultures is using porous matrices, which offer a 3D matrix where cells can be distributed evenly similar to *in vivo* conditions. Further, they provide an opportunity to develop high cell density cultures due to a high surface area to volume ratio [147]. These 3D structures have shown sensitivity of cells to the physical properties of the structure such as stiffness, pore size and void fraction in addition to chemical properties [148]. They have been generated and utilized in various tissue engineering applications [149].

The effect of co-culturing LSEC and HUVEC on HepaRG survival and functionality was investigated. Porous structures formed by freeze-drying of a CG solution, which have been extensively characterized in our group [94], were used. CG scaffolds made of 2% chitosan and

2% gelatin have a modulus of 5-12 kPa in hydrated conditions [96], making scaffolds i) conducive for adhesion of various cell types [150], and ii) optically transparent. How HepaRG function would change when cultured with liver native LSEC compared with non-native HUVEC was questioned. In addition, cultures were challenged with APAP. Significant effect of these culture configurations on HepaRG activity was shown.

5.2 MATERIALS AND METHODS

5.2.1 Chemicals

Chitosan (190–310 kDa MW and 85% degree of deacetylation, Catalog # 448877), gelatin type-A from porcine skin (Bloom300, Catalog # G2500), acetaminophen (APAP) (Catalog # A3035), acetaminophen-sulfate (Catalog #UC448), acetaminophen-gluconuride (Catalog # 43073), perchloric acid solution (Catalog # 311413), theophylline (Catalog # T1633), and sodium sulfate (Catalog # 71729) were all purchased from Sigma Aldrich Chemical Co. (St. Louis, MO). Absolute Ethanol (ACS grade, Catalog # 111000200), glacial acetic acid (ACS grade, Catalog # 281000ACS), and acetonitrile (Distilled/HPLC grade, Catalog # 300000DIS) were purchased from Pharmco-AAper (Shelbyville, KY). Phosphoric acid (85%, certified ACS Catalog # A242-212) was purchased from Fisher Scientific (Hampton, NH). Carboxyfluorescein diacetate succinimidyl ester (CFDA-SE) and live/dead cell viability assay kit (Catalog # L34951) were purchased from Invitrogen Corp. (Carlsbad, CA). eFluor® 670 (Catalog #) was purchased from eBioscience (San Diego, CA). Pierce™ BCA (bicinchoninic acid) Protein Assay Kit (Catalog # 23227) was purchased from Thermo Fisher Scientific (Waltham, MA).

5.2.2 Cells and Media

No-Spin HepaRG cells (terminally differentiated, hepatocellular carcinoma line, Catalog # NSHPRG), Base Medium with supplement (Catalog # MH100), Thawing and Plating Additive

(Catalog # MHTAP), and Plated Metabolism Additive (Catalog # MHMET) were purchased from Lonza (Basel, Switzerland). **Table 5.1** shows the maintenance and subculture process for all cells used in experiments. Liver sinusoidal endothelial cells (LSEC, Catalog # ACBRI 566), CSC Complete Medium with 10% serum (Catalog # 4Z0-500), CSC Passage Reagent Group (includes PRG1: an EDTA/dPBS solution, PRG2: a Trypsin/EDTA/dPBS solution, and PRG3: a Trypsin Inhibitor/PBS solution, Catalog # 4Z0-800) were all purchased from Cell Systems Corp. (Kirkland, WA). .

Table 5.1: Cell lines with materials and methods for culturing

Cells	Source	Maintenance medium	Centrifuge	Subculture process
HepaRG	Lonza	Base Medium with 12% Plated Metabolism Additive	100×g	Not subcultured. Plated using Base Medium with 12% Thawing and Plating Additive
LSEC	Cell Systems	CSC Complete Medium with 10% serum	150×g	Washed with EDTA/dPBS, detached using Trypsin/EDTA/dPBS, and neutralized with Trypsin Inhibitor Solution/PBS
HUVEC	BD Biosciences	200PRF Medium with 10% LSGS	125×g	Detached using trypsin/EDTA, and neutralized with trypsin neutralizer solution

Human umbilical vein endothelial cells (HUVEC-2) derived from single donors were purchased from BD Biosciences (San Jose, CA). Medium 200 phenol red free (PRF, Catalog # M-200PRF-500), low serum growth supplement (LSGS, Catalog # S-003-10), trypsin/EDTA (Catalog # R001100), trypsin neutralizer solution (Catalog # R002100) were all purchased from Life Technologies Corporation (Carlsbad, CA). The combinations of cell lines used in experiments are shown in **Table 5.2**

Table 5.2: Culturing combinations for 2D and 3D systems

Cell Culture Combinations		
HepaRG	**LSEC**	**HUVEC**
X		
X	X	
X		X

5.2.3 Porous Chitosan-Gelatin Scaffold Preparation

Discoid-shaped CG scaffolds of 10 cm diameter and 1 mm thickness were prepared as discussed in Chapter 4. In brief, dry CG scaffolds were placed in sealed petri dishes, wrapped in aluminum foil, and stored in a desiccator until time of use. The CG scaffolds were cut down to 34 mm diameter discs prior to the 24-hour neutralization process. A sterilized, 34 mm diameter nylon mesh was placed on the bottom of wells for 3D systems. Neutralized, CG scaffolds were placed on top of the mesh, rinsed with sterile PBS to remove trace ethanol, and soaked in HepaRG media for 2 hours.

5.2.4 Cell Culture in 2D and 3D Systems

In parallel with HepG2 experiments, HepaRG experiments were carried out in triplicate for each cell culture condition and system. In brief, one set of experiments contained pre-stained cells for imaging and viability analysis, while the other contained non-stained cells for enzyme activity analysis.

The same cell culture timeline used in HepG2 experiments were employed in HepaRG experiments. In brief, 0.5×10^6 HepaRG cells were seeded on Day 0 and allowed 24 hours to attach to the well bottom or CG scaffold, depending on dimensionality of the experiment, prior to the addition of media. Media was added to all cultures to render a total liquid volume of 2 mL.

On day 3, media was changed and, 100,000 LSEC or HUVEC were seeded in cocultures based on the physiological ratio of hepatocytes to endothelial cells in an adult liver. Endothelial cells were given allowed to attach, same as HepaRG. A ½ and ½ mixture of HepaRG and EC medium was used in cocultures to accommodate the two cell types. After the cultures were well established, (8 days) they were split into two groups:

Group 1: Controls: no APAP was added and cultured by adding medium, as before.

Group 2: Treated: Cells were challenged with APAP at a concentration of 150 µg/mL.

The same 5 mg/mL stock solution of APAP from HepG2 experiments was used.

A 25 µL sample was taken from each well every six hours for 24 hours, including a sample at the zero time point. The media changes and time point samples were stored in 2 mL centrifuge tubes at -20 °C until time of analysis.

5.2.5 Determining Cell Distribution

In order to understand the distribution and viability of cells, separate experiments were performed where HepaRG cells were pre-stained with eFluor® 670 following the vendor's protocol. In brief, a 10 µM solution of eFluor® 670 in PBS was mixed in equal parts with a hepatocyte cell suspension. The mixture was then incubated for 10 minutes at 37°C in the dark. Cells were washed twice with media prior to seeding. In co-culture studies, endothelial cells were stained with a 1 µM CFDA-SE solution, according to the vendor's protocol. In brief, a CFDA stain solution was added to cell suspension and incubated at 37 °C for 20 min, followed by washing of the excess stain with PBS and then cell seeding.

For 2D experiments, micrographs were taken on days 1, 3, 4, 6, and 8. After the seeding of EC's, digital and fluorescent micrographs were captured at the same location through an inverted microscope outfitted with a CCD camera.

All treated and non-treated CG scaffolds were harvested and fixed after 9 days in culture. Scaffolds were split into two parts, and the following three analyses were performed:

- Half of the split scaffolds from 3D experiments were stored in 1 mL of PBS and frozen until viability analysis was performed, as described in Chapter 4.

- The other half of the split scaffolds were immediately analyzed by confocal imaging using a confocal microscope as discussed in Chapter 4. In brief, images were taken throughout the scaffold thickness along the z-axis. At each step, the two fluorescent signals of hepatocyte and endothelial stains were collected. In co-cultures, the fluorescent signals of hepatocyte and EC's at the different steps along the z-axis were overlapped to obtain a single image at each location.

- The half CG scaffold used in confocal microscopy was washed with PBS to remove trace media. The CG scaffolds were then fixed as discussed in Chapter 4. In brief, scaffolds were submerged in a 3.7% formalin solution for 45 minutes at room temperature, washed with PBS (×2), and submerged in 2 mL of absolute ethanol. The 6-well plates in which the CG scaffolds were housed were tightly sealed using paraffin film and stored at 4 °C. CG scaffolds were then processed according to standard H/E staining protocols. The samples were sliced 4 μm thick and sealed in slides. Bright field micrographs were taken and cell morphology and distribution were analyzed. Twenty-four hours prior to SEM analysis, the fixed CG scaffolds were vacuum dried. Dry samples were attached to 10

mm diameter aluminum stubs using a conductive graphite glue and sputter-coated with gold for 1 minute.

5.2.6 Determining Cell Viability

All cultures and conditions were analyzed by fluorescence for viability, using the standard curves developed and discussed in Chapter 4. In 2D experiments, cell culture wells were aspirated of media, filled with 1 mL of PBS, and frozen at -80 ºC. In 3D, the experimental wells and half scaffolds were analyzed separately. The half scaffolds, placed into a new 6-well plate, and the 3D experimental wells were filled with 1 mL of sterile PBS and frozen at -80 ºC. The number of viable cells per well for each condition was determined by lysing cells via a repeated freeze-thaw cycle and measuring fluorescence released from pre-stained cells. A 150 µL sample was taken from each well and pipetted into a black, 96-well plate. Fluorescence was measured using a Spectramax GeminiXS spectrophotometer with excitation wavelengths of 485 and 615 nm and emission wavelengths of 538 nm and 660 nm for endothelial cells and hepatocytes respectively.

5.2.7 Protein Content and Albumin Secretion Analysis

A BCA assay was used to evaluate the total protein content of the supernatant of media changes, according to the vendor's protocol. Identical to HepG2 analysis methods, a sample diluted by mixing 25 µL of supernatant in 100 µL of PBS was mixed with 200 µL of the working reagent mixture. An Emax spectrophotometer was used to measure absorbance at 490 nm, and converted to concentration using the standard curves created and discussed in Chapter 4.

A Bromocresol Green (BCG) albumin assay kit was used to measure the albumin concentration of the supernatant collected during media changes. In brief, 5 µL of supernatant was pipetted into a clear, 96-well plate, followed by the addition of 200 µL of Reagent. Solutions were mixed by light tapping and then incubated for 5 minutes at room temperature. Absorbance was measured

using an Emax microplate reader (Molecular Devices) at 650 nm. Albumin concentration was converted from absorbance using an exponential standard curve. This assay was not performed in HepG2 experiments due to the presence of phenol red in the maintenance media, which interferes with absorbance readings.

5.2.8 APAP and Metabolite Analysis

Sample preparation was performed similar to previously reported methods [106] and identical to HepG2 metabolic analysis methods. In brief, 25 µL sample aliquots were deproteinated by the addition of a 6% perchloric acid solution, containing 10 mg/mL of theophylline at twice the sample volume. Supernatant was aspirated and placed into a glass vial for analysis. A 10 µL injection volume was analyzed by the same HPLC methods discussed in Chapter 4. Chromeleon® software was used to control of all components of the Dionex HPLC system. An isocratic mobile phase consisting of 93% 0.05 mM sodium sulfate solution and 7% acetonitrile was used for sample separation (pH 2.2). A constant flowrate of 1.5 mL/min and temperature of 30 °C were maintained throughout separation. APAP and metabolites were resolved on the C18 column, preceded by a guard column with a 5 µm particle diameter. Detection of APAP and metabolites was achieved using UV absorbance of 254 nm. Prior to analysis, samples were equilibrated to room temperature for 60 min. For clinical data comparison, APAP concentration values from HPLC analysis were converted to conversion.

5.2.9 Enzymatic Activity Analysis

Due to the inability of HPLC methods to detect APAP-GSH concentrations, enzyme activity along the bioactivation pathway was evaluated. A CYP 3A4 activity assay was used to assess enzyme activity for all cultures and conditions, as well as cell-free environments as discussed in Chapter 4. In brief, HepaRG cells were washed with medium prior to the addition of the

substrate and incubated at 37 ºC for 50 minutes in the experimental wells. Then 25 µL from each well was transferred into a white 96-well plate, followed by the addition of 25 µL of luciferin detection reagent for reaction initiation. The 96-well plate was incubated for 20 minutes at room temperature. A DTX 880 Multimode Detector was used to quantify luminescence and thus enzymatic activity.

5.2.10 Statistical Analysis

Each set of experiments (stained and non-stained) was performed in triplicate for each culture and condition combination. Viability and CYP 3A4 activity averages are based on results from non-stained and stained sets respectively. Total protein content and metabolism averages are based on data from both stained and non-stained experiments, for a total of six data points. In order to determine significance of variance, ANOVA analysis was performed.

5.3 RESULTS

5.3.1 Morphological Changes in 2D During Cell Culture Timeline

In 2D cultures, HepaRG cells were uniformly distributed and attached to tissue culture plastic on Day 1 (**Figure 5.1**). Some random migration of HepaRG cells were observed from Day 1 to Day 3. Reorganization of hepatocytes and EC, both LSEC and HUVEC, was observed in all 2D cultures. EC were observed to attach in and around established HepaRG colonies, suggesting cell-cell communication. The morphology of HepaRG cells appeared to differ throughout the culture timeline. As the HepaRG reorganized, regions of extremely compact cells with easily identifiable nuclei were observed (**Figure 5.1**). This change in morphology occurred in all culture conditions and systems.

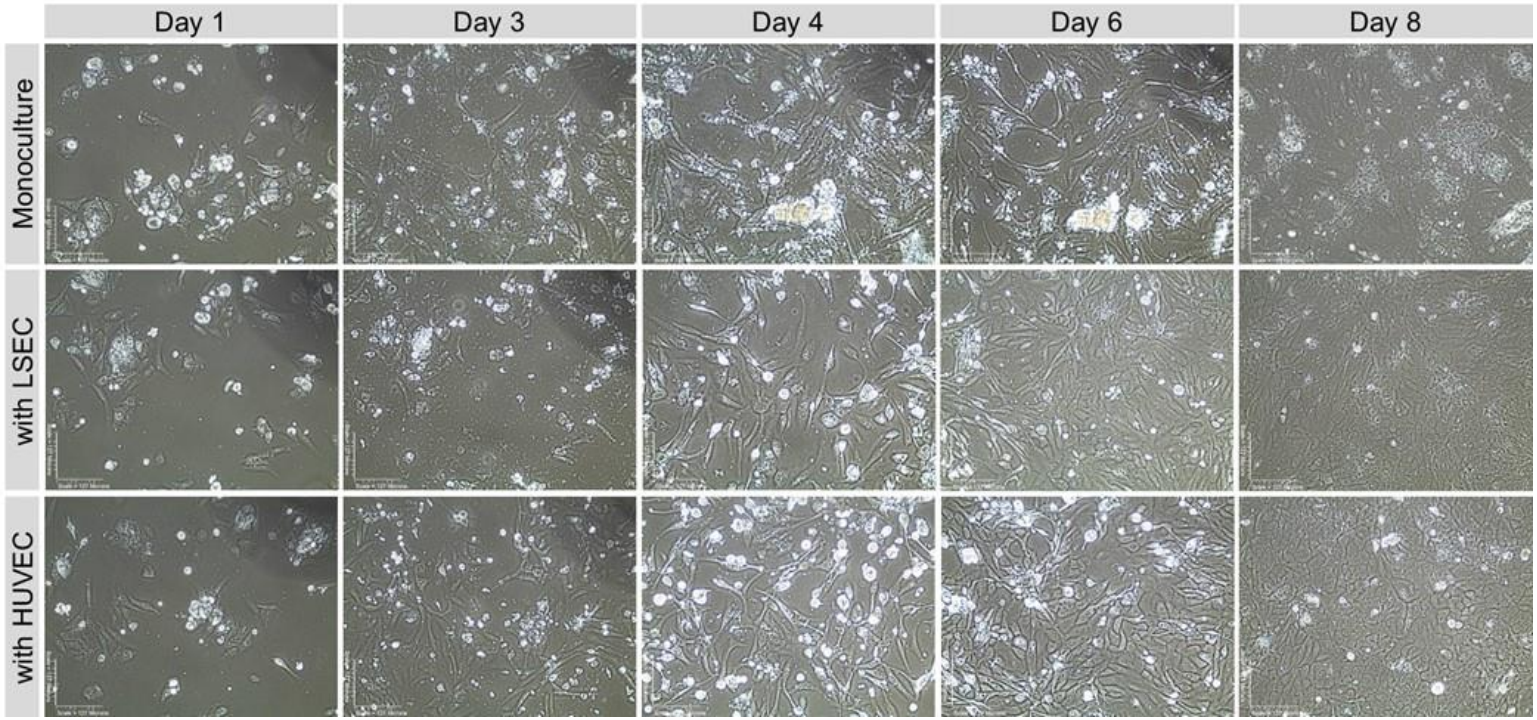

Figure 5.1: Digital micrographs of 2D cultures for observation of morphology and distribution

Fluorescent micrographs were captured at the same locale as light microscopy to compare and discern different cell types. CFDA-stained ECs attached to tissue culture plastic surfaces amongst and around the edges of HepaRG cells (**Figure 5.2**).

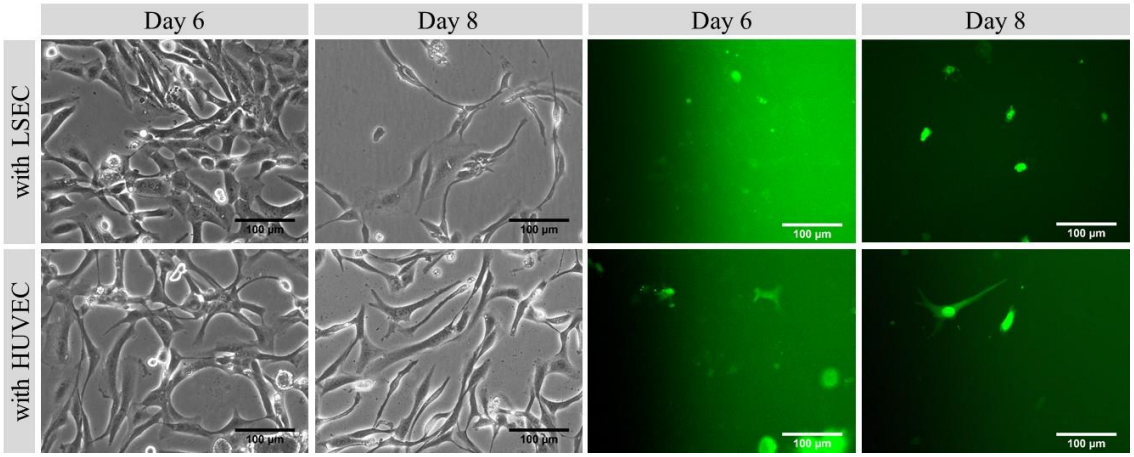

Figure 5.2: Digital and fluorescent micrographs show cell distribution in coculture with respect to time. The fluorescent images make HUVEC/LSEC (green fluorescence) discernable from HepG2

In all cultures, LSEC was smaller in size than HUVEC when comparing fluorescent images. The cytoplasmic portion of HUVEC were more prominent compared with LSEC.

5.3.2 Evaluating the Distribution of Cells in 3D Cultures

Unlike 2D cultures, evaluating cell distribution needs observations at different depths within the porous structure. Hence, confocal imaging was employed to evaluate cell distribution in 3D cultures. Comparison of fluorescent images at various depths demonstrated that the efluor-stained HepaRG, CFDA-stained LSEC, and CFDA-stained HUVEC were present in the scaffold (**Figure 5.3**). HepaRG were observed with considerably higher frequency compared to endothelial cells, in agreement with the seeding ratio of 5:1.

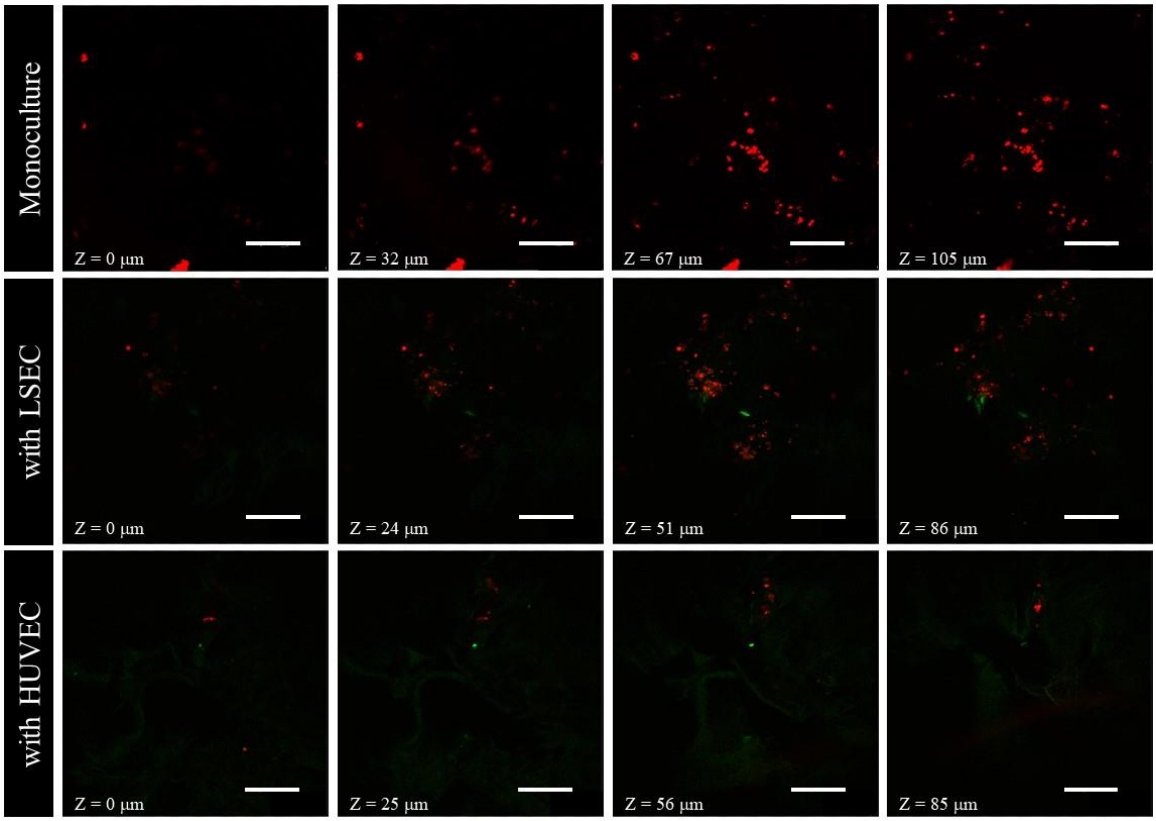

Figure 5.3: Confocal images of 3D cultures with HepG2 cells (red) and LSEC/HUVEC (-green) at different depths confirming 3D configuration. (scale = 100 µm)

Additional analyses using scanning electron microscopy and histology were performed to confirm cell distribution in 3D at the surface. Similar to previous reports, these analyses confirmed the presence of cells and some matrix elements in porous structures. Only a few representative micrographs are shown (**Figure 5.4**).

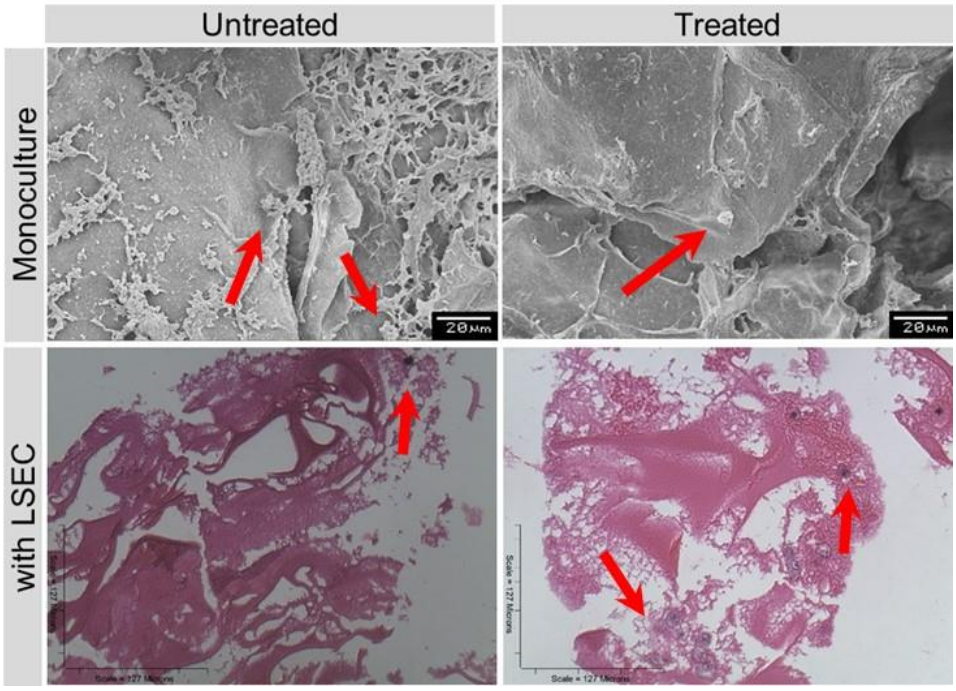

Figure 5.4: Micrographs of HepaRG cells after 9 days of cell culture (top row) at the scaffold surface captured by SEM and (bottom row) showing the cross-sectional view of H&E stained scaffolds. Arrows indicate the location of HepaRG cells

The combination of confocal imaging and SEM, confirmed that cells were distributed in 3D.

5.3.3 Evaluation of Cell Viability

Various imaging techniques qualitatively confirmed the presence of cells and their uniform distribution in both 2D and 3D cultures. In order to further understand those results quantitatively, viability of cells was determined using pre-stained cells. As two different fluorescent stains were used to identify hepatocytes and ECs, they were also used to quantify the number of each cell type. These results showed (**Figure 5.5a**) that HepaRG viability on Day 9 was nearly double in 3D monoculture relative to 2D monoculture, suggesting improved viability in 3D configuration. Interestingly, the presence of LSEC significantly improved the survival rate

in 2D culture and similar viability was observed in 3D cultures. However, presence of HUVEC in 2D cultures did not change cell viability. On the contrary, presence of HUVEC in 3D cultures decreased cell viability.

When EC viability was analyzed, these results varied by dimensionality (**Figure 5.5b**). Higher EC viability was observed in 3D cultures compared with 2D cultures for both cell lines. Presence of a higher number of HUVEC in 3D cultures with reduced HepaRG cultures suggest that these interactions may not be favorable for the survival of HepaRG cells and origin of EC affects survival of HepaRG cells.

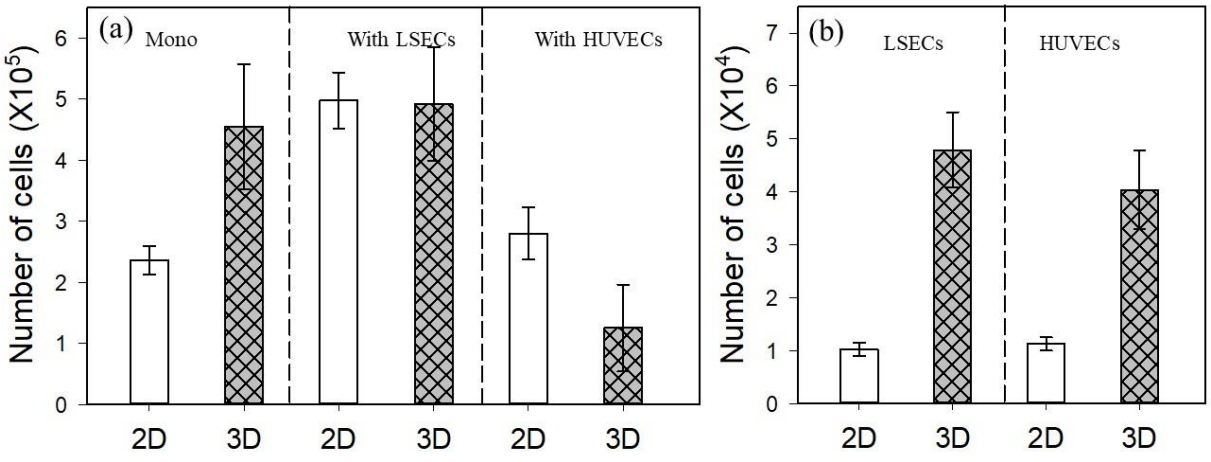

Figure 5.5: Relative viability for a) HepaRG cells in monoculture and co-culture with LSEC or HUVEC and b) LSEC and HUVEC in coculture

5.3.4 Assessment of Total Protein Content and Urea and Albumin Synthesis

In order to better understand the viable cell population and the effect of co-culture on hepatocytes, first, total protein content was evaluated during nine day culture. Since a 1:1 mixture of HepaRG medium with respective EC medium was used, the total protein content for the three media mixtures (pure HepaRG medium, ½ and ½ HepaRG and LSEC media, and ½ and

½ HepaRG and HUVEC media) were analyzed. When fresh media was analyzed, the protein content of the HepaRG and LSEC mixture had the highest protein content, followed by pure HepaRG medium, and then the HepaRG and HUVEC mixture. The protein content of the ½ and ½ mixtures were normalized for total protein content to pure HepaRG medium. Both monoculture and co-culture with LSEC showed increase in protein content during the culture duration (**Figure 5.6a**). An abrupt increase in protein content was observed from Day 8 to Day 9, which could be partially attributed to some toxicity effect of APAP damaging the cell membrane. This could also be due to the adaptation of cells for acute toxicity.

However, co-cultures with HUVEC showed a reduction in the total protein content from day 4 and a moderate increase at day 9. This could be due to a reduced number of viable cells. There was no significant difference between the protein content of 2D and 3D cultures. Protein content was not affected by dimensionality or co-culturing with HUVEC.

Urea is solely synthesized in the liver and is commonly used to assess hepatocyte function. Urea production (normalized by the total protein content of media changes) was relatively constant over the nine day period for all experimental setups, with the exception of 3D and 2D co-culture with HUVEC's (**Figure 5.6b**). In both monocultures and co-cultures with LSEC, a decreasing trend was observed during the culture period. On the contrary, an increase in urea content or similar levels of production were observed in both 2D and 3D co-cultures with HUVEC. This trend could be confounded by the fact that the urea values were normalized by the total protein content. In any case, these results suggest that the cells that were viable had similar functionality.

In order to further understand the cell viability and function of HepaRG cells, albumin secretion was assessed in culture supernatants. Albumin secretion in HepaRG monocultures increased (**Figure 5.6c**) in the beginning until day 4 and then remained relatively constant in both 2D and

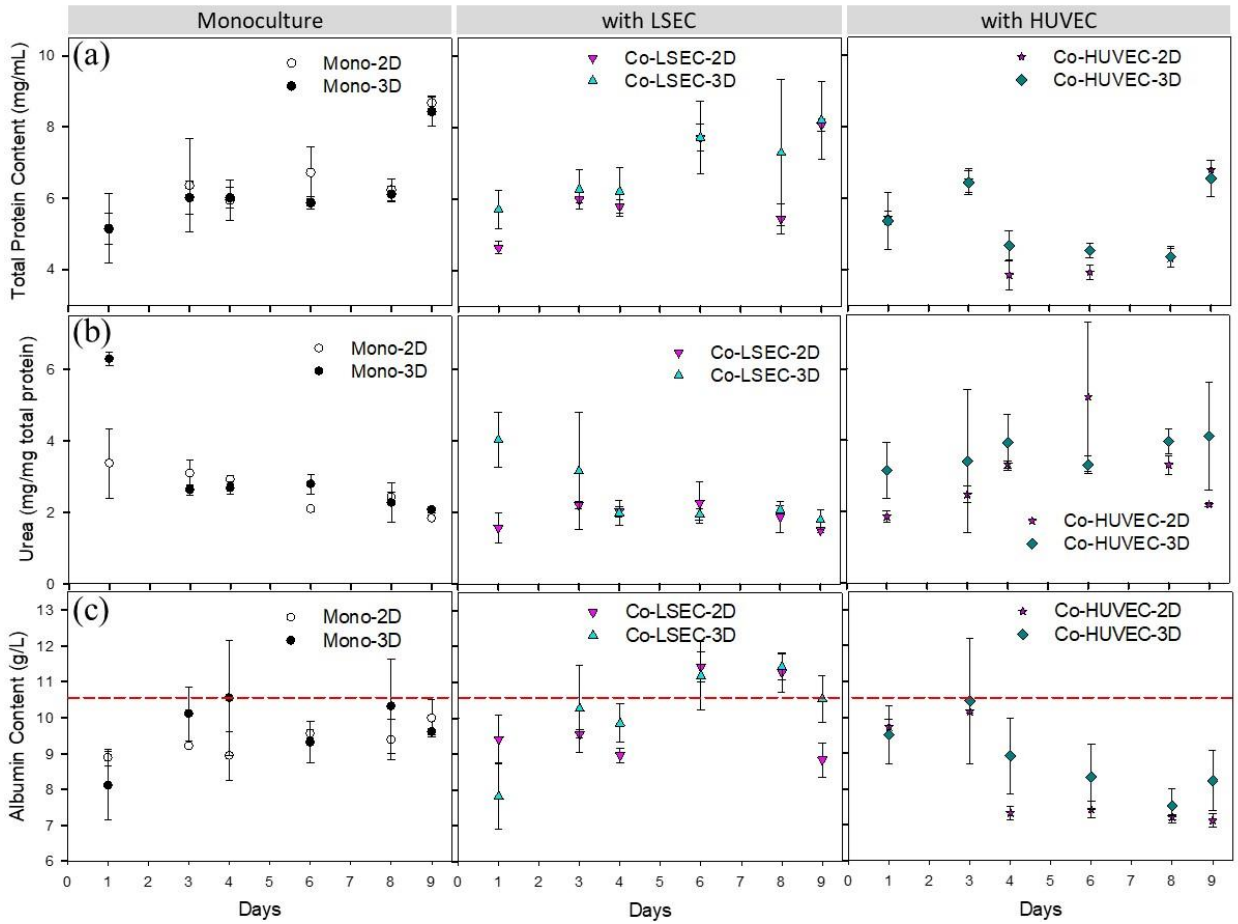

Figure 5.6: Concentration time profiles for (a) the total protein content, (b) urea synthesis, and (c) albumin synthesis in experimental setups

3D cultures. Co-cultures with LSEC showed further improvements over the nine day period for all experimental setups, with the pattern mimicking the total protein content. Similarly, co-culture experiments with HUVEC showed reduced albumin secretion after four days, mimicking the total protein content. Comparison of 2D cultures to 3D cultures suggests that the configuration did not affect the functionality of HepaRG cells. However, type of cells used in co-cultures significantly influenced the performance of HepaRG cells.

5.3.5 APAP Metabolism

As the intent of this work was to evaluate various cell culture conditions for use in drug screening, hepatic function was assessed through drug metabolism studies. APAP conversion was highest in 3D co-culture with LSEC, followed by 2D co-culture with LSEC and 3D co-culture with HUVEC (**Figure 5.7a**). Two dimensional co-culture with LSEC and 3D co-culture with HUVEC yielded similar APAP conversions at sample time points of 12 hours through 24 hours.

Production of the APAP-sulfate conjugate followed a general increasing trend for most cultures, but 2D cocultures yielded results with the highest production values (**Figure 5.7b**).

The production of APAP-glucuronide was much lower than expected when compared with simulation predictions. Two dimensional co-culture with HUVEC yielded the highest production value, followed by 2D co-culture with LSEC (**Figure 5.7c**). Three dimensional cultures appeared to produce very little APAP-glucuronide.

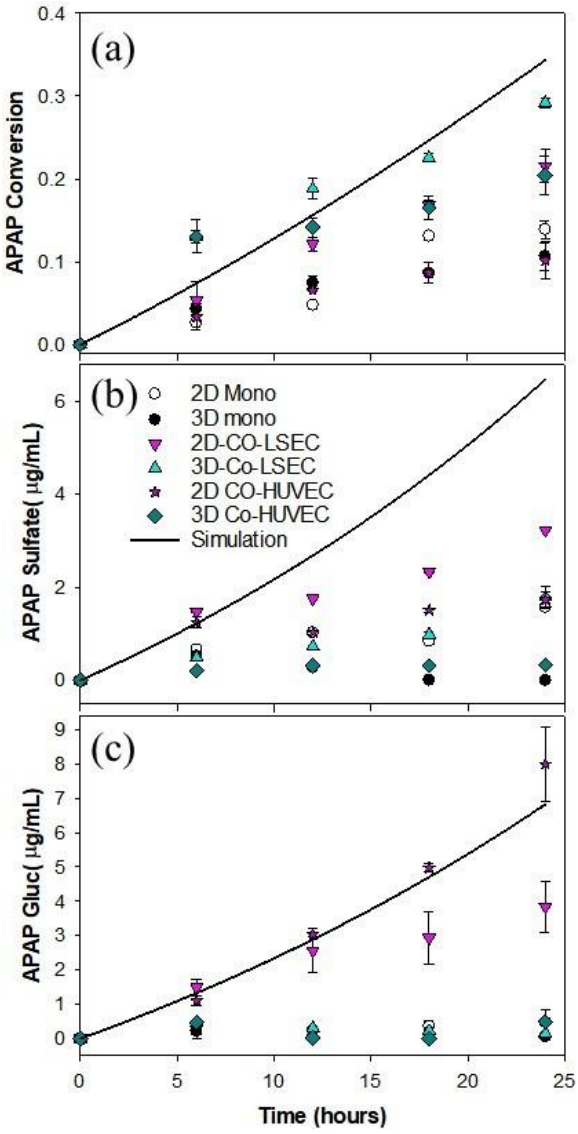

Figure 5.7: Metabolic profiles for (a) APAP conversion, (b) APAP-sulfate concentration production, and (c) APAP-glucuronide concentration production

5.3.6 Changes in CYP Enzyme Activity

The most abundant cytochrome P450 enzyme in the liver is CYP 3A4. CYP 3A4 is responsible for the metabolism of more than 50 % of all marketed drugs. Further, others have shown that HepaRG cells have the highest CYP34 activity, relative to other hepatocyte cell lines [143]. In

order to understand culturing effects on enzyme activity changes in CYP 3A4 enzyme activity were assessed. These results showed that CYP 3A4 activity was significantly higher in all 2D cultures when compared with 3D counterparts. The highest CYP3A4 activity was observed in HepaRG monoculture, followed by co-cultures with LSEC. Higher CYP 3A4 activities were observed in untreated 2D cultures for both monocultures and co-cultures with HUVEC (**Figure 5.8)**.

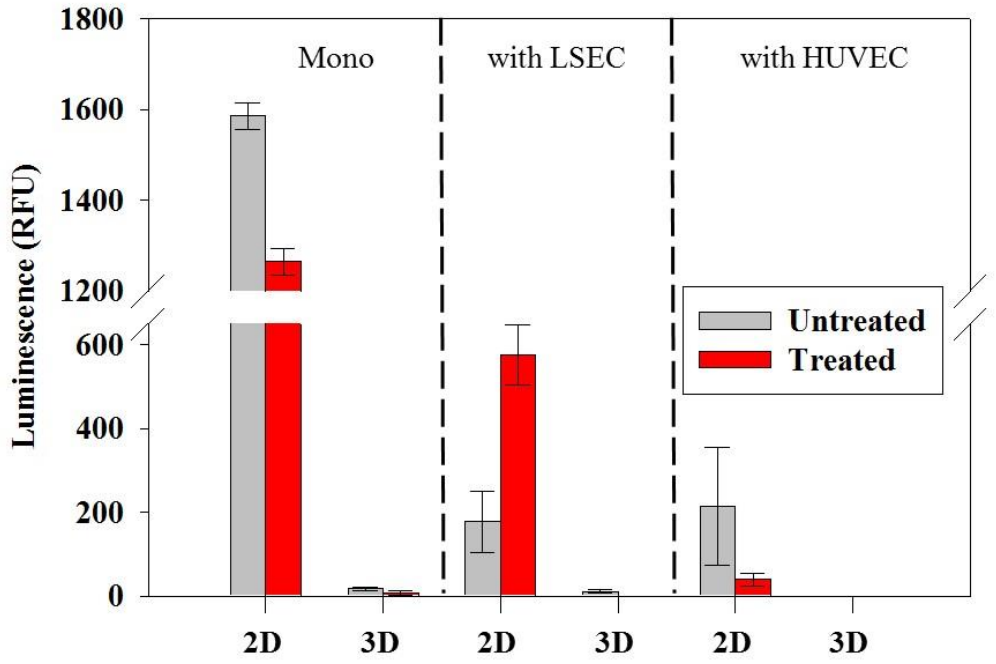

Figure 5.8: CYP 3A4 activity in HepaRG tissue cultures

This is in contrast to findings with HepG2, where only co-cultures with HUVEC had higher activity in untreated cultures. The relative luminescence values were significantly higher than those observed in HepG2 experiments, suggesting that the bioactivation pathway is more active in HepaRG cells.

5.4 DISCUSSION

In this study, the influence of culturing HepaRG cells in combination with LSEC and HUVEC on cell viability and functionality was investigated. Morphological changes in HepaRG were observed over the culturing timeline. Migration of HepaRG cells through Day 8 was observed, similar to that reported for the first three days [151]. HepaRG also demonstrated abilities to reorganize themselves into colonies in 2D, suggesting the occurrence of homogeneous cell-cell communication. The formation of bile canaliculi was observed, as others have shown during shorter culture periods [141]. The functionality of bile canaliculi specific transporters should be investigated to confirm their presence. In 3D porous structures, HepaRG cells were observed both individually and in clusters. The relative viability data for HepaRG was highest, and comparable to initial seeding, in both 2D and 3D co-cultures with LSEC and 3D monocultures. This suggests that the CG porous scaffolds are conducive for culturing HepaRG cells and the microarchitecture of those scaffolds are also suitable. Further, total protein secretion was not sensitive to dimensionality. The relatively constant value throughout the culture timeline suggests that protein secretion functions were stable and maintained. In addition, one could blend heparan sulfate to chitosan and gelatin and form porous structures to mimic the liver architecture. One could also add other cell types such as Kupffer cells in 3D liver tissue constructs to test the effect on metabolism of APAP [152].

In co-cultures, LSEC and HUVEC attachment was observed amongst and/or around HepaRG colonies, suggesting the occurrence of heterogeneous cell-cell communication. HepaRG cells demonstrated sensitivity to the EC line used. HepaRG viability in the presence of HUVEC decreased significantly relative to LSEC. This is unlike the results obtained using the HepG2 derived C3A cell line in combination with HUVEC [153]. Those co-cultures showed improvements in albumin synthesis by day 3 and less toxicity towards APAP. On the contrary,

there was a reduction in albumin secretion on day 6 in co-cultures of HepaRG and HUVEC cells. Further investigation into whether these sensitivities are due to changes in media composition [154] or cell-cell interaction is necessary. Also, this study focused on evaluating the functionality of HepaRG cells. Evaluation of EC activity in these set ups need to be performed as well. Some have shown the importance of HepG2 cells in remodeling of HUVEC and their importance in providing physical support [155]. In order to understand the such interactions, one could measure the production of nitric oxide (NO) and hydrogen peroxide by EC and compare the difference in the level between HUVEC and LSEC.

In this study, a 1mM concentration of APAP was used, unlike other studies which have used higher concentrations [118]. Comparison of total protein secretion with and without APAP challenge showed some increases in conditions containing APAP. This could be due to either cells responding to APAP or some toxicity. Further, investigation into understanding the cell growth during the culture time would help understand these issues. Some using HepaRG spheroid cultures, some have shown the effect of APAP metabolism and alterations in enzymes [144]. However, direct comparison with such results are hindered by cell distribution of APAP. The trend for APAP-sulfate production was observed in simulation and experimental metabolic profiles. APAP-glucuronide production in experimentation did not match well with simulation; however, production was increased compared with HepG2 profiles.

Enzymatic activity for CYP 3A4 was higher in co-culture with HUVEC for 2D and 3D cultures. The enzymatic activity of CYP 3A4 was difficult to detect in 3D cultures. In 2D, CYP 3A4 activity was significantly higher in HepaRG cultures compared to HepG2. This was particularly evident in monocultures. The increased CYP 3A4 activity in HepaRG cultures compared with HepG2 is in agreement with previous reports [107, 156]. The addition of EC decreased activity. HepaRG activity alone may be higher than that seen *in vivo*; thus rendering co-cultures superior.

Some researchers have reported higher activity in HepaRG compared with primary human hepatocytes for CYP 3A4. This study revealed that HepaRG cultures are metabolically superior to HepG2 cultures. Co-culture with HepaRG cells performed best, particularly with LSEC. This indicates metabolic results are sensitive to the endothelial cell line used in co-culture. Further investigation into diffusion limitations of APAP-glucuronide and APAP-GSH in the scaffold region should be pursued.

In this study, evaluation of whether the use of a terminally differentiated cell line, like HepaRG, would yield different results than an immortalized cell line, like HepG2, when set up under identical conditions was performed. The initial seeding distributions of HepaRG were observed to be homogeneous in 2D. Between Days 1 and 3, rearrangement of HepaRG cells into colonies was observed, similar to that seen in HepG2 experiments. In addition to rearrangement, the development of bile canaliculi was observed when dense HepaRG colonies were formed. In co-culture experiments, both LSEC and HUVEC were attached amongst and around the outer edges of the established HepaRG colonies, again suggesting the occurrence of heterogeneous cell-cell communication, similar to HepG2 experiments. The distribution of cells in 3D was confirmed by multiple approaches. The relative viability of HepaRG on Day 9 was comparable to the initial seeding density for 3D monocultures and 2D and 3D co-cultures with LSEC. Monocultures in 2D and co-cultures with HUVEC in 2D exhibited around 50% viability, compared with initial seeding. The relative viability for endothelial cells was higher in 3D for both LSEC and HUVEC. Total protein secretion was comparable between 2D and 3D on respective days and within respective cultures (monoculture, co-culture with LSEC, and co-culture with HUVEC), through Day 9. Total protein secretion remained relatively constant within respective cultures throughout the culture process, indicating maintenance of that particular function. Experimental metabolic profiles for HepaRG cultures were also compared with scaled simulation profiles from Aim 1.

Co-culture in 3D with LSEC yielded results that closely matched simulation, followed by 2D co-cultures with LSEC and 3D co-cultures with HUVEC. APAP-glucuronide formation results from HepaRG experiments were significantly lower than simulation, but also higher than in HepG2 experiments. The increasing trend in the APAP-sulfate amount produced with respect to time was observable in both 2D and 3D LSEC co-cultures, as well as 2D co-culture with HUVEC; however, all APAP-sulfate production results were slightly lower than those observed in HepG2 experiments and in simulation. The metabolite APAP-GSH was still not detectable by the HPLC methods used, though the CYP 3A4 enzymatic assay demonstrated much higher activity in HepaRG experiments compared with HepG2. Enzymatic activity was considerably higher in 2D than 3D experiments. This could be due to diffusion limitations of the detection reagent into or out of the scaffold. Enzyme activity was activated in treated co-cultures with LSEC, but activated in non-treated cultures in monocultures.

CHAPTER VI

CONCLUSIONS AND RECCOMMENDATIONS

6.1 CONCLUSIONS

The goal of this study was to create a tissue culture platform for use in drug development for which experimental results could be connected to clinical data by incorporation of computational modeling, thereby creating a method of validation for experimental results. There has been significant development in generating 3D synthetic tissues using various techniques [109, 157-159]. Three dimensional systems provide a new integrative level, which is a complex environment where cells can interact, create cellular networks, and extend processes. Many synthetic tissues are developed based on the fundamental understanding that cell-cell and cell-matrix interactions in 3D systems are crucial to integrate the extensive signaling pathways, and the biophysics that regulate the development and regeneration of tissues [149]. Cell-cell interactions between hepatocytes and nonparenchymal cells have been shown to alter the functionality of hepatocytes [101], prolonging CYP-450 activity and albumin production. While

tissue culture models using a wide range of techniques have demonstrated the ability to provide PK values and metabolic profiles, there is currently no method for validating local tissue culture results by tying to clinical data. I decided to address the lack of a validation methodology by incorporating computational modeling to act as a bridge for scaling between local tissue culture and clinical data. To achieve this goal, the project was split into three aims. Aim 1 was to i) develop a computational model that was capable of mimicking clinical data at physiologically relevant conditions using kinetic constants from literature, and ii) determine whether the computational model could be used for scaling between different initial doses, cell densities, and bioreactor sizes. Aim 2 was to evaluate the impact various tissue culturing techniques had on i) metabolic function by comparing experimental results to scaled simulated metabolic profiles, ii) enzymatic activity, and iii) protein synthesis, using a commonly used cell line, HepG2. Aim 3 employed the same evaluation methods and endpoints, but used an alternative hepatocyte cell line, HepaRG.

6.1.1 Conclusions from Aim 1:

I investigated numerous kinetic constants for the three metabolic pathways of APAP metabolism. In addition to compiling kinetic constant values for enzyme specific and total contributions to the different metabolic paths, I also explored multiple forms by which reaction rates could be expressed, including i) individually by each enzyme ii) as a grouped sum contributing to total metabolism, iii) individually by each enzyme, but weighted by abundance or contribution to metabolism. The metabolic distribution of APAP and metabolites 24 hours after dosing for different combinations of kinetic constants and reaction rate considerations were compared with clinical distributions at the same time point. At the physiological hepatocyte density, the combination of i) a bioactivation reaction rate equation employing individualized kinetic parameters weighted by each enzyme's contribution to metabolism and ii) kinetic constants given

in literature as total contributions to metabolism for both the sulfation and glucuronidation pathways yielded a metabolic distribution that most closely matched clinical distribution. The effect of initial dose was evaluated to determine whether results would follow mechanistic trends. The glucuronidation pathway is considered high capacity; therefore, a trend of increased APAP-Gluc production should be seen with an increase in dose. The sulfation pathway is considered high affinity; therefore, a trend of decreased APAP-sulfate production with an increase in dose should be observed. Both of these trends were observed with contribution weighted kinetics were considered, further confirming the validity of the computational model. Cell density scaling was also investigated. As expected, APAP conversion and all metabolite yields increased as cell density increased. Exploration of changing the well-size of the static bioreactor indicated that metabolic profiles were not sensitive to such changes, suggesting scaling of using the computational model was possible. The ability to i) match clinical metabolic distribution, ii) follow dose related mechanistic trends, iii) adhere to expected results for changes in cell density, and iv) lack sensitivity to changes in bioreactor size, affirmed the ability of the developed computational model to be used to tie together experimental and clinical data as a method for validation.

6.1.2 Conclusions from Aim 2:

Aim 2 was devoted to determining the culturing condition which yielded metabolic and hepatic function data that most closely matched clinical data using commonly used HepG2 cells. In 2D, initial seeding distributions of HepG2 cells were observed to be homogeneous over the plate bottom, and rearrangement of HepG2 cells into colonies was observed between Days 1 and 3 for both mono and cocultures. Endothelial cells, both LSEC and HUVEC, were shown to attach amongst and around the outer edges of HepG2 established colonies, suggesting the occurrence of cell-cell communication. Cell growth/spreading in 2D was qualitatively observed in all cultures

and was particularly high in cocultures with HUVEC. In 3D cultures, cell distribution in all 3 dimensions was confirmed by multiple approaches. A relative viability assessment for hepatocytes showed that HepG2 viability was comparable across all cultures. In the case of the relative viability assessment for endothelial cells, HUVEC demonstrated higher viability than LSEC. Total protein secretion was evaluated as a measure of hepatocyte function, and was comparable in 2D and 3D cultures relative to each mono or coculture condition for each day, through Day 8. A major focus of Aim 2 was to compare experimental metabolic profiles with scaled simulation profiles from Aim 1. Three dimensional coculture with HUVEC yielded an APAP consumption profile that more closely matched simulation, followed closely by 2D and 3D coculture with LSEC and 3D monoculture. For the major APAP metabolic product, APAP-glucuronide, all experimental results were significantly lower than simulation. Experiments using other drugs have reported up to a thousand-fold decrease in APAP-glucuronide production compared with primary hepatocytes. Similar APAP-sulfate production trends were observed between simulation and experimental data, with the exception of 3D monocultures and 3D cocultures with LSEC. The metabolite APAP-GSH, produced by CYP450s, was not detectable by the HPLC methods used. An enzymatic assay was performed to determine whether CYP 3A4, one of the major contributors to APAP bioactivation, was active. The assay indicated that CYP 3A4 was active in all 2D culture conditions and 3D cocultures with HUVEC. CYP 3A4 activity was undetectable in the other 3D culture settings. Activity was higher for all cocultures with HUVEC. Increased enzymatic activity was observed in monocultures and cocultures with LSEC that were challenged with APAP. Observance of the activation of CYP3A4 activity in untreated cocultures with HUVEC indicate that coculture of hepatocytes with a non-native liver cell line can cause changes in behavior as activation should occur in treated hepatic cultures. Considering all of the metabolic, functional, and enzymatic data, I would consider the coculture with LSEC in 2D to be superior to the other systems.

6.1.3 Conclusions from Aim 3:

In Aim 3, I wanted to determine whether use of a terminally differentiated cell line, like HepaRG, would yield different results than an immortalized cell line, like HepG2, when set up under identical conditions. The initial seeding distributions of HepaRG were observed to be homogeneous in 2D. Between Days 1 and 3, rearrangement of HepaRG cells into colonies was observed, similar to that seen in HepG2 experiments. In addition to rearrangement, the development of bile canaculi was observed when dense HepaRG colonies were formed. In coculture experiments, both LSEC and HUVEC were attached amongst and around the outer edges of the established HepaRG colonies, again suggesting the occurrence of cell-cell communication, similar to HepG2 expeeriments. The distribution of cells in 3D was confirmed by multiple approaches. The relative viability of HepaRG on Day 9 was comparable to the initial seeding density for 3D monocultures and 2D and 3D cocultures with LSEC. Monocultures in 2D and cocultures with HUVEC in 2D exhibited around 50% viability, compared with initial seeding. The relative viability for endothelial cells was higher in 3D for both LSEC and HUVEC. Total protein secretion was comparable between 2D and 3D on respective days and within respective cultures (monoculture, coculture with LSEC, and coculture with HUVEC) , through Day 9. Total protein secretion remained relatively constant within respective cultures throughout the culture process, indicating maintenance of that particular function. Experimental metabolic profiles for HepaRG cultures were also compared with scaled simulation profiles from Aim 1. Coculture in 3D with LSEC yielded results that closely matched simulation, followed by 2D cocultures with LSEC and 3D cocultures with HUVEC. APAP-glucuronide formation results from HepaRG experiments were still significantly lower than simulation, but also higher than in HepG2 experiments. The increasing trend in the APAP-sulfate amount produced with respect to time was observable in both 2D and 3D LSEC cocultures, as well as 2D coculture with HUVEC;

however, all APAP-sulfate production results were slightly lower than those observed in HepG2 experiments and in simulation. The metabolite APAP-GSH was still not detectable by the HPLC methods used, though the CYP 3A4 enzymatic assay demonstrated much higher activity in HepaRG experiments compared with HepG2. Enzymatic activity was considerably higher in 2D than 3D experiments. This could be due to diffusion limitations of the detection reagent into or out of the scaffold. Enzyme activity was activated in treated cocultures with LSEC, but activated in non-treated cultures in monocultures.

6.2 RECOMMENDATIONS

6.2.1 Investigate Higher Cell Densities in 3D

In aim one, changes in cell density were shown to affect the distribution of metabolic profiles. The number of cells in this study was limited to half a million cells due to the use of 2D cultures. As a measure of further validation, alterations in dell density in experimental settings should be investigated. I suggest using larger cell densities in 3D systems, as 2D were limited, in order to obtain greater values of metabolic production.

6.2.3 Explore the Addition of Other Non-Parenchymal Liver Cells

The goal of tissue engineering is to mimic the architecture and composition of the liver in an attempt to increase functionality. In this study, cocultures out performed monocultures in terms of metabolic analysis. With this in mind, the addition of a third cell type to tissue culture systems could further supplement appropriate cell to cell communications. The kupffer cell performs important immune response functions in the liver; thus, cell-cell communication between hepatocytes and kupffer cells could play an important role maintaining appropriate hepatic function.

6.2.4 Expand the Methodology to Other Known Drugs

While this methodology appears to work for acetaminophen, it is important to further validate the methodology by application to other well researched drugs. Of particular interest would be drugs that follow a different reaction rate equation than acetaminophen. All pathways of acetaminophen metabolism have been reported to follow the Michalis-Menten reaction rate equation. I suggest investigation of drug metabolism that follows a first order reaction rate or Hill equation reaction rate for further validation of this methodology.

6.2.5 Explore Flow Systems

Flow through systems are of particular interest to tissue engineers. Flow systems can constantly provide fresh, nutrient-rich medium to support cell survival and growth. Moreover, flow systems can also flush out toxic waste products that may inhibit proper cell function. Under these conditions, tissue culture platforms may be able to be cultured for increased time periods, which is extremely important when considering repeated dosing studies. Flow systems can also apply mechanical stress that is important to the development of certain tissues in correlation to performance. Investigation of a flow system would require the addition of convective considerations in the computational model, making it more complex and requiring more solving power and time. These considerations would need to be investigated prior to experimentation.

6.2.5 Expand the Research to Newly Developed Drugs

The optimal goal of this project was to develop a testing and validating methodology that was adaptable to various conditions and reactions. An adaptable model would suggest that this methodology could be applied to newly developed or in the process of being developed drugs. By obtaining kinetic constants from laboratory experiments, one could input experimental data and use the computational model to predict *in vivo* metabolic profiles.

REFERENCES

1. Herper, M. *The Cost of Creating a New Drug NOw $5 Billion, Pushing Big Pharma to Change*. Pharma and Healthcare 2013; Available from: http://www.forbes.com/sites/matthewherper/2013/08/11/how-the-staggering-cost-of-inventing-new-drugs-is-shaping-the-future-of-medicine/2/.
2. Bissell, D.M., et al., *Drug-induced liver injury: Mechanisms and test systems.* Hepatology, 2001. **33**(4): p. 1009-1013.
3. Aarons, L., et al., *Role of modelling and simulation in Phase I drug development.* European Journal of Pharmaceutical Sciences, 2001. **13**(2): p. 115-122.
4. Ekins, S., *In silico approaches to predicting drug metabolism, toxicology and beyond.* Biochemical Society Transactions, 2003. **31**: p. 611-614.
5. Huang, S.M., et al., *The Utility of Modeling and Simulation in Drug Development and Regulatory Review.* Journal of Pharmaceutical Sciences, 2013. **102**(9): p. 2912-2923.
6. Nowak, P., M. Wozniakiewicz, and P. Koscielniak, *Simulation of drug metabolism.* Trac-Trends in Analytical Chemistry, 2014. **59**: p. 42-49.
7. DiMasi, J.A., R.W. Hansen, and H.G. Grabowski, *The price of innovation: new estimates of drug development costs.* J Health Econ, 2003. **22**(2): p. 151-85.
8. Joseph DiMasi, H.G., Ronald Hansen. *Costs to Develop and Win Marketing Approval for a New Drug is $2.6 Billion*. 2014; Available from: http://csdd.tufts.edu/news/complete_story/pr_tufts_csdd_2014_cost_study.
9. Björnsson, E.S., *Hepatotoxicity by Drugs: The Most Common Implicated Agents.* International Journal of Molecular Sciences, 2016. **17**(2): p. 224.
10. Shanks, N., R. Greek, and J. Greek, *Are animal models predictive for humans?* Philosophy, Ethics, and Humanities in Medicine : PEHM, 2009. **4**: p. 2-2.
11. Sliwoski, G., et al., *Computational methods in drug discovery.* Pharmacological reviews, 2014. **66**(1): p. 334-395.
12. Igarashi, T., *The duration of toxicity studies required to support repeated dosing in clinical investigation — a toxicologist's opinion*, in *The Timing of Toxicological Studies to Support Clinical Trials*, C. Parkinson, et al., Editors. 1994, Springer Netherlands: Dordrecht. p. 67-74.
13. Sankar, U., *The Delicate Toxicity Balance in Drug Discovery*, in *The Scientist*. 2005.
14. Claude Spriet-Pourra, M.A., *Drug withdrawl from sale*. Scrip Reports. 1994, Richmond, Surrey: PBJ Publications.
15. Heywood, R., *Clinical Toxicity- Could it have been predicted? Post-marketing experience*, in *Animal Toxicity Studies: Their Relevance for Man*, C.E. Lumley and S.R. Walker, Editors. 1990, Quay Publishing: Lancaster, UK. p. 57-67.

16. Gebhardt, R., et al., *New hepatocyte in vitro systems for drug metabolism: Metabolic capacity and recommendations for application in basic research and drug development, standard operation procedures.* Drug Metabolism Reviews, 2003. **35**(2-3): p. 145-213.
17. Weise, F., et al., *Analysis and Comparison of Oxygen Consumption of HepG2 Cells in a Monolayer and Three-Dimensional High Density Cell Culture by use of a MatriGrid (R).* Biotechnology and Bioengineering, 2013. **110**(9): p. 2504-2512.
18. Griffith, L.G. and G. Naughton, *Tissue engineering--current challenges and expanding opportunities.* Science, 2002. **295**(5557): p. 1009-14.
19. Schmitmeier, S., et al., *Development and characterization of a small-scale bioreactor based on a bioartificial hepatic culture model for predictive pharmacological in vitro screenings.* Biotechnology and Bioengineering, 2006. **95**(6): p. 1198-1206.
20. Ijima, H., et al., *Development of a practical small-scale circulation bioreactor and application to a drug metabolism simulator.* Biochemical Engineering Journal, 2009. **44**(2-3): p. 292-296.
21. Novik, E., et al., *A microfluidic hepatic coculture platform for cell-based drug metabolism studies.* Biochem Pharmacol, 2010. **79**(7): p. 1036-44.
22. Tostoes, R.M., et al., *Human liver cell spheroids in extended perfusion bioreactor culture for repeated-dose drug testing.* Hepatology, 2012. **55**(4): p. 1227-36.
23. Ebrahimkhani, M.R., et al., *Bioreactor technologies to support liver function in vitro.* Advanced Drug Delivery Reviews, 2014. **69–70**(0): p. 132-157.
24. ElectrospinningCompany. *Why 3D cell culture?* ; Available from: http://www.electrospinning.co.uk/why-3d-cell-culture/.
25. Gibco, i., *Cell culture basics*
26. Achilli, T.-M., J. Meyer, and J.R. Morgan, *Advances in the formation, use and understanding of multi-cellular spheroids.* Expert opinion on biological therapy, 2012. **12**(10): p. 1347-1360.
27. Edmondson, R., et al., *Three-Dimensional Cell Culture Systems and Their Applications in Drug Discovery and Cell-Based Biosensors.* Assay and Drug Development Technologies, 2014. **12**(4): p. 207-218.
28. Polo, M.L., et al., *Responsiveness to PI3K and MEK inhibitors in breast cancer. Use of a 3D culture system to study pathways related to hormone independence in mice.* PLoS One, 2010. **5**(5): p. e10786.
29. Hartmanshenn, C., M. Scherholz, and I.P. Androulakis, *Physiologically-based pharmacokinetic models: approaches for enabling personalized medicine.* J Pharmacokinet Pharmacodyn, 2016. **43**(5): p. 481-504.
30. Lerapetritou, M.G., et al., *Tissue-level modeling of xenobiotic metabolism in liver: An emerging tool for enabling clinical translational research.* Clin Transl Sci, 2009. **2**(3): p. 228-37.
31. Patten, C.J., et al., *Cytochrome P450 enzymes involved in acetaminophen activation by rat and human liver microsomes and their kinetics.* Chemical Research in Toxicology, 1993. **6**(4): p. 511-518.

32. Chen, W., et al., *Oxidation of acetaminophen to its toxic quinone imine and nontoxic catechol metabolites by baculovirus-expressed and purified human cytochromes P450 2E1 and 2A6.* Chem Res Toxicol, 1998. **11**(4): p. 295-301.
33. Dong, H., et al., *Involvement of human cytochrome P450 2D6 in the bioactivation of acetaminophen.* Drug Metab Dispos, 2000. **28**(12): p. 1397-400.
34. Ganetsky, M., et al., *Effect of Excipients on Acetaminophen Metabolism and Its Implications for Prevention of Liver Injury.* The Journal of Clinical Pharmacology, 2013. **53**(4): p. 413-420.
35. Reith, D., et al., *Simultaneous modelling of the Michaelis-Menten kinetics of paracetamol sulphation and glucuronidation.* Clin Exp Pharmacol Physiol, 2009. **36**(1): p. 35-42.
36. Jibril, F., et al., *Intravenous versus Oral Acetaminophen for Pain: Systematic Review of Current Evidence to Support Clinical Decision-Making.* Can J Hosp Pharm, 2015. **68**(3): p. 238-47.
37. Drendel, A.L., et al., *A randomized clinical trial of ibuprofen versus acetaminophen with codeine for acute pediatric arm fracture pain.* Annals of emergency medicine, 2009. **54**(4): p. 553-560.
38. Watkins, P.B., et al., *Aminotransferase elevations in healthy adults receiving 4 grams of acetaminophen daily: a randomized controlled trial.* Jama, 2006. **296**(1): p. 87-93.
39. Atkuri, K.R., et al., *N-Acetylcysteine—a safe antidote for cysteine/glutathione deficiency.* Current opinion in pharmacology, 2007. **7**(4): p. 355-359.
40. Allen, D.D., et al., *Cell lines as in vitro models for drug screening and toxicity studies.* Drug development and industrial pharmacy, 2005. **31**(8): p. 757-768.
41. Yang, Z. and H.-R. Xiong, *In vitro, Tissue-Based Models as a Replacement for Animal Models in Testing of Drugs at the Preclinical Stages*, in *Biomedical Tissue Culture*. 2012, InTech.
42. Jiang, X.L., et al., *Application of physiologically based pharmacokinetic modeling to predict acetaminophen metabolism and pharmacokinetics in children.* CPT Pharmacometrics Syst Pharmacol, 2013. **2**: p. e80.
43. Kumar, N., et al., *Applying computational modeling to drug discovery and development.* Drug discovery today, 2006. **11**(17): p. 806-811.
44. Maes, M., M. Vinken, and H. Jaeschke, *Experimental models of hepatotoxicity related to acute liver failure.* Toxicol Appl Pharmacol, 2016. **290**: p. 86-97.
45. Brown, R., et al., *Would acetaminophen be approved by the FDA today.* GEMS104 drug development and regulation, 2012.
46. Bjornsson, E.S., *Hepatotoxicity by Drugs: The Most Common Implicated Agents.* International Journal of Molecular Sciences, 2016. **17**(2).
47. Weil, K., et al., *Paracetamol for pain relief after surgical removal of lower wisdom teeth.* Cochrane Database Syst Rev, 2007(3): p. CD004487.

48. Lauschke, V.M., et al., *Novel 3D Culture Systems for Studies of Human Liver Function and Assessments of the Hepatotoxicity of Drugs and Drug Candidates.* Chem Res Toxicol, 2016. **29**(12): p. 1936-1955.
49. DeLeve, L.D., *Liver sinusoidal endothelial cells and liver regeneration.* The Journal of Clinical Investigation, 2013. **123**(5): p. 1861-1866.
50. Nguyen, D.G., et al., *Bioprinted 3D Primary Liver Tissues Allow Assessment of Organ-Level Response to Clinical Drug Induced Toxicity In Vitro.* PLOS ONE, 2016. **11**(7): p. e0158674.
51. German, C.L. and S.V. Madihally, *Applications of Computational Modelling and Simulation of Porous Medium in Tissue Engineering.* Computation, 2016. **4**(1).
52. Devarapalli, M., B.J. Lawrence, and S.V. Madihally, *Modeling nutrient consumptions in large flow-through bioreactors for tissue engineering.* Biotechnol Bioeng, 2009. **103**(5): p. 1003-15.
53. Podichetty, J.T., et al., *Modeling pressure drop using generalized scaffold characteristics in an axial-flow bioreactor for soft tissue regeneration.* Ann Biomed Eng, 2014. **42**(6): p. 1319-30.
54. Podichetty, J.T. and S.V. Madihally, *Modeling of porous scaffold deformation induced by medium perfusion.* Journal of Biomedical Materials Research Part B: Applied Biomaterials, 2014. **102**(4): p. 737-748.
55. Bertz, R.J. and G.R. Granneman, *Use of In Vitro and In Vivo Data to Estimate the Likelihood of Metabolic Pharmacokinetic Interactions.* Clinical Pharmacokinetics, 1997. **32**(3): p. 210-258.
56. Shimada, T., et al., *Interindividual Variations in Human Liver Cytochrome-P-450 Enzymes Involved in the Oxidation of Drugs, Carcinogens and Toxic-Chemicals - Studies with Liver-Microsomes of 30 Japanese and 30 Caucasians.* Journal of Pharmacology and Experimental Therapeutics, 1994. **270**(1): p. 414-423.
57. German, C.L., *Modeling liver metabolism for drug development*. 2014, Oklahoma State University.
58. Podichetty, J.T. and S.V. Madihally, *Modeling of porous scaffold deformation induced by medium perfusion.* J Biomed Mater Res B Appl Biomater, 2014. **102**(4): p. 737-48.
59. Falk, B., S. Garramone, and S. Shivkumar, *Diffusion coefficient of paracetamol in a chitosan hydrogel.* Materials Letters, 2004. **58**(26): p. 3261-3265.
60. Mutlib, A.E., et al., *Kinetics of Acetaminophen Glucuronidation by UDP-Glucuronosyltransferases 1A1, 1A6, 1A9 and 2B15. Potential Implications in Acetaminophen–Induced Hepatotoxicity.* Chemical Research in Toxicology, 2006. **19**(5): p. 701-709.
61. Ben-Shachar, R., et al., *The biochemistry of acetaminophen hepatotoxicity and rescue: a mathematical model.* Theoretical Biology and Medical Modelling, 2012. **9**(1): p. 1-22.
62. Shimada, T., et al., *Interindividual variations in human liver cytochrome P-450 enzymes involved in the oxidation of drugs, carcinogens and toxic chemicals: studies with liver*

microsomes of 30 Japanese and 30 Caucasians. Journal of Pharmacology and Experimental Therapeutics, 1994. **270**(1): p. 414-423.
63. Court, M.H., et al., *Interindividual variability in acetaminophen glucuronidation by human liver microsomes: identification of relevant acetaminophen UDP-glucuronosyltransferase isoforms.* J Pharmacol Exp Ther, 2001. **299**(3): p. 998-1006.
64. Achour, B., et al., *Simultaneous quantification of the abundance of several cytochrome P450 and uridine 5'-diphospho-glucuronosyltransferase enzymes in human liver microsomes using multiplexed targeted proteomics.* Drug Metabolism and Disposition, 2014: p. dmd. 113.055632.
65. DEFENDI, G.L., *Acetaminophen Toxicity in Children: Diagnosis, Clinical Assessment, and Treatment of Acute Overingestion.*
66. Prescott, L.F., *Kinetics and metabolism of paracetamol and phenacetin.* British Journal of Clinical Pharmacology, 1980. **10**(Suppl 2): p. 291S-298S.
67. Damalakiene, L., et al., *Intracellular distribution of nontargeted quantum dots after natural uptake and microinjection.* Int. J. Nanomed, 2013. **8**: p. 555-568.
68. Norouzzadeh, M., et al., *Determining population doubling time and the appropriate number of HepG2 cells for culturing in 6-well plate.* 2016.
69. Kicic, A., A.C. Chua, and E. Baker, *Desferrithiocin is a more potent antineoplastic agent than desferrioxamine.* British journal of pharmacology, 2002. **135**(6): p. 1393-1402.
70. Bannwarth, B. and F. Pehourcq, *[Pharmacologic basis for using paracetamol: pharmacokinetic and pharmacodynamic issues].* Drugs, 2003. **63 Spec No 2**: p. 5-13.
71. Saad, Y. and M.H. Schultz, *GMRES: a generalized minimal residual algorithm for solving nonsymmetric linear systems.* SIAM J. Sci. Stat. Comput., 1986. **7**(3): p. 856-869.
72. Sohlenius-Sternbeck, A.K., *Determination of the hepatocellularity number for human, dog, rabbit, rat and mouse livers from protein concentration measurements.* Toxicol In Vitro, 2006. **20**(8): p. 1582-6.
73. Obach, R.S., *Nonspecific binding to microsomes: Impact on scale-up of in vitro intrinsic clearance to hepatic clearance as assessed through examination of warfarin, imipramine, and propranolol.* Drug Metabolism and Disposition, 1997. **25**(12): p. 1359-1369.
74. Tyapochkin, E., P.F. Cook, and G. Chen, *para-Nitrophenyl Sulfate Activation of Human Sulfotransferase 1A1 Is Consistent with Intercepting the E·PAP Complex and Reformation of E·PAPS.* The Journal of Biological Chemistry, 2009. **284**(43): p. 29357-29364.
75. Chen, G. and E. Tyapochkin, *CATALYTIC MECHANISM OF HUMAN SULFOTRANSFERASE 1A1.* The FASEB Journal, 2007. **21**(6): p. LB28.
76. Gamage, N.U., et al., *Structure of a human carcinogen-converting enzyme, SULT1A1. Structural and kinetic implications of substrate inhibition.* J Biol Chem, 2003. **278**(9): p. 7655-62.
77. Kuepfer, L., et al., *Applied Concepts in PBPK Modeling: How to Build a PBPK/PD Model.* CPT Pharmacometrics Syst Pharmacol, 2016. **5**(10): p. 516-531.

78. Diaz Ochoa, J.G., et al., *A multi-scale modeling framework for individualized, spatiotemporal prediction of drug effects and toxicological risk.* Front Pharmacol, 2012. **3**: p. 204.
79. Ben-Shachar, R., et al., *The biochemistry of acetaminophen hepatotoxicity and rescue: a mathematical model.* Theoretical Biology and Medical Modelling, 2012. **9**(1): p. 1-22.
80. Reddyhoff, D., et al., *Timescale analysis of a mathematical model of acetaminophen metabolism and toxicity.* Journal of Theoretical Biology, 2015. **386**: p. 132-146.
81. Gebhardt, R. and M. Matz-Soja, *Liver zonation: Novel aspects of its regulation and its impact on homeostasis.* World Journal of Gastroenterology : WJG, 2014. **20**(26): p. 8491-8504.
82. Ishibashi, H., et al., *Liver architecture, cell function, and disease.* Semin Immunopathol, 2009. **31**(3): p. 399-409.
83. Geraud, C., et al., *Liver sinusoidal endothelium: a microenvironment-dependent differentiation program in rat including the novel junctional protein liver endothelial differentiation-associated protein-1.* Hepatology, 2010. **52**(1): p. 313-26.
84. Godoy, P., et al., *Recent advances in 2D and 3D in vitro systems using primary hepatocytes, alternative hepatocyte sources and non-parenchymal liver cells and their use in investigating mechanisms of hepatotoxicity, cell signaling and ADME.* Arch Toxicol, 2013. **87**(8): p. 1315-530.
85. Ramaiahgari, S.C., et al., *A 3D in vitro model of differentiated HepG2 cell spheroids with improved liver-like properties for repeated dose high-throughput toxicity studies.* Archives of toxicology, 2014. **88**(5): p. 1083-1095.
86. Tolosa, L., et al., *HepG2 cells simultaneously expressing five P450 enzymes for the screening of hepatotoxicity: identification of bioactivable drugs and the potential mechanism of toxicity involved.* Archives of toxicology, 2013. **87**(6): p. 1115-1127.
87. Takayama, K., et al., *3D spheroid culture of hESC/hiPSC-derived hepatocyte-like cells for drug toxicity testing.* Biomaterials, 2013. **34**(7): p. 1781-1789.
88. Carrel, A., *On the Permanent Life of Tissue Outside of the Organism.* J. Exp. Med.,, 1912. **15**(3): p. 516–528.
89. Knazek, R.A., et al., *Cell culture on artificial capillaries: an approach to tissue growth in vitro.* Science, 1972. **178**(56): p. 65-6.
90. Bhatia, S.N., et al., *Effect of cell-cell interactions in preservation of cellular phenotype: cocultivation of hepatocytes and nonparenchymal cells.* Faseb J, 1999. **13**(14): p. 1883-900.
91. Mooney, D.J., et al., *Long-term engraftment of hepatocytes transplanted on biodegradable polymer sponges.* J Biomed Mater Res, 1997. **37**(3): p. 413-20.
92. Madihally, S.V., A.W. Flake, and H.W. Matthew, *Maintenance of CD34 expression during proliferation of CD34+ cord blood cells on glycosaminoglycan surfaces.* Stem Cells, 1999. **17**(5): p. 295-305.
93. Kim, B.S. and D.J. Mooney, *Scaffolds for engineering smooth muscle under cyclic mechanical strain conditions.* J Biomech Eng, 2000. **122**(3): p. 210-5.

94. Huang, Y., et al., *In vitro characterization of chitosan-gelatin scaffolds for tissue engineering.* Biomaterials, 2005. **26**(36): p. 7616-27.
95. Huang, Y., M. Siewe, and S.V. Madihally, *Effect of spatial architecture on cellular colonization.* Biotechnol Bioeng, 2006. **93**(1): p. 64-75.
96. Ratakonda, S., et al., *Assessing viscoelastic properties of chitosan scaffolds and validation with cyclical tests.* Acta Biomater, 2012. **8**(4): p. 1566-75.
97. Tillman, J., A. Ullm, and S.V. Madihally, *Three-dimensional cell colonization in a sulfate rich environment.* Biomaterials, 2006. **27**(32): p. 5618-26.
98. Iyer, P., K.J. Walker, and S.V. Madihally, *Increased matrix synthesis by fibroblasts with decreased proliferation on synthetic chitosan-gelatin porous structures.* Biotechnol Bioeng, 2011.
99. Goulet, F., C. Normand, and O. Morin, *Cellular interactions promote tissue-specific function, biomatrix deposition and junctional communication of primary cultured hepatocytes.* Hepatology, 1988. **8**(5): p. 1010-1018.
100. Morin, O. and C. Normand, *Long-term maintenance of hepatocyte functional activity in co-culture: requirements for sinusoidal endothelial cells and dexamethasone.* J Cell Physiol, 1986. **129**(1): p. 103-10.
101. DeLeve, L.D., *Liver sinusoidal endothelial cells and liver regeneration.* J Clin Invest, 2013. **123**(5): p. 1861-6.
102. Xu, B., et al., *Capillarization of Hepatic Sinusoid by Liver Endothelial Cell-Reactive Autoantibodies in Patients with Cirrhosis and Chronic Hepatitis.* The American Journal of Pathology, 2003. **163**(4): p. 1275-1289.
103. Kim, K., et al., *Preserved liver-specific functions of hepatocytes in 3D co-culture with endothelial cell sheets.* Biomaterials, 2012. **33**(5): p. 1406-1413.
104. Huang, Y., M. Siewe, and S.V. Madihally, *Effect of spatial architecture on cellular colonization.* Biotechnology and Bioengineering, 2006. **93**(1): p. 64-75.
105. Tormos, C.J., C. Abraham, and S.V. Madihally, *Improving the stability of chitosan-gelatin-based hydrogels for cell delivery using transglutaminase and controlled release of doxycycline.* Drug Deliv Transl Res, 2015. **5**(6): p. 575-84.
106. Brunner, L.J. and S. Bai, *Simple and rapid assay for acetaminophen and conjugated metabolites in low-volume serum samples.* Journal of Chromatography B, 1999. **732**(2): p. 323-329.
107. Gerets, H.H.J., et al., *Characterization of primary human hepatocytes, HepG2 cells, and HepaRG cells at the mRNA level and CYP activity in response to inducers and their predictivity for the detection of human hepatotoxins.* Cell Biology and Toxicology, 2012. **28**(2): p. 69-87.
108. No, D.Y., et al., *Functional 3D Human Primary Hepatocyte Spheroids Made by Co-Culturing Hepatocytes from Partial Hepatectomy Specimens and Human Adipose-Derived Stem Cells.* PLOS ONE, 2012. **7**(12): p. e50723.

109. Lauschke, V.M., et al., *Novel 3D Culture Systems for Studies of Human Liver Function and Assessments of the Hepatotoxicity of Drugs and Drug Candidates.* Chemical Research in Toxicology, 2016. **29**(12): p. 1936-1955.
110. Khetani, S.R. and S.N. Bhatia, *Microscale culture of human liver cells for drug development.* Nat Biotech, 2008. **26**(1): p. 120-126.
111. Chiew, G.G.Y., et al., *Physical supports from liver cancer cells are essential for differentiation and remodeling of endothelial cells in a HepG2-HUVEC co-culture model.* Scientific Reports, 2015. **5**.
112. Ye, M., et al., *Size- and time-dependent alteration in metabolic activities of human hepatic cytochrome P450 isozymes by gold nanoparticles via microsomal coincubations.* Nanoscale Research Letters, 2014. **9**(1): p. 642-642.
113. Lash, L.H., D.A. Putt, and H. Cai, *Drug Metabolism Enzyme Expression and Activity in Primary Cultures of Human Proximal Tubular Cells.* Toxicology, 2008. **244**(1): p. 56-65.
114. Shulman, M. and Y. Nahmias, *Long-Term Culture and Coculture of Primary Rat and Human Hepatocytes.* Methods in molecular biology (Clifton, N.J.), 2013. **945**: p. 287-302.
115. Szkolnicka, D., et al., *Accurate Prediction of Drug-Induced Liver Injury Using Stem Cell-Derived Populations.* Stem Cells Translational Medicine, 2014. **3**(2): p. 141-148.
116. Donato, M.T., et al., *Validated assay for studying activity profiles of human liver UGTs after drug exposure: inhibition and induction studies.* Analytical and Bioanalytical Chemistry, 2010. **396**(6): p. 2251-2263.
117. McLean, A.J., et al., *Age-related pseudocapillarization of the human liver.* J Pathol, 2003. **200**(1): p. 112-7.
118. Michaut, A., et al., *A cellular model to study drug-induced liver injury in nonalcoholic fatty liver disease: Application to acetaminophen.* Toxicology and Applied Pharmacology, 2016. **292**: p. 40-55.
119. Nelson, L.J., et al., *Acetaminophen cytotoxicity is ameliorated in a human liver organotypic co-culture model.* Scientific Reports, 2015. **5**.
120. Orbach, S.M., et al., *Investigating acetaminophen hepatotoxicity in multi-cellular organotypic liver models.* Toxicology in Vitro, 2017. **42**: p. 10-20.
121. Roe, A.L., et al., *The effect of high dose endotoxin on CYP3A2 expression in the rat.* Pharmaceutical research, 1998. **15**(10): p. 1603-1608.
122. Masubuchi, Y., K. Enoki, and T. Horie, *Down-regulation of hepatic cytochrome P450 enzymes in rats with trinitrobenzene sulfonic acid-induced colitis.* Drug Metabolism and Disposition, 2008. **36**(3): p. 597-603.
123. Bespalov, A., et al., *Drug Tolerance: A Known Unknown in Translational Neuroscience.* Trends Pharmacol Sci, 2016. **37**(5): p. 364-78.
124. Mosedale, M. and P.B. Watkins, *Drug-induced liver injury: Advances in mechanistic understanding that will inform risk management.* Clinical Pharmacology & Therapeutics, 2017. **101**(4): p. 469-480.
125. Park, B.K. and A.M. Breckenridge, *Clinical implications of enzyme induction and enzyme inhibition.* Clin Pharmacokinet, 1981. **6**(1): p. 1-24.

126. Mumtaz, M., *Principles and practice of mixtures toxicology*. 2011: John Wiley & Sons.
127. Miwa, G.T. and A.Y.H. Lu, *Kinetic isotope effects and 'metabolic switching' in cytochrome P450-catalyzed reactions.* BioEssays, 1987. **7**(5): p. 215-219.
128. Stillwell, W., *Chapter 1 - Introduction to Biological Membranes*, in *An Introduction to Biological Membranes (Second Edition)*. 2016, Elsevier. p. 3-15.
129. Abu-Absi, S.F., L.K. Hansen, and W.S. Hu, *Three-dimensional co-culture of hepatocytes and stellate cells.* Cytotechnology, 2004. **45**(3): p. 125-40.
130. Gu, J., et al., *Establishment of a three-dimensional co-culture system by porcine hepatocytes and bone marrow mesenchymal stem cells in vitro.* Hepatol Res, 2009. **39**(4): p. 398-407.
131. Thomas, R.J., et al., *The effect of three-dimensional co-culture of hepatocytes and hepatic stellate cells on key hepatocyte functions in vitro.* Cells Tissues Organs, 2005. **181**(2): p. 67-79.
132. Boland, T., et al., *Cell and organ printing 2: fusion of cell aggregates in three-dimensional gels.* Anat Rec A Discov Mol Cell Evol Biol, 2003. **272**(2): p. 497-502.
133. Jakab, K., et al., *Tissue engineering by self-assembly of cells printed into topologically defined structures.* Tissue Eng Part A, 2008. **14**(3): p. 413-21.
134. Burg, T., et al. *Systems engineering challenges in inkjet biofabrication*. in *SoutheastCon, 2007. Proceedings. IEEE*. 2007.
135. Xu, T., et al., *Inkjet printing of viable mammalian cells.* Biomaterials, 2005. **26**(1): p. 93-9.
136. Fedorovich, N.E., et al., *Hydrogels as extracellular matrices for skeletal tissue engineering: state-of-the-art and novel application in organ printing.* Tissue Eng, 2007. **13**(8): p. 1905-25.
137. Varghese, D., et al., *Advances in tissue engineering: cell printing.* J Thorac Cardiovasc Surg, 2005. **129**(2): p. 470-2.
138. Bjornsson, E.S., *Epidemiology and risk factors for idiosyncratic drug-induced liver injury.* Semin Liver Dis, 2014. **34**(2): p. 115-22.
139. Takahashi, Y., et al., *3D spheroid cultures improve the metabolic gene expression profiles of HepaRG cells.* Bioscience reports, 2015. **35**(3): p. e00208.
140. Mueller, D., et al., *3D organotypic HepaRG cultures as in vitro model for acute and repeated dose toxicity studies.* Toxicology in Vitro, 2014. **28**(1): p. 104-112.
141. Cerec, V., et al., *Transdifferentiation of hepatocyte-like cells from the human hepatoma HepaRG cell line through bipotent progenitor.* Hepatology, 2007. **45**(4): p. 957-67.
142. Aninat, C., et al., *EXPRESSION OF CYTOCHROMES P450, CONJUGATING ENZYMES AND NUCLEAR RECEPTORS IN HUMAN HEPATOMA HepaRG CELLS.* Drug Metabolism and Disposition, 2006. **34**(1): p. 75-83.
143. Lübberstedt, M., et al., *HepaRG human hepatic cell line utility as a surrogate for primary human hepatocytes in drug metabolism assessment in vitro.* Journal of Pharmacological and Toxicological Methods, 2011. **63**(1): p. 59-68.

144. Rebelo, S.P., et al., *HepaRG microencapsulated spheroids in DMSO-free culture: novel culturing approaches for enhanced xenobiotic and biosynthetic metabolism.* Arch Toxicol, 2015. **89**(8): p. 1347-58.
145. Ramaiahgari, S.C., et al., *A 3D in vitro model of differentiated HepG2 cell spheroids with improved liver-like properties for repeated dose high-throughput toxicity studies.* Arch Toxicol, 2014. **88**(5): p. 1083-95.
146. Rose, K.A., et al., *Co-culture of Hepatocytes and Kupffer Cells as an In Vitro Model of Inflammation and Drug-Induced Hepatotoxicity.* Journal of pharmaceutical sciences, 2016. **105**(2): p. 950-964.
147. LeCluyse, E.L., et al., *Organotypic liver culture models: meeting current challenges in toxicity testing.* Crit Rev Toxicol, 2012. **42**(6): p. 501-48.
148. Lawrence, B.J. and S.V. Madihally, *Cell colonization in degradable 3D porous matrices.* Cell Adh Migr, 2008. **2**(1): p. 9-16.
149. Petrie, R.J., et al., *Nonpolarized signaling reveals two distinct modes of 3D cell migration.* J Cell Biol, 2012. **197**(3): p. 439-55.
150. Iyer, P., K.J. Walker, and S.V. Madihally, *Increased matrix synthesis by fibroblasts with decreased proliferation on synthetic chitosan-gelatin porous structures.* Biotechnol Bioeng, 2012. **109**(5): p. 1314-25.
151. Coulouarn, C., et al., *Hepatocyte - Stellate Cell Crosstalk in the Liver Engenders a Permissive Inflammatory Microenvironment that Drives Progression in Hepatocellular Carcinoma.* Cancer research, 2012. **72**(10): p. 2533-2542.
152. Shi, L., et al., *Role of estrogen in hepatocellular carcinoma: is inflammation the key?* J Transl Med, 2014. **12**: p. 93.
153. Nelson, L.J., et al., *Acetaminophen cytotoxicity is ameliorated in a human liver organotypic co-culture model.* Scientific Reports, 2015. **5**: p. 17455.
154. Tomizawa, M., et al., *Cell death in a co-culture of hepatocellular carcinoma cells and human umbilical vascular endothelial cells in a medium lacking glucose and arginine.* Oncology Letters, 2017. **13**(1): p. 258-262.
155. Chiew, G.G., et al., *Physical supports from liver cancer cells are essential for differentiation and remodeling of endothelial cells in a HepG2-HUVEC co-culture model.* Sci Rep, 2015. **5**: p. 10801.
156. Guillouzo, A., et al., *The human hepatoma HepaRG cells: A highly differentiated model for studies of liver metabolism and toxicity of xenobiotics.* Chemico-Biological Interactions, 2007. **168**(1): p. 66-73.
157. Godoy, P., et al., *Recent advances in 2D and 3D in vitro systems using primary hepatocytes, alternative hepatocyte sources and non-parenchymal liver cells and their use in investigating mechanisms of hepatotoxicity, cell signaling and ADME.* Archives of toxicology, 2013. **87**(8): p. 1315-1530.
158. Bachmann, A., et al., *3D Cultivation Techniques for Primary Human Hepatocytes.* Microarrays, 2015. **4**(1): p. 64-83.

159. Edmondson, R., et al., *Three-dimensional cell culture systems and their applications in drug discovery and cell-based biosensors.* Assay Drug Dev Technol, 2014. **12**(4): p. 207-18.

Carrie Lynn German

Candidate for the Degree of

Doctor of Philosophy

Thesis: EVALUATING TISSUE CULTURE PLATFORMS FOR USE IN DRUG DEVELOPMENT: A MULTI-METHOD VALIDATIONAL APPROACH

Major Field: Chemical Engineering

Biographical:

Born in Stillwater, Oklahoma August 10, 1982.

Education:

Completed the requirements for the Doctor of Philosophy in your major at Oklahoma State University, Stillwater, Oklahoma in December, 2017

Completed the requirements for the Master of Science in your major at Oklahoma State University, Stillwater, Oklahoma in July, 2014

Completed the requirements for the Bachelor of Science in your major at Oklahoma State University, Stillwater, Oklahoma in May, 2006

Experience:

Teaching Assistant, Oklahoma State University	2012 – 2017
Research Associate, Oklahoma State University	2014 – 2017
Research Assistant, Oklahoma State University	2012 – 2014
Research Experience for Teachers, Oklahoma State University	2011

Professional Memberships:

Tissue Engineering & Regenerative Medicine International Society
American Institute of Chemical Engineers
Graduate Society for Interdisciplinary Toxicology
Phi Kappa Phi Honor Society
Omega Chi Honor Society, Mu Chapter